MATHEMATICAL MODELING OF ZIKA VIRUS TRANSMISSION AND MULTIPLE PATHOGEN INTERACTIONS

by

OMOMAYOWA OLAWOYIN

Presented to the Faculty of the Graduate School of
The University of Texas at Arlington in Partial Fulfillment
of the Requirements
for the Degree of

DOCTOR OF PHILOSOPHY

THE UNIVERSITY OF TEXAS AT ARLINGTON

May 2019

ACKNOWLEDGEMENTS

I would first like to thank God for his faithfulness in my life. I would also like to thank my parents, Afolabi and Bosede Oguntokun, for instilling in me the value of education and for all they sacrificed to ensure that I had the resources needed to succeed. A big thank you goes to my husband, siblings, extended family, friends, and mentors for their prayers, support, and encouragement throughout my graduate studies. I would like to express my deepest appreciation to my advisor, Christopher Kribs, for his guidance. I am grateful to have learned from him and could not have asked for a better advisor. I would like to thank the other members of my committee, Hristo Kojouharov, James Grover, Benito Chen, and Gaik Ambartsoumian, for their valuable feedback. In addition, I want to thank Dr. Pauline van den Driessche for valuable feedback on initial work developing the models in Chapter 4 and calculating reproductive numbers, and Dr. Frank Hilker for suggesting relevant articles for Chapter 4 and providing a preprint of [1]. I would like to acknowledge the National Science Foundation (NSF) for supporting this work through the Louis Stokes Alliance for Minority Participation Bridge to Doctorate Program (Grant No. HRD-1026806) and the NSF Graduate Research Fellowship Program (Grant No. 1746052).

April 22, 2019

ABSTRACT

MATHEMATICAL MODELING OF ZIKA VIRUS TRANSMISSION AND MULTIPLE PATHOGEN INTERACTIONS

Omomayowa Olawoyin, Ph.D.

The University of Texas at Arlington, 2019

Supervising Professor: Christopher Kribs

The purpose of this dissertation is twofold: to deepen our understanding of the complex transmission routes of the Zika virus (ZIKV), and to study multiple pathogen interactions (specifically cocirculation of Zika and dengue and discrete-time coinfection models) through the lens of invasion reproductive numbers (IRNs) which measure the ability of a disease to invade a population endemic with another disease(s).

In addition to being transmitted to humans through the bite of infected female *Aedes aegypti* mosquitoes, studies show that the ZIKV can also be sexually and vertically transmitted within both populations. We develop a new mathematical model of the ZIKV which incorporates sexual transmission in humans and mosquitos, vertical transmission in mosquitos, and mosquito to human transmission through bites. Analysis of this deterministic model shows that although the secondary transmission pathways cause minor qualitative changes on a Zika outbreak, they have important consequences for control strategies and estimates of Zika's basic reproductive number (BRN).

Over the past five years, cocirculation of dengue and Zika has increased; however, very little is known about its epidemiological consequences. Using a dengue and Zika coinfection model that incorporates altered infectivity of mosquitoes (due to coinfection), and antibody-dependent enhancement (ADE) within the human population, we study the impact of cocirculation on the spread of both diseases. Central to our analysis is the derivation and interpretation of the basic reproductive number (BRN) and IRN of both pathogens. Our results identify threshold conditions under which one disease facilitates the spread of the other and show that ADE has a greater impact on disease persistence than altered vector infectivity.

IRNs are utilized frequently in continuous-time models with multiple interacting pathogens; however, they are yet to be explored in discrete-time systems. We extend the concept of IRNs to discrete-time models by showing how to calculate them for a set of two-pathogen SIS models with coinfection. In our exploration, we address how sequencing events impacts the BRN and IRN, and analyze a formulation of the discrete-time model which assumes that events occur simultaneously. Results show that while the BRN is unaffected by variations in the order of events, the IRN differs. Furthermore, although the simultaneous model lacks the simplification property that other models possess and the mathematics involved in its analysis is complex, the model exhibits competitive exclusion under cross-immunity which is not observed in the sequential formulations.

TABLE OF CONTENTS

CHAPTER 1

Introduction

1.1 Vector-Borne Disease Modeling

More than half of the world's population is at risk for vector-borne diseases, illnesses that are caused by pathogens transmitted to humans via snails, mosquitoes, ticks, flies, or other animals. These diseases (examples of which include malaria, dengue, yellow fever, and Zika) result in over one million deaths annually and account for approximately 17% of all infectious diseases [2]. Although historically limited to (sub)tropical and developing countries, the range of vector-borne diseases has increased with urbanization, climate change, and international travel.

Mathematical models are especially useful in studying vector-borne diseases. These models provide insight on disease spread and the effectiveness of control measures, while obviating the need for heavy economic commitments or lofty epidemiological experiments. One of the earliest mathematical models of vector-borne diseases was formulated by a British medical doctor, Sir Ronald Ross, to study malaria transmission. In his model, Ross used differential equations to describe the change in susceptible and infectious human and mosquito populations and discovered a threshold mosquito density under which malaria could be eradicated. Decades later, George Macdonald extended the work of Sir Ross and developed the classical Ross-Macdonald model. Amongst other things, his model incorporated latency within mosquito classes and introduced the basic reproductive number (BRN), the expected number of secondary infections caused by a single infected individual in a completely susceptible population, of malaria. Over the past several decades, the Ross-Macdonald model

has been extended to study various illnesses and remains an integral component of vector-borne disease modeling [3].

1.2 Zika Virus

One particular vector-borne disease that has received international attention is Zika. Zika is caused by the Zika virus (ZIKV) which is transmitted to humans primarily through the bite of infected female *Aedes* mosquitoes. This virus was first isolated in a rhesus monkey in Uganda in 1947 and the first human infection was discovered in Nigeria in 1953. Prior to the 21st century, Zika spread sporadically in Africa and Asia. In 2007, however, a series of massive outbreaks began, first in Micronesia (2007), then French Polynesia (2013), and more recently the Americas (2014). Since its introduction into the western hemisphere, over 200,000 confirmed cases (and approximately 600,000 suspected cases) of Zika have been reported in the region [4].

The clinical manifestations and transmission mechanisms of Zika complicate the study of this disease. For one, 80% of individuals infected with ZIKV are asymptomatic. Those that are symptomatic typically experience fever, rash, conjunctivitis, or myalgia. While ZIKV infection lasts approximately two weeks (followed by life-long immunity), severe forms of the disease have been associated with Guillain-Barré syndrome, Congenital Zika Syndrome, and increased microcephaly in newborns. Furthermore, although Zika is primarily spread by mosquitoes, the virus can be sexually and vertically transmitted (from a mother to her offspring) within human and mosquito populations [4, 5]. Since there are currently no vaccines for Zika, disease prevention efforts focus on the use of biological controls, insecticides, repellents, or bird nets.

1.3 Pathogen Interactions

With the rapid spread of pathogens across the globe, cocirculation of multiple diseases within the same geographical region is inevitable (for example Chagas disease and chikingunya in Latin America, and Zika and dengue in Southeast Asia). As a result, it is important to consider how these pathogens interact and how their interactions impact disease spread (e.g. whether they lead to copersistence or competitive exclusion).

One way to examine the interplay between multiple pathogens is through a key epidemiological quantity called the invasion reproductive number (IRN). The IRN describes the number of secondary infections produced by an infected individual in a population where one (or more) other pathogen is endemic [6]. If a disease's IRN is greater than 1, it can spread in a population endemic with other disease(s), but if it is less than 1, the disease will die off. One of the earliest mathematical models to discuss the use of IRNs is [6]. In this article, Porco and Blower develop a vaccination model for controlling two subtypes of HIV and show that four distinct outcomes are possible-eradication of both subtypes, persistence of both subtypes, eradication of only the endemic subtype, and persistence of only the invading subtype. In addition to [6], IRNs have been considered in numerous continuous-time models such as [7, 8, 9]. However, it is important to note that IRNs have not previously been discussed in the context of discrete-time models, where biological events occur within specific time intervals.

1.4 Outline

In this thesis, we model Zika transmission and multiple pathogen interactions (as it pertains to the ZIKV and more generally discrete-time models). In Chapter

2, we examine the impact of multiple transmission pathways (vector-human transmission, sexual transmission in humans and mosquitoes, and vertical transmission in mosquitoes) on the spread and control of the ZIKV. Specifically, we focus on how additional transmission mechanisms effect Zika's BRN, the timing of an outbreak, the number of people infected, and the effectiveness of control measures. In Chapter 3, we model the cocirculation of dengue and Zika to determine how the presence of one disease affects that of the other. Central to our analysis is the IRN of each pathogen, which provides a way to measure the effects of antibody-dependent enhancement and altered infectivity of coinfected mosquitoes on the dengue-Zika interplay. Lastly, in Chapter 4, we expand the analytical tools used in modeling multiple pathogen interactions by extending the concept of IRNs to simple discrete-time coinfection models. We show that the ordering of events (which does not exist in continuous-time models) greatly impacts reproductive numbers in discrete-time.

CHAPTER 2

Effects of Multiple Transmission Pathways on Zika Dynamics

2.1 Introduction

Zika is a vector-borne disease transmitted to humans primarily through the bite of infected female *Aedes aegypti* mosquitoes. The Zika virus (ZIKV) was first found in Uganda in 1947 and has since spread sporadically to regions in Africa and Asia [10]. However, since 2015, Zika has been reported in over 50 countries in the Americas including the United States and has been associated with serious clinical implications such as Guillain-Barré syndrome and increased microcephaly in newborns [10]. To date, there have been approximately 200,000 confirmed cases of Zika and approximately 2,600 confirmed congenital syndrome cases associated with ZIKV infection [11].

Transmission of Zika within human and mosquito populations is quite complex. Although ZIKV is primarily transmitted to humans through the bite of infected *Aedes* mosquitoes, recent reports have confirmed sexual and perinatal transmission among humans [12]. In addition to these transmission routes, the virus can spread vertically from a female mosquito to her offspring [5] and has the potential to spread sexually in *Aedes* mosquitoes. While sexual transmission of ZIKV within mosquito populations is not yet confirmed (in part because of the lack of studies investigating transmission of ZIKV within mosquitoes), this transmission route is highly probable given evidence of sexual transmission of the Dengue virus (DENV), a closely related flavivirus, in Aedes mosquitoes [13].

Since little is known about Zika, mathematical models are essential to understanding the transmission dynamics of the disease, deriving key epidemiological quantities, and informing the creation of disease control strategies [14]. Most of the early mathematical models of Zika were employed to estimate the basic reproductive number, R_0, of the virus (the number of secondary infections that a single infected individual can make in a completely susceptible population). By examining the 2013/2014 Zika outbreak in French Polynesia through a simple compartmental model which incorporates only human-vector transmission, R_0 was found to range between 2.6-4.8 [15]. This range for R_0 is consistent with other estimates [16, 10].

As evidence of sexual transmission of ZIKV emerged, researchers began to investigate the impact of this additional transmission pathway on the spread of the disease. In [10], authors present one of the first mathematical models to examine the combined effects of direct (sexual) and indirect (vector to human) modes of ZIKV transmission in the human population. Their deterministic model utilized data from several South American countries and showed that sexual transmission contributes very little to R_0 (3%) but has the potential to increase the risk of infection and epidemic size of an outbreak. To further explore the contribution of sexual and vector transmission of Zika, an age-and-sex structured model was developed in [17]. Analysis of the model revealed that human-mosquito interaction parameters have a more significant impact on R_0 than do sexual transmission parameters which contribute less than 5% to the reproductive number. However, sexual transmission was shown to strongly contribute to an outbreak in regions where mosquito populations are sparse. In addition to the two transmission mechanisms studied in the previous models, the effect of migration on disease spread was investigated in [18]. As with other studies, it was shown that sexual transmission alone cannot drive the spread of Zika but that

this transmission pathway and migration can increase the magnitude and duration of outbreaks.

Researchers in [19] are among the first to develop and analyze a mathematical model of Zika which incorporates vertical transmission of the virus in humans (in addition to transmission of the disease through mosquito bites). Sensitivity analysis of the model showed that mosquito demographic parameters and human-mosquito transmission parameters play critical roles in the diffusion of Zika. The authors also investigated the effects of varying levels of control techniques on Zika and found that personal protection strategies were more effective at controlling the spread of disease than delayed conception or mosquito-reduction.

Although incorporating the additional transmission mechanisms of ZIKV into mathematical models adds to their complexity, these epidemiological details can impact the initial growth rate of an outbreak and estimates of the basic reproductive number [20, 21, 22, 23]. In a general exploration of the sensitivity of parameter estimates to model structure, Lloyd [20] shows that models with algebraically identical R_0 expressions can have drastically different initial growth rates due to variations in the biological assumptions of the models (e.g. SIR versus SEIR classes and exponential versus gamma distribution of infectious and latent periods). The sensitivity of the initial growth rate of an outbreak to the model structure can lead to inaccurate estimates of the basic reproductive number of a disease. As detailed in the within-host study of viral dynamics in [21] and the disease management context of [23], this results in unrealistic predictions of the effectiveness of control measures needed to curtail the spread of a pathogen.

While individually, some of the transmission mechanisms of the ZIKV are unlikely, in combination they can affect the persistence of Zika. The different components can increase the size and duration of outbreaks, result in peak infections

occurring sooner in Zika outbreak history, and allow the virus to circulate at low levels until favorable environmental conditions cause an outbreak. In contrast to previous studies which focus on at most two transmission pathways of the ZIKV, we introduce a new mathematical model which incorporates (1) sexual and (2) vertical ZIKV transmission within mosquito populations as well as (3) sexual transmission in humans and (4) vector to human transmission. We omit vertical ZIKV transmission in humans both to simplify our model and because the infectious period of Zika (at most two weeks [24]) is too short for an infant class to contribute to further sexual or vertical transmission of the disease. By analyzing the simultaneous ZIKV transmission cycles in humans and vectors, something which no other model has done, we aim to answer the following research question: what is the relative contribution of the individual and combined transmission mechanisms (1-4) on the spread of Zika? Quantifying the effects of these transmission pathways will not only contribute to a better understanding of the overall population dynamics of Zika but may also aid in the formation of control strategies.

In the following sections, we formulate a mathematical model incorporating transmission modes 1-4 and compare it with a simplified vector transmission model to determine the combined effects of secondary transmission pathways on the spread of Zika. We derive and numerically approximate the basic reproductive numbers of both models which are used to determine whether an epidemic will occur ($R_0 > 1$ implies sustained disease spread within a population). We also analyze the sensitivity of the basic reproductive number, peak time, and final epidemic size to variations in parameter values. In addition, we explore how differential timing of control measures (based on the proportion of people infected in each model) may affect the outcome of an outbreak. Lastly, we investigate how secondary transmission pathways impact estimates of Zika's R_0.

2.2 Model Formation

The deterministic mathematical model discussed in this paper utilizes a system of nonlinear ordinary differential equations to capture the overall trends in Zika dynamics and estimate the likely contribution of each transmission route. In the model, we consider two populations: humans and mosquitoes. Humans are compartmentalized into susceptible, exposed, symptomatic, asymptomatic, and recovered, classes (S_h, E_h, I_h, A_h, R_h) with the total number of humans denoted by N_h. In the vector population, we consider susceptible, exposed, and infectious female mosquitoes (S_{vf}, E_{vf}, I_{vf}), infectious male mosquitoes (I_{vm}), and susceptible and infected juvenile mosquitoes (S_e, I_e). The total number of adult female, adult male, and juvenile mosquitoes is given by N_{vf}, N_{vm}, and N_e respectively. We also include demographics for the mosquito population and not the human population because the lifespan of the mosquito is much shorter than that of a human. A complete list of the state variables used in this model is shown in Table 2.1.

Susceptible humans become exposed to ZIKV after it is transmitted to them through the bite of an infectious female mosquito or through sexual contact with an infected person. This infected person could be symptomatic or asymptomatic since the sexual transmission of ZIKV from both classes has been documented [10, 25]. After a person is infected with ZIKV, he or she incubates the virus at rate δ before becoming infectious. Infectious humans recover at rate γ and are assumed to have lifelong immunity following recovery. This assumption is based on evidence from other flaviviruses, such as DENV, and the presence of ZIKV neutralizing antibodies in human and animal sera [26, 27, 28]. We neglect ZIKV induced mortality in this model because symptoms of Zika (rash, fever, conjunctivitis, and muscle and joint pain) are mild and rarely result in death [29].

State Variable	Description
S_h	Susceptible Humans
E_h	Exposed Humans
I_h	Symptomatic Infected Humans
A_h	Asymptomatic Infected Humans
R_h	Recovered Humans
N_h	Total Number of Humans
S_{vf}	Susceptible Adult Female Mosquitoes
E_{vf}	Exposed Adult Female Mosquitoes
I_{vf}	Infectious Adult Female Mosquitoes
I_{vm}	Infectious Adult Male Mosquitoes
S_e	Susceptible Juvenile Mosquitoes
I_e	Infectious Juvenile Mosquitoes
N_e	Total Number of Juvenile Mosquitoes
N_{vm}	Total Number of Adult Male Mosquitoes
N_{vf}	Total Number of Adult Female Mosquitoes

Table 2.1: **Epidemiological Classes**

Susceptible adult female mosquitoes become exposed to ZIKV after feeding on an infected person. We assume that asymptomatic humans can transmit ZIKV to mosquitoes, as is the case in [30]. During exposure to ZIKV, mosquitoes undergo an incubation period of 7-10 days before becoming infectious [12]. Once a mosquito is infectious, we assume that it does not clear the virus.

The life cycle of *Aedes* mosquitoes consists of four successive stages: egg, larva, pupa, and adult. In this model, we begin our observation of the mosquito population following the hatching of eggs (at rate r) and combine the two aquatic stages (larva and pupa) into the juvenile mosquito compartments S_e and I_e. The growth of the juvenile vector population is limited by the carrying capacity K of the breeding site. These juvenile vectors mature at a rate γ_e into either susceptible or infectious

adult mosquitoes. We assume that those infected juvenile mosquitoes that mature into infectious male mosquitoes can transmit ZIKV to female vectors through sexual contact. This assumption is based on experimental studies which show evidence of venereal transmission of viruses from male to female *Aedes* mosquitoes [5, 31]. We do not include sexual transmission from female to male mosquitoes since female mosquitoes are not shown to transmit DENV through sexual contact. Finally, since male mosquitoes do not feed on humans, we assume that they can only become carriers of ZIKV through vertical transmission from their mother.

A flowchart of ZIKV transmission is illustrated in Figure 2.1. The system of equations that will henceforth be referred to as the full model is given by (2.1) and the parameter values are shown in Table 2.2.

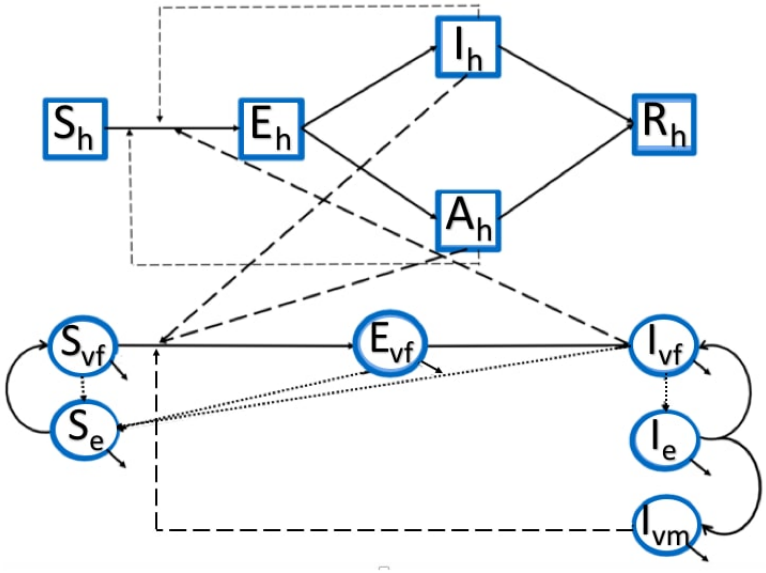

Figure 2.1: **ZIKV Transmission Model Schematic:** The solid lines in this flow chart represent movement between different state variables. Thin dashed lines represent disease transmission between different classes of the same population, thick dashed lines represent disease transmission across different populations, and dotted lines represent birth in the mosquito population.

$$
\begin{aligned}
\dot{S}_h &= -b\beta_{vh}\tfrac{I_{vf}S_h}{N_h} - a\tfrac{S_h}{N_h}(\beta_a A_h + \beta_I I_h) \\
\dot{E}_h &= b\beta_{vh}\tfrac{I_{vf}S_h}{N_h} + a\tfrac{S_h}{N_h}(\beta_a A_h + \beta_I I_h) - \delta E_h \\
\dot{I}_h &= \phi\delta E_h - \gamma I_h \\
\dot{A}_h &= (1-\phi)\delta E_h - \gamma A_h \\
\dot{R}_h &= \gamma(I_h + A_h) \\
\dot{S}_{vf} &= \alpha\gamma_e S_e - b\tfrac{S_{vf}}{N_h}(\beta_{hs} I_h + \beta_{ha} A_h) - s\beta_{mf}\tfrac{I_{vm}S_{vf}}{N_{vm}} - \mu S_{vf} \\
\dot{E}_{vf} &= b\tfrac{S_{vf}}{N_h}(\beta_{hs} I_h + \beta_{ha} A_h) + s\beta_{mf}\tfrac{I_{vm}S_{vf}}{N_{vm}} - (\delta_v + \mu)E_{vf} \\
\dot{I}_{vf} &= \delta_v E_{vf} - \mu I_{vf} + \gamma_e\alpha I_e \\
\dot{I}_{vm} &= \gamma_e I_e(1-\alpha) - \mu I_{vm} \\
\dot{S}_e &= r(1-\tfrac{N_e}{K})(N_{vf} - qI_{vf}) - (\gamma_e + \mu_e)S_e \\
\dot{I}_e &= rq(1-\tfrac{N_e}{K})I_{vf} - (\gamma_e + \mu_e)I_e
\end{aligned}
\tag{2.1}
$$

2.3 Parameter Estimates

The parameter values used in this model were retrieved from previously published literary sources as shown in Table 2.2. However, due to the scarcity of available data on the transmission dynamics of ZIKV, some of the values, namely b, β_{vh}, β_{hs}, and β_{mf}, are based on DENV studies since DENV and ZIKV are of the same genus and are both spread by *Aedes aegypti* mosquitoes. Since no studies were found investigating sexual transmission of ZIKV in *Aedes aegypti* mosquitoes, the β_{mf} parameter was retrieved from a study on *Aedes albopictus* and is an average of the transmission probability of DENV in this species across various days after female mosquito blood meals [13]. Lastly, since clinical studies suggest that the viral load of asymptomatically infected ZIKV patients is approximately half of the viral load of symptomatic patients, we assume that the transmission probability of asymptomatic people is half of the transmission probability of symptomatic people [32, 33]. The initial suscepti-

ble human population (76, 182 people) in our work represents the calculated at-risk population for Zika in El Salvador that is presented in [24]. Assuming that at demographic equilibrium there are 6 adult female mosquitoes per person (a ratio within the range of values found in literature [34, 35, 36]), the carrying capacity, K, was derived through back calculation of the equilibrium value of adult female mosquitoes, $N_{vf}^{*} = K(\frac{\alpha\gamma_e}{\mu} - \frac{\mu_e+\gamma_e}{r})$.

2.4 Results

To understand the contribution of additional transmission pathways (1-3) on the spread of Zika, we compare the basic reproductive numbers and key epidemiological quantities of dynamical system (2.1) with those of a vector-only transmission model (2.2) which incorporates disease transmission in the human and vector populations solely through mosquito bites.

Symbol	Description (Units)	Value (Range)	Source
b	Mosquito biting rate (days^{-1})	0.50 $(0.33 - 1)$	[37]
ϕ	Proportion of symptomatic infections (Dimensionless)	0.20	[26]
a	Sexual contact rate between humans (days^{-1})	0.14 $(0.01 - 0.20)$	[17]
q	Vertical transmission probability in mosquitoes (Dimensionless)	0.01	[38]
β_{vh}	Transmission probability, mosquito to human (Dimensionless)	0.30 $(0.10 - 0.75)$	[37]
β_{hs}	Transmission probability symptomatic human to mosquito (Dimensionless)	0.30 $(0.10 - 0.75,$ baseline)	[37]
β_{ha}	Transmission probability asymptomatic human to mosquito (Dimensionless)	$\beta_{hs}/2$	Assumed
β_a	Transmission probability- asymptomatic humans to susceptible humans (Dimensionless)	$\beta_I/2$	Assumed
β_I	Transmission probability- symptomatic humans to susceptible humans (Dimensionless)	0.35 $(0 - 1)$	Assumed
δ	Incubation rate in humans (days^{-1})	0.2 $(0.14 - 0.50)$	[10]
γ	Recovery rate (days^{-1})	0.14 $(0.07 - 0.30)$	[24]
γ_e	Maturation rate- mosquitoes (days^{-1})	0.06 $(0.06 - 0.20)$	[39]
μ	Natural mortality rate of adult female mosquitoes (days^{-1})	0.07 $(0.03 - 0.09)$	[39]
μ_e	Natural mortality rate of juvenile mosquitoes (days^{-1})	0.07 $(0.03 - 0.47)$	[39]
δ_v	Incubation rate in mosquitoes (days^{-1})	0.10 $(0.06 - 0.22)$	[24]
α	Proportion of female juvenile mosquitoes (Dimensionless)	0.5	[40]
β_{mf}	Transmission probability-infected male vectors to susceptible female vectors (Dimensionless)	0.45 $(0.15 - 0.65)$	[13]
r	Egg hatching rate (days^{-1})	0.40 $(0.13 - 1)$	[41]
K	Carrying capacity (total number of juvenile mosquitoes)	$4,413,320$	Assumed
s	Mosquito sexual contact rate (days^{-1})	1	[40]
N_h	Total number of humans	$76,182$	[24]

Table 2.2: **Model Parameters and Values**

$$
\begin{aligned}
\dot{S}_h &= -b\beta_{vh}\tfrac{I_{vf}S_h}{N_h} \\
\dot{E}_h &= b\beta_{vh}\tfrac{I_{vf}S_h}{N_h} - \delta E_h \\
\dot{I}_h &= \phi\delta E_h - \gamma I_h \\
\dot{A}_h &= (1-\phi)\delta E_h - \gamma A_h \\
\dot{R}_h &= \gamma(I_h + A_h) \\
\dot{S}_{vf} &= \alpha\gamma_e S_e - b\tfrac{S_{vf}}{N_h}(\beta_{hs}I_h + \beta_{ha}A_h) - \mu S_{vf} \\
\dot{E}_{vf} &= b\tfrac{S_{vf}}{N_h}(\beta_{hs}I_h + \beta_{ha}A_h) - (\delta_v + \mu)E_{vf} \\
\dot{I}_{vf} &= \delta_v E_{vf} - \mu I_{vf} \\
\dot{S}_e &= r(1 - \tfrac{S_e}{K})N_{vf} - (\gamma_e + \mu_e)S_e
\end{aligned}
\tag{2.2}
$$

2.4.1 Disease-Free Equilibria

The disease-free equilibrium is the point where no disease is present within the population. For system (2.1), this occurs when $I_h = I_{vf} = I_e = 0$. Setting all of the differential equations in (2.1) equal to zero, we find an infinite line of non-isolated disease-free equilibria of the form $[S_h^*, 0, 0, 0, R_h^*, S_{vf}^*, 0, 0, 0, S_e^*, 0]$, where S_h^* and R_h^* are free variables such that $S_h^* + R_h^* = N_h$, $S_{vf}^* = \frac{\alpha\gamma_e S_e^*}{\mu}$, and $S_e^* = K(1 - \frac{\mu(\mu_e+\gamma_e)}{\alpha r\gamma_e})$. The value of S_e^* is only biologically feasible (i.e. greater than zero) when $r > \frac{\mu(\mu_e+\gamma_e)}{\alpha\gamma_e}$.

Similarly, we find non-isolated disease-free equilibria for system (2.2) of the form $[S_h^{**}, 0, 0, 0, R_h^{**}, S_{vf}^{**}, 0, 0, S_e^{**}]$, where S_h^{**} and R_h^{**} are free variables such that $S_h^{**} + R_h^{**} = N_h$, $S_{vf}^{**} = S_{vf}^*$, and $S_e^{**} = S_e^*$. The authors note that an endemic equilibrium exists for system (2.1) and involves the transmission of ZIKV solely within the mosquito population. Due to the focus of the current study on the contribution of Zika transmission pathways to the spread of the disease within the human population, we omit detailed computation of the endemic equilibrium.

2.4.2 Basic Reproductive Number

The next-generation operator method proposed by Diekmann and Heesterbeck [42] was used to derive the basic reproductive numbers of system (2.1) and (2.2), denoted R_{0f} and R_{0v} respectively. To obtain R_{0f}, we begin by separating the state variables into uninfected (X), noninfectious infected (Y), and infectious (Z) classes;

$$X = \begin{pmatrix} S_h \\ S_{vf} \\ S_e \\ R_h \end{pmatrix}, Y = \begin{pmatrix} E_h \\ E_{vf} \end{pmatrix}, Z = \begin{pmatrix} I_h \\ A_h \\ I_{vf} \\ I_{vm} \\ I_e. \end{pmatrix}$$

After substituting the equilibrium values of the Y classes into the differential equations for the Z classes, we generate the Jacobian matrix

$$A = (\frac{\partial}{\partial Z})(\frac{dZ}{dt}).$$

Evaluating A at the disease-free equilibrium for system (2.1), we obtain $A = M - D$, with

$$M = \begin{pmatrix} \frac{\phi a \beta_I S_h^*}{N_h} & \frac{\phi a \beta_a S_h^*}{N_h} & \frac{\phi b \beta_{vh} S_h^*}{N_h} & 0 & 0 \\ \frac{(1-\phi) a \beta_I S_h^*}{N_h} & \frac{(1-\phi) a \beta_a S_h^*}{N_h} & \frac{(1-\phi) b \beta_{vh} S_h^*}{N_h} & 0 & 0 \\ \frac{\delta_v b \beta_{hs} S_{vf}^*}{(\delta_v+\mu) N_h} & \frac{\delta_v b \beta_{ha} S_{vf}^*}{(\delta_v+\mu) N_h} & 0 & \frac{\delta_v s \beta_{mf} S_{vf}^*}{(\delta_v+\mu) N_{vm}^*} & \gamma_e \alpha \\ 0 & 0 & 0 & 0 & \gamma_e (1-\alpha) \\ 0 & 0 & qr(1 - \frac{N_e^*}{K}) & 0 & 0 \end{pmatrix}$$

and

$$D = \begin{pmatrix} \gamma & 0 & 0 & 0 & 0 \\ 0 & \gamma & 0 & 0 & 0 \\ 0 & 0 & \mu & 0 & 0 \\ 0 & 0 & 0 & \mu & 0 \\ 0 & 0 & 0 & 0 & \gamma_e + \mu_e \end{pmatrix},$$

where $N^*_{vm} = K(1-\alpha)(\frac{\gamma_e}{\mu} - \frac{\mu_e+\gamma_e}{\alpha r})$, and $N^*_e = K(1 - \frac{\mu(\mu_e+\gamma_e)}{\alpha r \gamma_e})$.

Since S^*_h can take on any value at the disease-free equilibrium, we take $S^*_h = N_h$ and calculate R_{0f}, which is the dominant eigenvalue of MD^{-1}. Due to the complexity of the analytic expression for R_{0f} we estimate it using parameter values in Table 2.2 and obtain $R_{0f} \approx 2.32$.

Similarly, R_{0v} is calculated as the dominant eigenvalue of the next generation matrix $M_v D_v^{-1}$, where

$$M_v = \begin{pmatrix} 0 & 0 & \frac{\phi b \beta_{vh} S^{**}_h}{N_h} \\ 0 & 0 & \frac{(1-\phi) b \beta_{vh} S^{**}_h}{N_h} \\ \frac{\delta_v b \beta_{hs} S^{**}_{vf}}{(\delta_v+\mu) N_h} & \frac{\delta_v b \beta_{ha} S^{**}_{vf}}{(\delta_v+\mu) N_h} & 0 \end{pmatrix}$$

and

$$D_v = \begin{pmatrix} \gamma & 0 & 0 \\ 0 & \gamma & 0 \\ 0 & 0 & \mu \end{pmatrix}.$$

Taking $S_h^{**} = N_h$, we have

$$M_v D_v^{-1} = \begin{pmatrix} 0 & 0 & e \\ 0 & 0 & f \\ c & d & 0 \end{pmatrix}$$

where $e = \frac{\phi b \beta_{vh}}{\mu}$, $f = \frac{(1-\phi) b \beta_{vh}}{\mu}$, $c = \frac{\delta_v b \beta_{hs} S_{vf}^{**}}{(\delta_v+\mu)\gamma N_h}$, and $d = \frac{\delta_v b \beta_{ha} S_{vf}^{**}}{(\delta_v+\mu)\gamma N_h}$. The simpler matrix structure in this scenario leads to the analytic expression $R_{0v} = \sqrt{ec + fd}$ where the first term under the radical contains parameters involved in disease transmission between symptomatic humans and mosquitos and the second term involves transmission between asymptomatic humans and mosquitos.

Using parameter values in Table 2.2, we obtain $R_{0v} \approx 2.21$. Hence, the secondary transmission pathways increase the basic reproductive number by an estimated 5%.

2.4.3 Visualizing ZIKV Dynamics

To visualize the difference between the dynamics of the vector-only model and full model, we generate numerical simulations in Mathematica using the baseline parameter values. Assuming that there are 6 adult female mosquitoes per person and about seven juvenile mosquitoes per adult female mosquito (values within previously reported ranges, [34, 35, 36]), we estimate the initial susceptible adult female and juvenile mosquito populations to be $457,092$ and $3,199,644$ respectively. The initial susceptible adult male mosquito population for system (2.1) is the same as the initial susceptible adult female mosquito population. Starting with only one infected individual (or mosquito) in each infected class, we observe through Figure 2.2 and Table 2.3 that the full model predicts an outbreak occurring (and ending) approximately

two weeks sooner than the vector-only model with more infections during the first half of the epidemic.

In order to track the effect of additional transmission pathways on the course of a Zika outbreak, we graph the ratio of infected humans in a set of models that each include one or more secondary transmission pathways (in addition to transmission via mosquito bites) to infected humans in the vector-only model. The set of models considered includes a human sexual transmission model, mosquito vertical transmission model, mosquito vertical and sexual transmission model, and full model. The human sexual transmission, mosquito vertical transmission, and mosquito vertical and sexual transmission models were derived by simply deleting terms or equations in the full model that did not correspond to the additional transmission route(s) under investigation.

As expected, the fastest growth in infected humans is seen with the full model, where about 2.5 times as many people are infected with ZIKV at the peak of the epidemic than in the vector-only model. At the point when the epidemic is growing fastest, the human sexual transmission model predicts almost 1.8 times as many Zika cases. Through Figure 2.3, we see that sexual transmission in the mosquito population greatly impacts the initial growth of an outbreak and results in up to 1.5 times as many Zika infections at the epidemic's peak than model (2.2). This is approximately 42% higher than the ratio of Zika cases observed at the peak of an epidemic when modeling only vertical transmission in the mosquito population.

2.4.4 Sensitivity Analysis

Since the additional transmission pathways of ZIKV resulted in an increase in the basic reproductive number and decrease in the peak time (the time of the maximum number of infected humans) of a Zika outbreak, we conduct a sensitivity

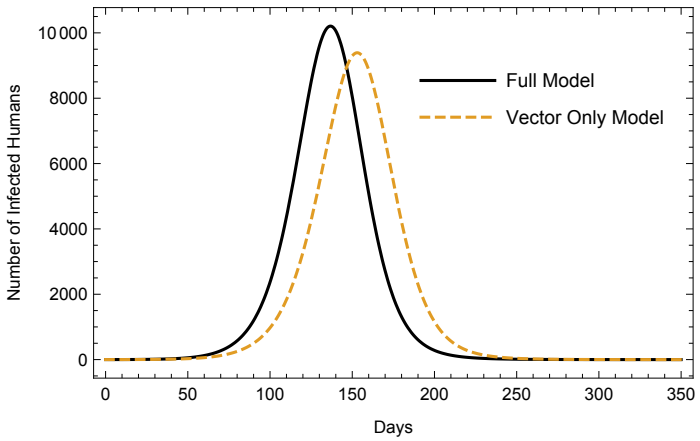

Figure 2.2: **ZIKV Dynamics: Full Model vs. Vector-Only Model**

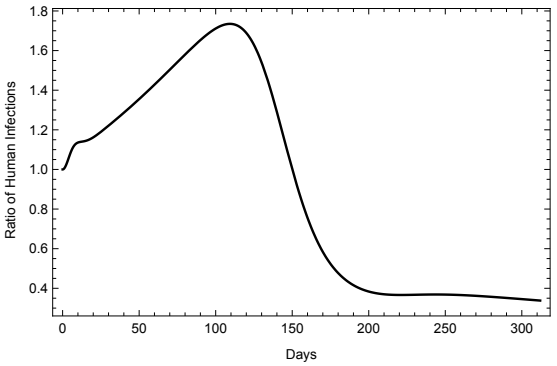

(a) Human Sexual Transmission

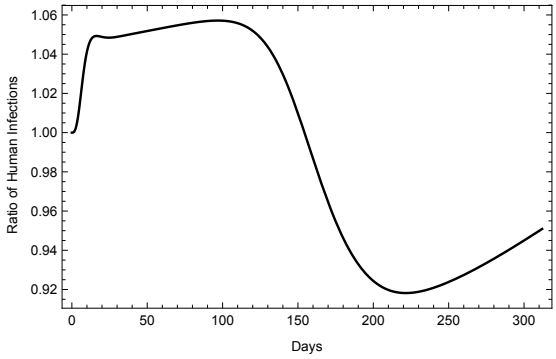

(b) Mosquito Vertical Transmission

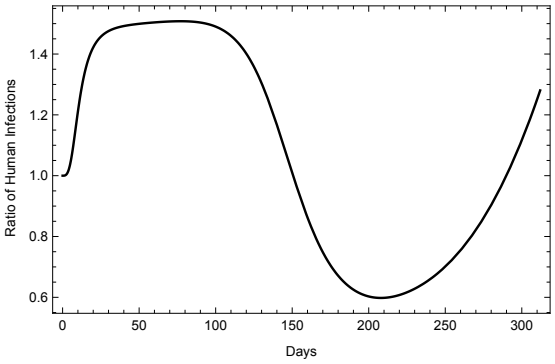

(c) Mosquito Vertical and Sexual

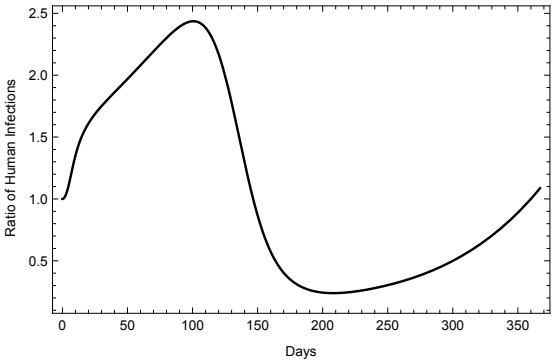

(d) Full Model

Figure 2.3: **The Ratio of Human Infections Over Time.** The figures show the ratio of Zika cases in models including secondary transmission pathways a, b, c, or d to Zika cases in the vector-only model over the time course of an outbreak.

	Vector-Only Model	Full Model
Duration	312 days	300 days
Final Size*	.99	.99
Peak Time	153 days	137 days
Peak Size*	.12	.13

Table 2.3: **Comparison of ZIKV Dynamics**, *-*Proportion of At-Risk Population Infected*

analysis to determine how variations in individual parameter values impact R_{0f} and the peak time. In particular, we increase each parameter by 0.1% (while keeping other parameters at the baseline values found in Table 2.2) and calculate the normalized sensitivity index. This index, as described in [43] is given by $\frac{\partial u}{\partial p}\frac{p}{u}$, where u represents the output variable and p represents the specific parameter under investigation. No simple analytic expression exists for either R_{0f} or the peak time (the expression for R_{0f} is complex and not easily manipulated), thus we compute the normalized sensitivity index numerically using $\frac{\Delta u}{\Delta p}\frac{p}{u}$. The results of the sensitivity analysis shown in Figures 2.4 and 2.5 reveal that R_{0f} is most sensitive to parameter values involved in the vector to human transmission of ZIKV such as the biting rate (b), transmission probabilities (β_{vh}, β_{hs}), and the mortality rate of adult female mosquitos (μ). The peak time is also greatly impacted by the mortality rate of adult female mosquitos (μ) and the biting rate (b), and is highly sensitive to parameters that impact juvenile mosquito stages such as the proportion of female juvenile mosquitoes (α) and maturation rate (γ_e). These results indicate that methods which decrease b, β_{vh}, and β_{hs}, and increase μ would be most beneficial at reducing R_{0f} while methods which decrease b, α, and γ_e, and increase μ may significantly delay the peak time of an outbreak. Although not shown here, a sensitivity analysis was also performed for the final epidemic size and yielded indices of magnitude less than 0.1 for all parameters except for μ which had a sensitivity index of -0.13.

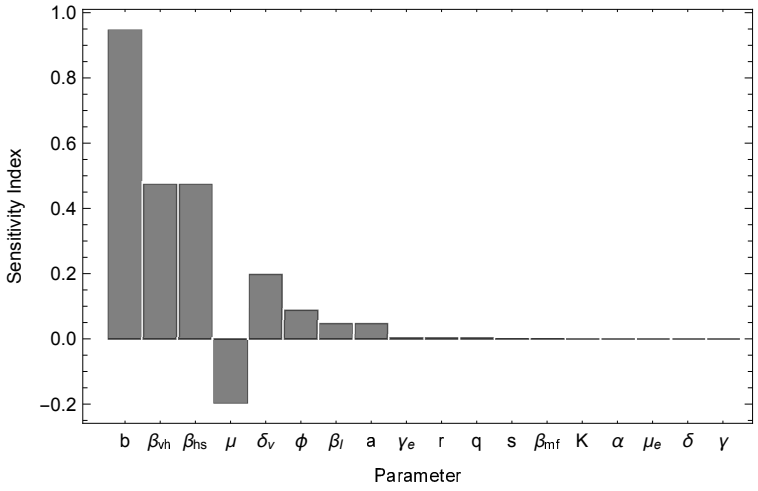

Figure 2.4: **Sensitivity Analysis for R_{0f}:** Sensitivity Indices are listed in order of decreasing magnitude.

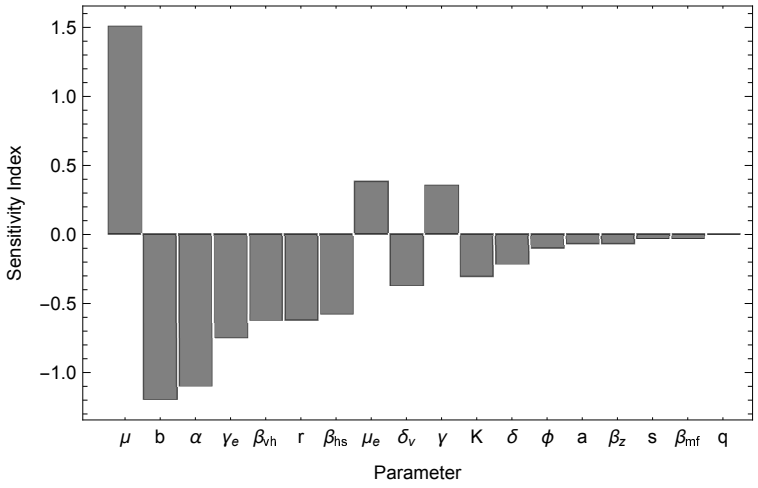

Figure 2.5: **Sensitivity Analysis for Peak Time:** Sensitivity Indices are listed in order of decreasing magnitude.

2.4.5 Consequences for Implementing Control Measures

Assuming that public health officials utilize predictive modeling tools to determine the timing and intensity of control strategies, the variation in the magnitude of infected individuals between the vector-only and full models (as seen in Figure 2.3) may impact the outcome of such strategies. Here, we examine how differences in the

type of model used to describe the spread of Zika impact the final size of an epidemic and estimates of the basic reproductive number of the virus.

As a result of the various aspects of vector-borne diseases (i.e. seasonality, type of vector, and location) there is no universal threshold that is used to determine when vector control methods should begin. Instead, public health officials must make decisions to implement control measures based on when they predict that the prevalence of a disease will be high enough to warrant them. In the case of Zika, their prediction will vary depending on whether the secondary transmission routes of the pathogen are taken into account.

To illustrate this, we assume that due to certain factors (i.e. limited resources), it would be more economical to implement Zika control measures when approximately 5% of the population is infected with the virus. In this scenario, we consider the possibility that public health workers rely on model predictions instead of case reports for the number of Zika infected individuals present over time. This is because reported cases may not be a good indicator of the actual number of Zika infections in a population due to low reporting rates, a large asymptomatic class associated with ZIKV, and misdiagnosis of Zika (since it is clinically similar to diseases like Chikungunya and Dengue).

If the secondary transmission pathways of ZIKV are neglected, the vector-only transmission model (2.2) predicts that the 5% threshold will be reached 123 days after the first ZIKV infection. However, if the additional transmission mechanisms of ZIKV (1-4) are considered, model (2.1) predicts that controls should begin 108 days after ZIKV introduction. Using model (2.1), which provides a more holistic view of Zika transmission than the vector-only model, we explore how this difference in the implementation of control measures may affect the final size of a ZIKV outbreak.

Since there are currently no vaccines for ZIKV, control methods focus on vector reduction through larvicides and adulticides and prevention of mosquito bites through the use of repellents. To stimulate the effect of applying each of the three control measures mentioned above, we vary the parameters μ_e, μ, and b. This is because the use of larvicides and adulticides will increase the juvenile and adult mosquito mortality rates, while using repellents will reduce mosquito biting rate. Presumably, an effective control measure will decrease the basic reproductive numbers, R_{0f} and R_{0v} below one. Observing the change in R_{0f} and R_{0v} as each of the control parameter values is varied, we find that larvicides and adulticides must reduce the average juvenile and adult mosquito lifetimes below 9 and 11 days respectively and that repellents must prevent a mosquito from biting for at least 5 days. With this, we choose our control parameters to be $\mu_{ec} = 0.107$ days^{-1}, $\mu_c = 0.089$ days^{-1}, and $b_c = 0.180$ days^{-1} and observe the effects of enacting each control individually and in combination. As adulticides are typically the last resort in integrated vector control strategies [44], the only double control scenario that we employ is the use of repellents and larvicides.

When we consider a continuous application of larvicides, adulticides, and repellents from the time that controls are initiated to the end of the epidemic, we find that a slight delay in the application of control measures (initiation at day 123 versus day 108) results in up to 28% more people infected with Zika in the full model (depending on the type of control that is used (Table 2.4)).

Since control measures are typically administered in discrete intervals rather than continuously over an entire outbreak period, we considered a separate scenario where larvicides and adulticides are applied at specific times, namely every two days for ten days and thereafter once a week as suggested by the World Health Organization in [44]. In this case, delayed application of control measures resulted in a similar

Initiation of Control Measures (days)	Control Type				
	L	A	R	L & R	L, A, & R
108	0.99	0.93	0.48	0.39	0.38
123	0.99	0.96	0.73	0.67	0.66

Table 2.4: **Proportion of At-Risk Population Infected with Continuous Application of Controls**, L-larvicide, A-adulticide, R-repellent

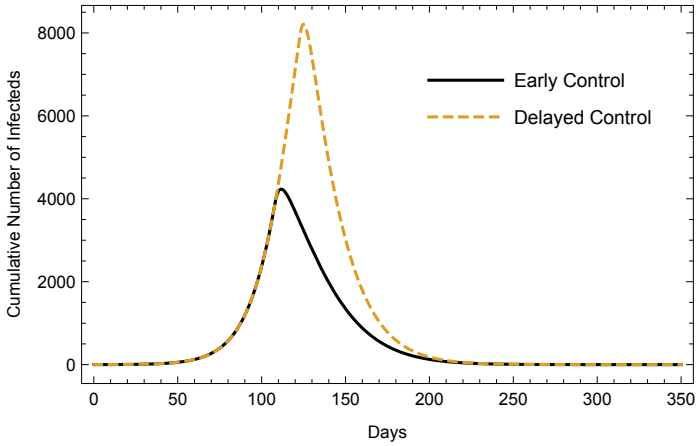

Figure 2.6: **Cumulative Infections Under Continuous Application of Larvicides, Adulticides, & Repellents.** Early control refers to initiation of the combined control measures at day 108 while delayed control refers to initiation at day 123

percent increase (25%, full results not shown) in the number of people infected with Zika in the full model.

Another way that public health officials may utilize mathematical models is to estimate the basic reproductive number of a disease through incidence data. These estimates play a crucial role in the formation of control strategies and may vary between different models, as described in [20, 21, 22, 23]. To examine how differences in model structure affect R_0 estimates, we fit initial Zika incidence data to models (2.1) and (2.2) separately, and in each case estimate transmission parameters. β_{vh}, β_{hs}, and β_{ha}. Using Mathematica's build-in function FindFit, with the other parameters fixed at baseline values, we fit the respective models to time-series data for the number of

ZIKV infected individuals (both symptomatic and asymptomatic) generated by the full model. We then use the best-fit transmission parameter values to estimate R_0. For illustrative purposes, we assume that public health officials fit the vector-only model to incidence data from the first 75 days of an outbreak. The results of the data fitting can be seen in Figure 2.7. Although the curve aligns quite well with the data points, we find that the fitted model estimates R_0 to be approximately 3 (with $\beta_{vh} \approx 0.35$, $\beta_{hs} \approx 0.48$, and $\beta_{ha} \approx 0.1$). This is 30% higher than that R_0 value obtained from the full model.

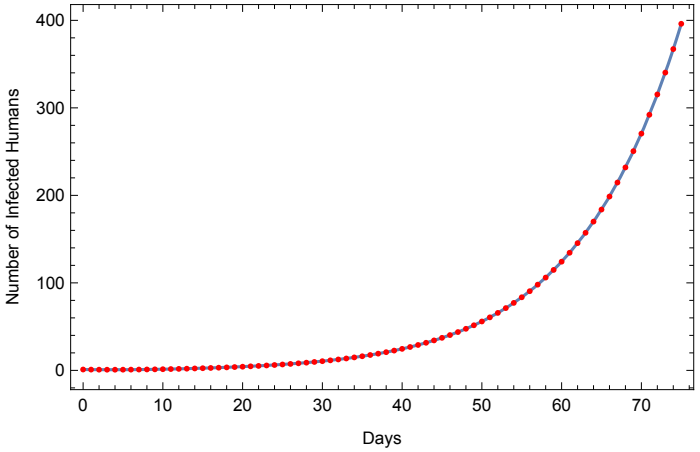

Figure 2.7: **Fitting Vector-Only Model to Zika Incidence Data.** Vector-only model is fit to ZIKV incidence data produced by full model (dots).

2.5 Discussion and Concluding Remarks

Mathematical models are useful in predicting disease dynamics and estimating key parameters that can be used to combat the spread of a disease. While it is common for researchers to simplify these models in order to better analyze them, the simplifications often overlook certain biological components of a disease which

may dramatically influence its spread. In this paper, we illustrate the impact of such simplifications in the context of Zika virus dynamics.

We examine a new mathematical model which incorporates multiple transmission avenues of the unique Zika arbovirus and compare it with a model that only incorporates the transmission of the virus through direct human and mosquito contacts. Since many researchers agree that the transmission of Zika through mosquito bites drives the spread of this disease [10, 16], it may be easy to overlook (or even dismiss) the secondary transmission routes. However, we have shown that these additional pathways not only increase the basic reproductive number of Zika and shift the outbreak to occur sooner than expected, but they also have important consequences for Zika control strategies.

When reflecting on the different ways that public health authorities may use Zika models to inform control efforts, our results show that if only the human-mosquito contacts are considered, authorities run the risk of enacting controls too late and overestimating the basic reproductive number. Delaying the implementation of control strategies based on using the vector-only model, inevitably results in more people infected at the end of an outbreak than if the full model were used. The overestimation of R_0 that is associated with fitting model (2.2) to initial Zika incidence data from the full model is reminiscent of the work in [20, 21, 22, 23] where differences in model assumptions (e.g. the inclusion of latent periods and distribution of latent and infectious periods) result in strikingly different estimates of R_0 obtained from the initial growth rate of a disease or pathogen. While use of simpler models in [20, 21, 22, 23] to estimate the basic reproductive number consistently resulted in underestimations, using our simplified vector-only model to estimate R_0 from initial growth results in an overestimate. This is because secondary transmission pathways increase the initial growth of an epidemic much more than they increase R_0. The

overestimation of R_0 may lead to aggressive control efforts, which although not be as detrimental to the overall health of the public as grossly underestimating this quantity, will result in wasted resources. Hence, we recommend that public health officials take into consideration the additional transmission pathways of Zika when enacting controls and estimating crucial disease parameters.

While the mathematical model considered in this study is unique in its combination of multiple ZIKV transmission pathways, some of its results resemble those of previous studies. For one, the numerical approximations of R_{0v} and R_{0f} in section 2.4.2 are comparable with other estimates of R_0 for Zika [10, 17]. In addition, since the basic reproductive number for Zika increased by only 5% between the vector-only and full models, our study supports the notion that vector transmission is primarily responsible for the spread of ZIKV as described in [10, 16, 17]. The percent increase in R_0 that is described in section 2.4.2 is comparable to the percent increase in R_0 for studies that consider only sexual transmission [10, 17]. Thus, our analysis suggests that ZIKV transmission within mosquito populations does not contribute substantially to the initial spread of the disease.

The few studies that describe sensitivity analysis as it pertains to Zika modeling have focused on the effects of parameter values on R_0 (e.g. [17, 19]), however the present study is distinct in that it also analyzes the sensitivity of other important epidemiological quantities such as the final size and peak time. Sensitivity analysis for these latter output variables has not been discussed elsewhere. Similar to [17, 19], our results show that Zika's basic reproductive number is most sensitive to the mosquito biting rate and transmission probability parameters (a fact which supports vector-to-human transmission as a driving force in the beginning of an outbreak). Therefore, in order to reduce the possibility of a ZIKV epidemic, public health campaigns should

emphasize measures which lower the biting rate and probability of transmission of the virus between humans and mosquitos.

Although we agree that R_0 is a vital epidemiological quantity, we note that this value describes the transmissibility of disease within a completely susceptible population and only tells whether or not a disease will spread. Given that a disease *will* spread, public health officials may look to other epidemiological quantities, such as the final epidemic size and peak time to determine the intensity of an outbreak and inform control strategies. Hence understanding how the final epidemic size and peak time are affected by parameter values would be of great interest. We find that of the three output variables (R_{0f}, final epidemic size, and peak time), the final epidemic size is least sensitive to changes in parameter values (all except one of the sensitivity indices < 0.1) and the peak time is most sensitive to variations in parameters (the magnitude of seven of its sensitivity indices were > 0.5 with two of the seven indices having magnitude > 1). In addition, the peak time is shown to be most sensitive to the death rate of adult female mosquitos, a parameter which plays a crucial role in accelerating the demographic renewal of mosquitoes and reducing the duration of infection within the vector population.

It is in the sensitivity analysis for the peak time that we see the importance of parameters such as α, γ_e, and r which affect the dynamics of the juvenile mosquito stages. With regards to the peak time, these parameters have sensitivity indices with magnitude > 0.6. This suggests that in order to delay the peak time of a foreboding ZIKV outbreak and potentially provide public health officials with more time to mobilize their resources and gather information on the nature of the outbreak, attention should be paid to the juvenile mosquito stages and if possible to developing methods that retard mosquito maturation.

When considering the effectiveness of ZIKV control measures, our study shows (as does [19]) that combined personal protection and mosquito reduction strategies are the most effective at limiting the transmission of ZIKV and that individually, personal protection is more effective than vector reduction. The effect of differential timing of control measures based on the additional transmission pathways of ZIKV is unique to this study. To our knowledge, no other studies address how the timing of control measures impact the outcome of ZIKV outbreaks. Our investigation of this effect shows that although the transmission routes result in a slight qualitative change in ZIKV dynamics, neglecting them when predicting the initiation of control measures may have a profound impact on final size of epidemics. This discovery deepens our understanding of the complex transmission routes of ZIKV and the consequences that they may hold for public health officials.

In the future, the initiation and duration of controls that were implemented in the current model can be adapted to vector control strategies of particular cities to predict how their strategies affect disease outcomes in the face of Zika's additional transmission pathways. Furthermore, we would like to fit the full model to actual Zika incidence data of a specific region to obtain better estimates of parameter values. Lastly, due to the discrete nature of epidemiological data, it may also be beneficial to formulate a discrete time model that incorporates the additional transmission pathways of Zika and compare its predicted disease dynamics and effects of control with the results found in this paper.

CHAPTER 3

Coinfection, Altered Vector Infectivity, and Antibody-dependent Enhancement: The Dengue-Zika Interplay

3.1 Introduction

With approximately 50-100 million cases annually, dengue is one of the most prevalent mosquito-borne diseases in the world [45]. Over 40% of the world's population live in areas with high risk of dengue transmission and over 100 countries are endemic for the disease [46]. Dengue is transmitted to humans mainly through the bite of infected female *Aedes aegypti* mosquitoes and is caused by one or more viral serotypes of the *Flaviviridae* family (DENV-1 through 5) [47]. Although this illness is typically self-limiting, with infection by one serotype resulting in life-long immunity to that specific serotype, severe forms of the disease can cause dengue hemorrhagic fever and dengue shock syndrome [46]. Currently, no treatment exists for dengue and only one controversial vaccine (Dengvaxia®) has been licenced. As a result, mosquito control strategies remain the primary method of preventing dengue transmission.

Closely related to dengue is Zika, another disease of international concern. Zika was first discovered in Uganda in 1947 and has since spread across the globe, with outbreaks in Yap Island (2007), French Polynesia (2013), and more recently the Americas (2015) [10]. The Zika virus (ZIKV) is of the same family as the dengue serotypes and is also transmitted to humans primarily by *Aedes aegypti* mosquitoes (although it can also be sexually and vertically transmitted within the human population). While some clinical symptoms of Zika, such as acute fever, nausea, rash, joint pain, and

myalgia, are similar to dengue, Zika is unique in that it can cause serious complications in the form of Guillain-Barré syndrome and congenital Zika syndrome [10].

Due to having a shared vector, cocirculation of dengue and Zika is common in many geographical regions and increases the likelihood of dengue-Zika coinfections within human and mosquito populations. To date, clinical studies have reported human coinfections in countries such as Colombia, New Caledonia, Nicaragua, and Haiti [48, 49, 50, 51]. However, because of the rapid introduction of Zika into countries that are endemic with dengue, similarities in symptoms between the two diseases, underreporting, and the lack of proper serotesting in developing countries, it is believed that the prevalence of coinfections is higher than currently perceived [52].

In *Aedes aegypti* mosquitoes, infection with multiple arboviruses has been shown to affect viral dissemination, transmission, and replication [52, 53, 54]. Researchers in [55] reveal that for dengue and Zika specifically, coinfection can impact mosquito infectivity. The results of [55] indicate that while the number of dengue virus cDNA copies in coinfected mosquitoes is higher than in monoinfected mosquitoes (up to 12 times higher), Zika cDNA copies are lower in coinfected mosquitoes than in their monoinfected counterparts (6-9 times lower). This suggests that coinfection may cause mosquitoes to be more likely to transmit dengue and less likely to transmit Zika.

Within humans, dengue and Zika can display complex viral interactions in the form of antibody-dependent enhancement (ADE). ADE occurs when antibodies from a previous infection bind to a pathogen in a subsequent infection and, instead of neutralizing the pathogen, increase viral uptake and replication [56]. Many in vitro studies (e.g. [57, 58, 59, 60]) have shown that dengue antibodies cross-react with the ZIKV, increasing Zika infection of cells and production of viral progeny by over 100-fold. Likewise [61, 62] report the reciprocal effect of ZIKV antibodies increasing

dengue virus titers. Thus, immunity to one of the two viruses can potentially enhance transmission of the other virus within the human population.

While many mathematical models have been developed to understand the dynamics of Zika and dengue individually (e.g. [63, 64, 65]), only two exist, to the best of our knowledge, that incorporate both viruses simultaneously [66, 67]. The first mathematical model to describe transmission of dengue and Zika [66] also includes chikungunya, an arbovirus transmitted by the infamous *Aedes aegypti*. In [66], two compartmental models are introduced. The first is a system of 17 ordinary differential equations which considers single transmission of the three viruses, and the second is a system of 30 differential equations that incorporates coinfections within the human population. It is important to note that the models in [66] exclude sexual transmission of Zika between humans, neglect the possibility of coinfection within the mosquito population, and do not consider altered infectivity of humans (due to possible ADE) or mosquitoes (due to coinfection). Furthermore, because of the complexity of the systems, an analytic expression for the basic reproductive number (i.e. the number of secondary infections that a single infected individual can make in a completely susceptible population) of each system was not obtained, and no meaningful epidemiological conclusions were made. Instead, analysis was limited to finding a nontrivial equilibrium for each system and obtaining a Jacobian matrix and stability conditions for the equilibrium of the first system.

A second mathematical model which incorporates Zika and dengue (in addition to chikungunya) is discussed in [67]. Instead of considering coinfections, the model in [67] investigates the impact of a dengue-chikungunya-Zika superinfection hierarchy within humans, where infection with dengue completely replaces infection with chikingunya or Zika, and infection with chikungunya replaces Zika. This hierarchy was based on epidemiological records that showed a greater number of dengue cases

than chikungunya or Zika, and a greater number of chikungunya cases than Zika. Although the effect of a dengue vaccine on Zika is unknown, Okuneye et al. [67] include dengue vaccination in their model and assume that vaccination can reduce Zika susceptibility. Furthermore, the authors include sexual transmission of Zika and consider the possibility of ADE of dengue over Zika (but not ADE of Zika over dengue) by letting $\Theta_z > 1$, where Θ_z is the modification parameter for the infectiousness of Zika in relation to dengue. The way that Θ_z is incorporated in [67] assumes that ADE alters the susceptibility of hosts and vectors to Zika, rather than altering Zika infectivity of these populations. Analysis of the model included finding the basic reproductive number and conducting stability analysis on the disease-free equilibrium. The model was fit to outbreak data in Mexico and extended to study the effect of seasonality, temperature, and rainfall on disease burden. In addition to finding temperature and rainfall ranges for maximum transmission of the diseases, the authors in [67] found that altering the infectiousness of Zika only mildly affects transmission of the disease and that under their assumptions, the use of a dengue vaccine minimally impacts Zika dynamics.

While it is important to grasp the epidemiological significance of the cocirculation of dengue and Zika, neither of the two studies described above simultaneously explores the three facets of what will henceforth be called the dengue-Zika interplay– coinfection of humans and vectors, altered vector infectivity, and ADE of dengue and Zika. In this article, we develop the first Zika and dengue model that includes coinfection (in humans and mosquitoes), altered vector infectivity, and ADE for both viruses (i.e. viral enhancement of Zika given dengue antibodies and enhancement of dengue given Zika antibodies). The goal of the present study is to better understand the epidemiological consequences of the dengue-Zika interplay. In particular, through

a deterministic mathematical model that utilizes a system of nonlinear ordinary differential equations, we seek to answer the following research questions:

1. How does the endemic presence of dengue affect Zika's ability to spread in a region?
2. How does invasion of Zika affect the endemic presence of dengue?

With Zika rapidly spreading across the globe to regions endemic with dengue, examining the complex interactions between the two pathogens is vital to clarifying the public health impact of the cocirculation of both diseases and potentially informing future vaccine development and control strategies.

3.2 Model Development

The current study is placed in the context of dengue and Zika cocirculation in El Salvador. The total human population (given in Table 3.2) represents the calculated at-risk population for Zika in El Salvador during the 2015/2016 outbreak, as described in [24]. Since Zika and dengue are spread by the same vector and are in similar geographic regions, we assume that this number also represents the population at risk for dengue during that time.

A visual representation of the deterministic dengue and Zika coinfection model that we consider is shown in Figure 3.1, with the state variables and parameters described in Tables 3.1 and 3.2 respectively. In this model, we make the following assumptions:

1. Human and mosquito populations remain constant.
2. Only one dengue serotype is cocirculating in the study region (an assumption also made in [66] and [67]).
3. There is no disease-induced death in the human population as the case-fatality rate for each disease is low [68, 69].

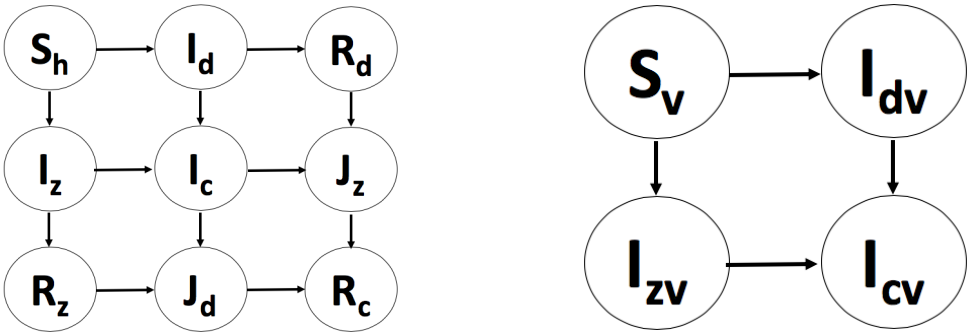

(a) Humans (b) Vectors

Figure 3.1: **Zika and Dengue Coinfection Model Schematic:** Arrows represent movement between different state variables within each population. Note that demographic renewal is not depicted in this diagram

4. ADE occurs after a person has recovered from a disease.
5. Humans and mosquitoes cannot simultaneously become coinfected with dengue and Zika (i.e. coinfection results only from sequential infection with each virus).
6. Coinfection alters the rate at which mosquitoes transmit dengue/Zika.

Humans are born fully susceptible to dengue and Zika at a rate of μN_h, where μ is the natural birth/death rate for humans and N_h is the total human population. Susceptible individuals can become infected with dengue from either a dengue-infected (I_{dv}) or coinfected female mosquito (I_{cv}). The mosquito-to-human dengue infection rate is given by β_{hd}. This rate is modified by a factor of ν_d to indicate the altered infectivity of coinfected mosquitoes. Once infected with dengue, humans can recover or become coinfected with Zika (by a Zika-infected (I_{zv}) or coinfected female mosquito (I_{cv})) and transition into the R_d or I_c class respectively. In a similar manner, fully susceptible humans become infected with Zika from a mosquito in the I_{zv} or I_{cv} compartment. The mosquito-to-human Zika infection rate is given by β_{hz} and is modified by a factor of ν_z for coinfected mosquitoes. Once infected with Zika, humans

State Variable	Description
S_h	Dengue & Zika-susceptible humans
I_d	Dengue-infected humans
I_z	Zika-infected humans
I_c	Dengue & Zika-coinfected humans
R_d	Dengue-recovered humans
R_z	Zika-recovered humans
J_d	Dengue-infected humans immune to Zika due to previous exposure
J_z	Zika-infected humans immune to Dengue due to previous exposure
R_c	Dengue & Zika-recovered humans due to previous exposure to both pathogens
S_v	Susceptible female Mosquitoes
I_{dv}	Dengue-infected female mosquitoes
I_{zv}	Zika-infected female mosquitoes
I_{cv}	Dengue & Zika-coinfected female mosquitoes

Table 3.1: **Epidemiological Classes**

either recover (with the Zika recovery rate given by γ_z) or become coinfected with dengue through a mosquito in I_{dv} or I_{cv}.

When a coinfected human recovers from dengue, he or she becomes dengue-immune and enters the J_z class. Meanwhile, singly infected humans who recover from dengue join the R_d compartment where they are susceptible to further infection with the ZIKV. For individuals in the J_z class, the rate of ZIKV infection is modified by a factor of k_z which represents the relative likelihood of Zika infection given the effect of ADE. Furthermore, coinfected humans who recover from Zika transition into the J_d class and are immune to ZIKV infection. Once in J_d, the rate of dengue infection is modified by a factor of k_d which signifies the relative likelihood of dengue infection given ADE. On the other hand, individuals who recover from a single infection with

Symbol	Description (Units)	Value	Reference
β_{hd}	Mosquito-to-human dengue infection rate (humans/(mosquito*day))	0.25	[64]
β_{hz}	Mosquito-to-human Zika infection rate (humans/(mosquito*day))	0.15	[37]
β_{vd}	Human-to-mosquito dengue infection rate (days^{-1})	0.25	[64]
β_{vz}	Human-to-mosquito Zika infection rate (days^{-1})	0.15	[37]
β_s	Zika human sexual transmission rate (days^{-1})	0.05	[70]
γ_d	dengue recovery rate (days^{-1})	0.14	[64]
γ_z	Zika recovery rate (days^{-1})	0.14	[24]
μ	Human birth/death rate (days^{-1})	4.47x10^{-5}	[64]
μ_v	Mosquito birth/death rate (days^{-1})	0.07	[39]
ν_d	Modification factor for dengue transmission by coinfected mosquitoes	12	[55]
k_d	Likelihood of dengue transmission given prior Zika infection	> 1	Assumed from [61, 62]
k_z	Likelihood of Zika transmission given prior dengue infection	> 1	Assumed from [57, 58, 59, 60]
ν_z	Modification factor for Zika transmission by coinfected mosquitoes	0.11	[55]
N_v	Total number of female mosquitoes	$457,092$	[70]
N_h	Total number of humans	$76,182$	[70]

Table 3.2: **Model Parameters**

Zika enter R_z and are susceptible to further infection with dengue. Lastly, individuals immune to dengue or Zika (i.e. those in J_d or J_z) that undergo subsequent infection with the secondary virus recover and become immune to both diseases (R_c).

In the vector population, mosquitoes are born into the susceptible class (S_v) at a rate of $\mu_v N_v$, where μ_v is the natural birth/death rate for mosquitoes and N_v is the total mosquito population. Susceptible mosquitoes are infected with dengue after feeding on a dengue-infected or coinfected human. In this case, the human-to-mosquito dengue infection rate is given by β_{vd}. Likewise, susceptible mosquitoes can become infected with Zika after feeding on a Zika-infected or coinfected human, with

a human-to-mosquito Zika infection rate of β_{vz}. These singly infected mosquitoes can be coinfected with both pathogens after feeding on a human infected with the second virus.

3.2.1 Model Equations

The system of nonlinear differential equations corresponding to the dengue and Zika coinfection model described above is given by (3.1).

$$\begin{aligned}
\dot{S}_h &= \mu N_h - \beta_{hd}\tfrac{S_h}{N_h}(I_{dv} + \nu_d I_{cv}) - \beta_{hz}\tfrac{S_h}{N_h}(I_{zv} + \nu_z I_{cv}) - \beta_s\tfrac{S_h}{N_h}(I_z + I_c + k_z J_z) - \mu S_h \\
\dot{I}_d &= \beta_{hd}\tfrac{S_h}{N_h}(I_{dv} + \nu_d I_{cv}) - \beta_{hz}\tfrac{I_d}{N_h}(I_{zv} + \nu_z I_{cv}) - \beta_s\tfrac{I_d}{N_h}(I_z + I_c + k_z J_z) - \gamma_d I_d - \mu I_d \\
\dot{I}_z &= \beta_{hz}\tfrac{S_h}{N_h}(I_{zv} + \nu_z I_{cv}) + \beta_s\tfrac{S_h}{N_h}(I_z + I_c + k_z J_z) - \beta_{hd}\tfrac{I_z}{N_h}(I_{dv} + \nu_d I_{cv}) - \gamma_z I_z - \mu I_z \\
\dot{I}_c &= \beta_{hz}\tfrac{I_d}{N_h}(I_{zv} + \nu_z I_{cv}) + \beta_s\tfrac{I_d}{N_h}(I_z + I_c + k_z J_z) + \beta_{hd}\tfrac{I_z}{N_h}(I_{dv} + \nu_d I_{cv}) - \gamma_d I_c - \gamma_z I_c - \mu I_c \\
\dot{R}_d &= \gamma_d I_d - \beta_{hz}\tfrac{R_d}{N_h}(I_{zv} + \nu_z I_{cv}) - \beta_s\tfrac{R_d}{N_h}(I_z + I_c + k_z J_z) - \mu R_d \\
\dot{R}_z &= \gamma_z I_z - \beta_{hd}\tfrac{R_z}{N_h}(I_{dv} + \nu_d I_{cv}) - \mu R_z \\
\dot{J}_d &= \beta_{hd}\tfrac{R_z}{N_h}(I_{dv} + \nu_d I_{cv}) + \gamma_z I_c - \gamma_d J_d - \mu J_d \\
\dot{J}_z &= \beta_{hz}\tfrac{R_d}{N_h}(I_{zv} + \nu_z I_{cv}) + \beta_s\tfrac{R_d}{N_h}(I_z + I_c + k_z J_z) + \gamma_d I_c - \gamma_z J_z - \mu J_z \\
\dot{R}_c &= \gamma_d J_d + \gamma_z J_z - \mu R_c \\
\dot{S}_v &= \mu_v N_v - \beta_{vd}\tfrac{S_v}{N_h}(I_d + I_c + k_d J_d) - \beta_{vz}\tfrac{S_v}{N_h}(I_z + I_c + k_z J_z) - \mu_v S_v \\
\dot{I}_{dv} &= \beta_{vd}\tfrac{S_v}{N_h}(I_d + I_c + k_d J_d) - \beta_{vz}\tfrac{I_{dv}}{N_h}(I_z + I_c + k_z J_z) - \mu_v I_{dv} \\
\dot{I}_{zv} &= \beta_{vz}\tfrac{S_v}{N_h}(I_z + I_c + k_z J_z) - \beta_{vd}\tfrac{I_{zv}}{N_h}(I_d + I_c + k_d J_d) - \mu_v I_{zv} \\
\dot{I}_{cv} &= \beta_{vz}\tfrac{I_{dv}}{N_h}(I_z + I_c + k_z J_z) + \beta_{vd}\tfrac{I_{zv}}{N_h}(I_d + I_c + k_d J_d) - \mu_v I_{cv}.
\end{aligned} \tag{3.1}$$

A majority of the baseline parameter values used for this model were obtained from previously published literary sources as indicated in Table 3.2. To obtain the Zika and dengue transmission modification factors, we observed the difference in viral cDNA copies between monoinfected and coinfected mosquitoes described in [55].

Based on this study, dengue virus cDNA copies in coinfected mosquitoes was 1.25-12 times higher than in monoinfected mosquitoes, while ZIKV cDNA copies were 6-9 times lower in coinfected mosquitoes than monoinfected mosquitoes. Assuming that these ranges correspond to the disease transmission capability of coinfected vectors, we use values within the ranges for ν_d and ν_z. Since the only studies on the effect of ADE on Zika and dengue have been conducted at the cellular level (i.e comparing viral titers and replication), the direct effect of ADE on dengue or Zika transmission is unknown. However, due to the large rise (up to two orders of magnitude) in viral load caused by ADE, we assume that ADE increases the likelihood of disease transmission and take k_d and k_z to be greater than one.

Under the assumption that human infection with the ZIKV is completely independent of DENV immunity (i.e. $k_z = 1$) *and* that the ability of vectors to transmit Zika is independent of their coinfection with dengue (i.e. $\nu_z = 1$), system (3.1) simplifies to

$$\begin{aligned}
\dot{\tilde{S}}_h &= \mu N_h - \beta_{hz}\tfrac{\tilde{S}_h}{N_h}\tilde{I}_{zv} - \beta_s\tfrac{\tilde{S}_h}{N_h}\tilde{I}_z - \mu\tilde{S}_h \\
\dot{\tilde{I}}_z &= \beta_{hz}\tfrac{\tilde{S}_h}{N_h}\tilde{I}_{zv} + \beta_s\tfrac{\tilde{S}_h}{N_h}\tilde{I}_z - \gamma_z\tilde{I}_z - \mu\tilde{I}_z \\
\dot{\tilde{R}}_z &= \gamma_z\tilde{I}_z - \mu\tilde{R}_z \\
\dot{\tilde{S}}_{dv} &= \mu_v N_v - \beta_{vz}\tfrac{\tilde{S}_{dv}}{N_h}\tilde{I}_z - \mu_v\tilde{S}_{dv} \\
\dot{\tilde{I}}_{zv} &= \beta_{vz}\tfrac{\tilde{S}_{dv}}{N_h}\tilde{I}_z - \mu_v\tilde{I}_{zv},
\end{aligned} \tag{3.2}$$

where $\tilde{S}_h = S_h + R_d + I_d$, $\tilde{I}_z = I_z + I_c + J_z$, $\tilde{R}_z = R_z + J_d + R_c$, $\tilde{S}_{dv} = S_v + I_{dv}$, and $\tilde{I}_{zv} = I_{zv} + I_{cv}$. Since the total human and vector populations, N_h and N_v respectively, are constant, (3.2) can be rewritten as

$$\begin{aligned}
\dot{\tilde{S}}_h &= \mu N_h - \beta_{hz}\tfrac{\tilde{S}_h}{N_h}(N_v - \tilde{S}_{dv}) - \beta_s\tfrac{\tilde{S}_h}{N_h}\tilde{I}_z - \mu\tilde{S}_h \\
\dot{\tilde{I}}_z &= \beta_{hz}\tfrac{\tilde{S}_h}{N_h}(N_v - \tilde{S}_{dv}) + \beta_s\tfrac{\tilde{S}_h}{N_h}\tilde{I}_z - \gamma_z\tilde{I}_z - \mu\tilde{I}_z \qquad (3.3) \\
\dot{\tilde{S}}_{dv} &= \mu_v N_v - \beta_{vz}\tfrac{\tilde{S}_v}{N_h}\tilde{I}_z - \mu_v\tilde{S}_v
\end{aligned}$$

A similar reduction of (3.1) can be obtained when $k_d = 1$ *and* $\nu_d = 1$. In this case, the model simplifies to system (3.3), with the exception that there is no sexual transmission term, and the z's in the subscripts of (3.3) are replaced with d's.

3.3 Equilibrium Points

To find equilibrium values of system (3.1), we set all of the differential equations to zero. Some of the equilibria are detailed in Table 3.3 and describe scenarios when no disease is present within the population (disease-free equilibrium), or when only one disease is present (dengue-only or Zika-only equilibrium). Although we were unable to find an analytic expression for a copersistence equilibrium, numerical explorations suggest the existence of a stable copersistence equilibrium when both the dengue and Zika IRNs (detailed in section 3.5) exceed 1. Existence criteria for the unique single pathogen equilibria are described in Lemma 3.3.1 and Theorem 3.3.2.

Lemma 3.3.1. *For* (3.1)*, a unique dengue-only equilibrium exists iff* $R_d = \sqrt{\frac{N_v}{N_h}\frac{\beta_{vd}}{\mu_v}\frac{\beta_{hd}}{\mu+\gamma_d}} > 1$.

The proof of Lemma 3.3.1 is in Appendix A.1.

Theorem 3.3.2. *For* (3.1)*, a unique Zika-only equilibrium exists iff* $R_z = \frac{1}{2}\left[\frac{\beta_s}{\gamma_z+\mu} + \sqrt{(\frac{\beta_s}{\gamma_z+\mu})^2 + 4\frac{\beta_{vz}\beta_{hz}N_v}{(\gamma_z+\mu)\mu_v N_h})}\right] > 1$.

Proof. As seen in Table 3.3, all of the nonzero points of the Zika-only equilibrium are expressed in terms of I_z^*, where I_z^* is the solution to the quadratic equation $aI_z^{*2} + bI_z^* + c = 0$. In this equation,

$$\begin{aligned} a &= \beta_s\beta_{vz}(\gamma_z + \mu)N_h, \\ b &= N_h[(\gamma_z + \mu)(\beta_{vz}\beta_{hz}N_v + N_h\beta_s\mu_v + \beta_{vz}\mu) - \beta_s\beta_{vz}\mu N_h], \text{and} \\ c &= N_h^2[\mu\mu_v(\gamma_z + \mu)N_h - \beta_s\mu\mu_v N_h - \beta_{hz}\beta_{vz}\mu N_v]. \end{aligned}$$

Using the quadratic formula, we have $I_z^* = \frac{-b\pm\sqrt{b^2-4ac}}{2a}$. Since $a > 0$, when $c > 0$, I_z^* takes the sign of $-b$. When $c < 0$, one positive ($\frac{-b+\sqrt{b^2-4ac}}{2a}$) and one negative ($\frac{-b-\sqrt{b^2-4ac}}{2a}$) solution are obtained.

Notice that

$$\begin{aligned} c &> 0 \iff \\ \mu\mu_v(\gamma_z + \mu)N_h - \beta_s\mu\mu_v N_h - \beta_{hz}\beta_{vz}\mu N_v &> 0 \iff \\ (\gamma_z + \mu) &> \tfrac{\beta_s\mu_v N_h + \beta_{vz}\beta_{hz}N_v}{\mu_v N_h} \iff \\ (\gamma_z + \mu)(\beta_{vz}\beta_{hz}N_v + (\beta_s\mu_v + \beta_{vz}\mu)N_h) &> (\tfrac{\beta_s\mu_v N_h + \beta_{vz}\beta_{hz}N_v}{\mu_v N_h})(\beta_{vz}\beta_{hz}N_v + (\beta_s\mu_v + \beta_{vz}\mu)N_h) \\ &> \beta_s\beta_{vz}\mu N_h. \end{aligned}$$

By this last inequality, have $(\gamma_z + \mu)(\beta_{vz}\beta_{hz}N_v + (\beta_s\mu_v + \beta_{vz}\mu)N_h) > \beta_s\beta_{vz}\mu N_h$. Finally, multiplying by N_h and subtracting $\beta_s\beta_{vz}\mu N_h$ on both sides of the inequality, we obtain $b > 0$. This implies that for $c > 0$, $I_z^* < 0$. Thus, the only biologically feasible solution for I_z^* occurs iff $c < 0$ and is given by $I_z^* = \frac{-b+\sqrt{b^2-4ac}}{2a}$.

Since

$$\begin{aligned}
c &< 0 \iff \\
\mu\mu_v(\gamma_z+\mu)N_h - \beta_s\mu\mu_v N_h - \beta_{hz}\beta_{vz}\mu N_v &< 0 \iff \\
1 - \tfrac{\beta_s}{\gamma_z+\mu} - \tfrac{\beta_{vz}\beta_{hz}N_v}{(\gamma_z+\mu)\mu_v N_h} &< 0 \iff \\
4(1 - \tfrac{\beta_s}{\gamma_z+\mu} - \tfrac{\beta_{vz}\beta_{hz}N_v}{(\gamma_z+\mu)\mu_v N_h}) &< 0 \iff \\
4 - 4\tfrac{\beta_s}{\gamma_z+\mu} + (\tfrac{\beta_s}{\gamma_z+\mu})^2 &< 4\tfrac{\beta_{vz}\beta_{hz}N_v}{(\gamma_z+\mu)\mu_v N_h}) + (\tfrac{\beta_s}{\gamma_z+\mu})^2 \iff \\
(2 - \tfrac{\beta_s}{\gamma_z+\mu})^2 &< 4\tfrac{\beta_{vz}\beta_{hz}N_v}{(\gamma_z+\mu)\mu_v N_h}) + (\tfrac{\beta_s}{\gamma_z+\mu})^2 \iff \\
1 &< \tfrac{1}{2}\left[\tfrac{\beta_s}{\gamma_z+\mu} + \sqrt{(\tfrac{\beta_s}{\gamma_z+\mu})^2 + 4\tfrac{\beta_{vz}\beta_{hz}N_v}{(\gamma_z+\mu)\mu_v N_h}) + (\tfrac{\beta_s}{\gamma_z+\mu})^2}\right],
\end{aligned}$$

this unique Zika-only equilibrium exists iff $R_z > 1$.

□

3.4 Basic Reproductive Number

To derive the basic reproductive number (BRN) of the ZIKV and DENV coinfection model we use the next-generation operator method proposed by van den Driessche and Watmough [71]. Evaluating the F and V matrices obtained from this method at the disease-free equilibrium, we have

$$F = \begin{pmatrix}
0 & 0 & 0 & 0 & 0 & \beta_{hd} & 0 & \beta_{hd}\nu_d \\
0 & \beta_s & \beta_s & 0 & \beta_s & 0 & \beta_{hz} & \beta_{hz}\nu_z \\
0 & 0 & 0 & 0 & 0 & 0 & 0 & 0 \\
0 & 0 & 0 & 0 & 0 & 0 & 0 & 0 \\
0 & 0 & 0 & 0 & 0 & 0 & 0 & 0 \\
\frac{\beta_{vd}N_v}{N_h} & 0 & \frac{\beta_{vd}N_v}{N_h} & \frac{\beta_{vd}N_v}{N_h} & 0 & 0 & 0 & 0 \\
0 & \frac{\beta_{vz}N_v}{N_h} & \frac{\beta_{vz}N_v}{N_h} & 0 & \frac{\beta_{vz}N_v}{N_h} & 0 & 0 & 0 \\
0 & 0 & 0 & 0 & 0 & 0 & 0 & 0
\end{pmatrix}$$

Equilibrium Type	S_h^*	I_d^*	I_z^*	I_c^*	R_d^*	R_z^*	J_d^*	J_z^*	R_c^*	S_v^*	I_{dv}^*	I_{zv}^*	I_{cv}^*
Disease-Free	N_h	0	0	0	0	0	0	0	0	N_v	0	0	0
Dengue-Only	$\frac{\mu N_h^2}{\beta_{hd} I_{dv}^* + \mu N_h}$	I_d^*	0	0	$\frac{\gamma_d}{\mu} I_d^*$	0	0	0	0	$\frac{\mu_v N_v N_h}{\beta_{vd} I_d^* + \mu_v N_h}$	$\frac{\beta_{vd} I_d^* N_v}{\beta_{vd} I_d^* + \mu_v N_h}$	0	0
Zika-Only	$\frac{\mu N_h^2}{\beta_{hz} I_{zv}^* + \beta_s I_z^* + \mu N_h}$	0	I_z^*	0	0	$\frac{\gamma_z}{\mu} I_z^*$	0	0	0	$\frac{\mu_v N_v N_h}{\beta_{vz} I_z^* + \mu_v N_h}$	0	$\frac{\beta_{vz} I_z^* N_v}{\beta_{vz} I_z^* + \mu_v N_h}$	0

Table 3.3: **Equilibrium Points.** In this table, $I_d^* = \frac{\mu N_h (\beta_{hd} \beta_{vd} N_v - \mu_v N_h (\gamma_d + \mu))}{\beta_{vd} (\gamma_d + \mu)(\mu N_h + \beta_{hd} N_v)}$ and $I_z^* = \frac{-b + \sqrt{b^2 - 4ac}}{2a}$, where a, b, and c are as described in Section 2

and

$$V = \begin{pmatrix} \gamma_d + \mu & 0 & 0 & 0 & 0 & 0 & 0 & 0 \\ 0 & \gamma_z + \mu & 0 & 0 & 0 & 0 & 0 & 0 \\ 0 & 0 & \gamma_d + \gamma_z + \mu & 0 & 0 & 0 & 0 & 0 \\ 0 & 0 & -\gamma_z & \gamma_d + \mu & 0 & 0 & 0 & 0 \\ 0 & 0 & -\gamma_d & 0 & \gamma_z + \mu & 0 & 0 & 0 \\ 0 & 0 & 0 & 0 & 0 & \mu_v & 0 & 0 \\ 0 & 0 & 0 & 0 & 0 & 0 & \mu_v & 0 \\ 0 & 0 & 0 & 0 & 0 & 0 & 0 & \mu_v \end{pmatrix}.$$

The BRN is the spectral radius of FV^{-1}, and is given by
$\max\{\sqrt{\frac{N_v}{N_h}\frac{\beta_{vd}}{\mu_v}\frac{\beta_{hd}}{\mu+\gamma_d}}, \frac{1}{2}\left[\frac{\beta_s}{\mu+\gamma_z} + \sqrt{(\frac{\beta_s}{\mu+\gamma_z})^2 + 4\frac{N_v}{N_h}\frac{\beta_{vz}}{\mu_v}\frac{\beta_{hz}}{\mu+\gamma_z}}\right]\} = \max\{R_d, R_z\}$.

The fractions $\frac{\beta_{vd}}{\mu_v}$ and $\frac{\beta_{hd}}{\mu+\gamma_d}$ in R_d are the product of the DENV infection rates and the average time a human or vector remains infected with dengue ($\frac{1}{\mu_v}$ days for vectors and $\frac{1}{\mu+\gamma_d}$ days for humans). The second term under the radical in R_z is similar to R_d and represents vector transmission of Zika. However, R_z also includes sexual transmission of Zika within the human population in the form $\frac{\beta_s}{\mu+\gamma_z}$, where β_s is the sexual transmission rate and $\frac{1}{\mu+\gamma_z}$ is the average duration of infection in humans.

3.5 IRNs

3.5.1 Dengue IRN

The dengue IRN, which describes the ability of dengue to spread in a population endemic with Zika, is also calculated using the next generation matrix method described by van den Driessche and Watmough (see [6, 7]), but with I_d, I_c, J_d, I_{dv},

and I_{cv} categorized as the infectious classes. Evaluating the F and V matrices at the Zika-only endemic equilibrium, we obtain

$$F = \begin{pmatrix} 0 & 0 & 0 & \beta_{hd}\frac{S_h^*}{Nh} & \nu_d\beta_{hd}\frac{S_h^*}{Nh} \\ 0 & 0 & 0 & \beta_{hd}\frac{I_z^*}{Nh} & \nu_d\beta_{hd}\frac{I_z^*}{Nh} \\ 0 & 0 & 0 & k_d\beta_{hd}\frac{R_z^*}{Nh} & k_d\nu_d\beta_{hd}\frac{R_z^*}{Nh} \\ \beta_{vd}\frac{S_v^*}{Nh} & \beta_{vd}\frac{S_v^*}{Nh} & \beta_{vd}\frac{S_v^*}{Nh} & 0 & 0 \\ \beta_{vd}\frac{I_{zv}^*}{Nh} & \beta_{vd}\frac{I_{zv}^*}{Nh} & \beta_{vd}\frac{I_{zv}^*}{Nh} & 0 & 0 \end{pmatrix}$$

and

$$V = \begin{pmatrix} \beta_{hz}\frac{I_{zv}^*}{N_h} + \beta_s\frac{I_z^*}{N_h} + \gamma_d + \mu & 0 & 0 & 0 & 0 \\ -\beta_{hz}\frac{I_{zv}^*}{N_h} - \beta_s\frac{I_z^*}{N_h} & \gamma_d + \gamma_z + \mu & 0 & 0 & 0 \\ 0 & -\gamma_z & \gamma_d + \mu & 0 & 0 \\ 0 & 0 & 0 & \beta_{vz}\frac{I_z^*}{N_h} + \mu_v & 0 \\ 0 & 0 & 0 & -\beta_{vz}\frac{I_z^*}{N_h} & \mu_v \end{pmatrix}.$$

Dengue's IRN is the spectral radius of FV^{-1} and is given by $\tilde{R}_d = R_d\sqrt{K_{vd}K_{hd}}$, where

$$K_{vd} = \frac{S_v^*}{N_v}[\frac{\beta_{vz}I_z^*}{\beta_{vz}I_z^* + \mu_v N_h}\nu_d + \frac{\mu_v N_h}{\beta_{vz}I_z^* + \mu_v N_h}] + \frac{I_{zv}^*}{N_v}\nu_d$$

and

$$K_{hd} = \frac{S_h^*}{N_h}\left(\frac{\beta_{hz}I_{zv}^* + \beta_s I_z^*}{(\beta_{hz}I_{zv}^* + \beta_s I_z^*) + (\mu+\gamma_d)N_h}[\frac{\mu+\gamma_d+k_d\gamma_z}{\mu+\gamma_d+\gamma_z}] + \frac{(\mu+\gamma_d)N_h}{(\beta_{hz}I_{zv}^* + \beta_s I_z^*) + (\mu+\gamma_d)N_h}\right) + \frac{I_z^*}{N_h}\frac{\mu+\gamma_d+k_d\gamma_z}{\mu+\gamma_d+\gamma_z} + \frac{R_z^*}{N_h}k_d.$$

It is important to note that when $k_d = v_d = 1$, $\tilde{R}_d = R_d$.

Epidemiologically, K_{vd} is the average relative dengue infectivity of mosquitoes in a setting where Zika is resident and K_{hd} is the average relative dengue infectivity of humans within that setting. While the proportion of susceptible mosquitoes that get Zika before dying ($\frac{S_v^*}{N_v}[\frac{\beta_{vz}I_z^*}{\beta_{vz}I_z^*+\mu_v N_h}]$) and the proportion of Zika infectious mosquitoes ($\frac{I_{zv}^*}{N_v}$) at the time that dengue arrives have relative dengue infectivity of ν_d, the relative dengue infectivity of the proportion of susceptible mosquitoes that die before contracting Zika ($\frac{S_v^*}{N_v}[\frac{\mu_v N_h}{\beta_{vz}I_z^*+\mu_v N_h}]$) is 1.

In the K_{hd} expression, the proportion of susceptible humans who get Zika before dying but recover from Zika prior to getting dengue ($\frac{S_h^*}{N_h}\frac{\beta_{hz}I_{zv}^*+\beta_s I_z^*}{(\beta_{hz}I_{zv}^*+\beta_s I_z^*)+(\mu+\gamma_d)N_h}\frac{\gamma_z}{\mu+\gamma_d+\gamma_z}$), the proportion of humans infected with Zika when dengue arrives who recover before getting dengue ($\frac{I_z^*}{N_h}\frac{\gamma_z}{\mu+\gamma_d+\gamma_z}$), and the proportion of humans already recovered from Zika when dengue is introduced ($\frac{R_z^*}{N_h}$) have a relative dengue infectivity of k_d. On the other hand, susceptibles who get Zika but die or get dengue before recovering from Zika ($\frac{S_h^*}{N_h}\frac{\beta_{hz}I_{zv}^*+\beta_s I_z^*}{(\beta_{hz}I_{zv}^*+\beta_s I_z^*)+(\mu+\gamma_d)N_h}\frac{\mu+\gamma_d}{\mu+\gamma_d+\gamma_z}$), susceptibles who die or get infected with dengue prior to getting Zika ($\frac{S_h^*}{N_h}\frac{(\mu+\gamma_d)N_h}{(\beta_{hz}I_{zv}^*+\beta_s I_z^*)+(\mu+\gamma_d)N_h}$), and those currently infected with Zika who die or get dengue before recovering from Zika ($\frac{I_z^*}{N_h}\frac{\mu+\gamma_d}{\mu+\gamma_d+\gamma_z}$) all have a relative dengue infectivity of 1.

3.5.2 Zika IRN

The Zika IRN describes the ability of Zika to spread in a population endemic with dengue and is computed in a similar manner as the dengue IRN. However, in

this case I_z, I_c, J_z, I_{zv}, and I_{cv} are categorized as the infectious classes. Evaluating F and V at the dengue-only endemic equilibrium, we obtain

$$F = \begin{pmatrix} \beta_s \frac{S_h^*}{N_h} & \beta_s \frac{S_h^*}{N_h} & \beta_s \frac{S_h^*}{N_h} & \beta_{hz} \frac{S_h^*}{Nh} & \nu_d \beta_{hz} \frac{S_h^*}{Nh} \\ \beta_s \frac{I_d^*}{N_h} & \beta_s \frac{I_d^*}{N_h} & \beta_s \frac{I_d^*}{N_h} & \beta_{hz} \frac{I_d^*}{Nh} & \nu_z \beta_{hz} \frac{I_d^*}{Nh} \\ k_z \beta_s \frac{R_d^*}{N_h} & k_z \beta_s \frac{R_d^*}{N_h} & k_z \beta_s \frac{R_d^*}{N_h} & k_z \beta_{hz} \frac{R_d^*}{Nh} & k_z \nu_z \beta_{hz} \frac{R_d^*}{Nh} \\ \beta_{vz} \frac{S_v^*}{N_h} & \beta_{vz} \frac{S_v^*}{N_h} & \beta_{vz} \frac{S_v^*}{N_h} & 0 & 0 \\ \beta_{vz} \frac{I_{dv}^*}{N_h} & \beta_{vz} \frac{I_{dv}^*}{N_h} & \beta_{vz} \frac{I_{dv}^*}{N_h} & 0 & 0 \end{pmatrix}$$

and

$$V = \begin{pmatrix} \beta_{hd} \frac{I_{dv}^*}{N_h} + \gamma_z + \mu & 0 & 0 & 0 & 0 \\ -\beta_{hd} \frac{I_{dv}^*}{N_h} & \gamma_d + \gamma_z + \mu & 0 & 0 & 0 \\ 0 & -\gamma_d & \gamma_z + \mu & 0 & 0 \\ 0 & 0 & 0 & \beta_{vd} \frac{I_d^*}{N_h} + \mu_v & 0 \\ 0 & 0 & 0 & -\beta_{vd} \frac{I_d^*}{N_h} & \mu_v \end{pmatrix}.$$

Zika's IRN is the spectral radius of FV^{-1} and is given by

$$\tilde{R}_z = \frac{1}{2} \left(\frac{\beta_s}{\mu + \gamma_z} K_{hz} + \sqrt{(\frac{\beta_s}{\mu + \gamma_z} K_{hz})^2 + 4 K_{hz} K_{vz} \frac{N_v}{N_h} \frac{\beta_{hz}}{\mu + \gamma_z} \frac{\beta_{vz}}{\mu_v}} \right),$$

where

$$K_{vz} = \frac{S_v^*}{N_v} [\frac{\beta_{vd} I_d^*}{\beta_{vd} I_d^* + \mu_v N_h} \nu_z + \frac{\mu_v N_h}{\beta_{vd} I_z^* + \mu_v N_h}] + \frac{I_{dv}^*}{N_v} \nu_z$$

and

$$K_{hz} = \frac{S_h^*}{N_h}\left(\frac{\beta_{hd}I_{dv}^*}{(\beta_{hd}I_{dv}^* + (\mu+\gamma_z)N_h}[\frac{\mu + k_z\gamma_d + \gamma_z}{\mu+\gamma_d+\gamma_z}] + \frac{(\mu+\gamma_z)N_h}{(\beta_{hd}I_{dv}^* + (\mu+\gamma_z)N_h}\right) + \frac{I_d^*}{N_h}\frac{\mu + k_z\gamma_d + \gamma_z}{\mu+\gamma_d+\gamma_z} + \frac{R_d^*}{N_h}k_z.$$

Notice that when $k_z = v_z = 1$, $\tilde{R}_z = R_z$. Furthermore, in a similar manner as K_{vd} and K_{hd}, the K_{vz} and K_{hz} expressions describe the relative Zika infectivity of vectors and humans respectively.

3.6 BRN/IRN Threshold Curves

In order to visualize how various aspects of the dengue-Zika interplay impact the persistence of each disease, we plot IRN threshold curves for $\tilde{R}_d = \tilde{R}_z = 1$ on the R_d vs. R_z axis. As seen in Figures 3.2 and 3.3, this results in four distinct regions of possible model outcomes (extinction of both diseases, E_0, persistence of only dengue, E_d, persistence of only Zika, E_z, and copersistence of both pathogens, E_{dz}). In these figures, the curve above the $R_z = 1$ line is $\tilde{R}_d = 1$ and the curve to the right of the $R_d = 1$ line is $\tilde{R}_z = 1$.

Figure 3.2 illustrates that ADE (i.e. $k_d, k_z > 1$) causes Zika and dengue to benefit from the presence of each other. In particular, due to ADE, the presence of dengue makes it possible for Zika to persist in regions where it would not have been able to persist on its own (i.e. in regions where $R_z < 1$). Similarly, this figure shows that the reciprocal effect of Zika presence on dengue is also true with ADE. In fact, as the likelihood of disease transmission by recovered individuals increases across various orders of magnitude, the E_{dz} region widens and makes it easier for dengue and Zika to copersist.

To disentangle the effects of altered infectivity of hosts from that of vectors, we let $k_d = k_z = 1$ (while keeping ν_d and ν_z at their baseline values) and obtain

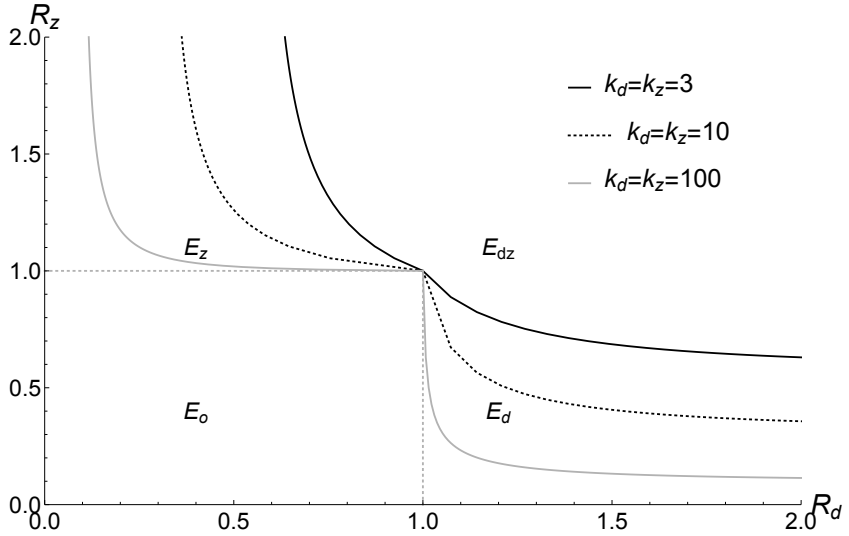

Figure 3.2: **Variations in IRN Threshold Curves with k_d and k_z.** The k_d and k_z parameter values used to generate the IRN threshold curves are as indicated, while other parameter values are kept at their baseline values.

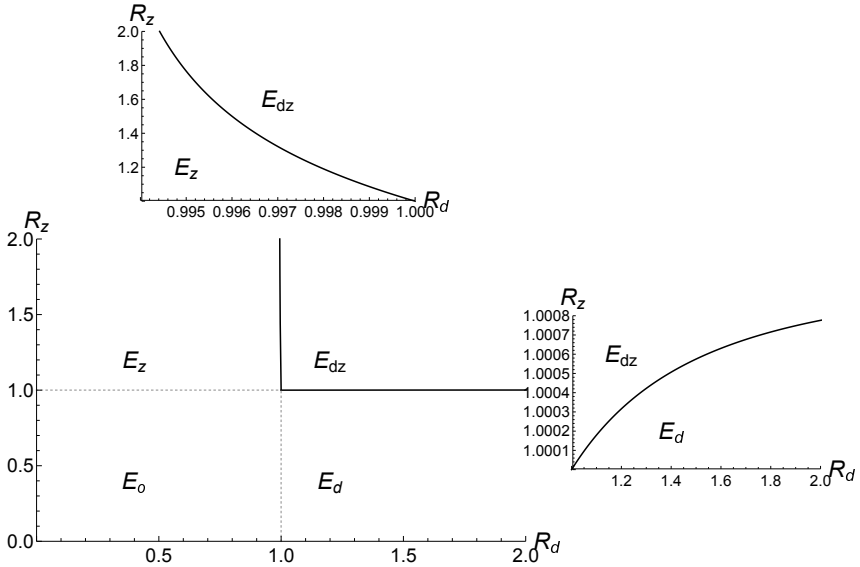

Figure 3.3: **IRN Threshold Curves for $k_d = k_z = 1$.** To generate this figure, we let $k_d = k_z = 1$ and keep other parameters at their baseline values. The miniature figures represent enlarged sections of the $\tilde{R}_d = 1$ (top figure) and $\tilde{R}_z = 1$ (bottom right figure) curves. This graph shows the relatively minimal effect of altered vector infectivity on transmission of the viruses.

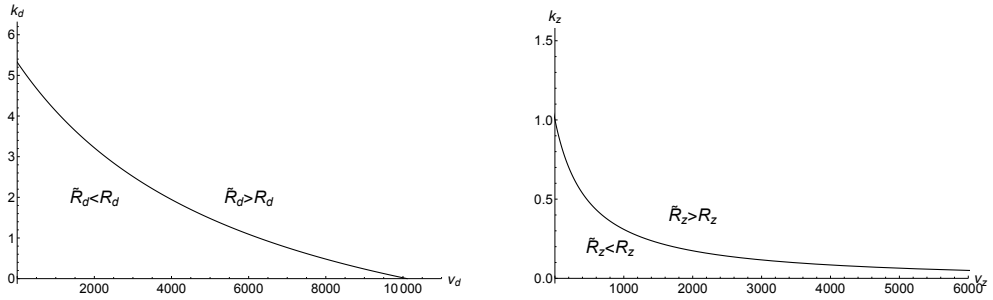

(a) ν_d vs. k_d (b) ν_z vs. k_z

Figure 3.4: **BRN & IRN Comparisons on ν Versus k Axes**

Figure 3.3. Since the $\tilde{R}_d = \tilde{R}_z = 1$ curves appear to be straight lines, it seems, at first glance, that altered infectivity of vectors does not affect persistence of Zika and dengue. However, after enlarging the IRN threshold curves, it is clear that Zika slightly facilitates the spread of dengue (as seen in the E_{dz} region where dengue is able to invade even though $R_d < 1$) while dengue hinders the spread of Zika (as evidenced by the narrow E_d region where Zika is not able to establish itself even though $R_z > 1$). This minor impact of ν_d and ν_z on the persistence of each pathogen can be attributed to the fact that coinfected mosquitoes have a higher likelihood of transmitting dengue and a lower likelihood of transmitting Zika than monoinfected mosquitoes.

A more detailed exploration of how the altered infectivity parameters impact dengue and Zika dynamics is conducted by plotting the $\tilde{R}_d = R_d$ and $\tilde{R}_z = R_z$ curves on the ν versus k axis. As shown in Figure 3.4, these curves divide the plane into two distinct regions, one where the IRN is greater than the BRN and the other where the IRN is less than the BRN. If Zika-recovered individuals are more than 5.2 times as likely as their Zika-naive counterparts to transmit dengue, the dengue IRN will always be greater than its BRN. On the other hand, any level of ADE (i.e. any $k_z > 1$) causes the Zika IRN to be greater than its BRN.

3.7 Discussion and Concluding Remarks

Although cocirculation of Zika and dengue is common due to the pathogens' shared vector, the impact of cocirculation on the presence of each pathogen has not received great mathematical modeling attention. In this study, we develop and analyze the first mathematical model of dengue and Zika that incorporates coinfection in humans and vectors, altered infectivity of coinfected vectors, and ADE. Through various analytical and numerical results, we highlight possible epidemiological consequences inherent in the cocirculation of both diseases.

The results of this work differ from those of [66] and [67], the only other mathematical modelling studies to consider dengue and Zika cocirculation. While the complexity of the model in [66] prevents the authors from finding the BRN, we provide an explicit expression for the BRN of our model. The R_d and R_z expressions in our BRN are structurally similar to those in [67]. However, they do not include the vaccination and ADE parameters present in [67]. The lack of ADE parameters in our BRN is due to the fact that ADE is incorporated in our model through altered infectivity of humans instead of altered susceptibility of humans and vectors. As a result, we are only able to assess the impact of ADE on the IRN (rather than on the BRN as discussed in [67]).

A major contribution of the present article to the study of dengue and Zika is the calculation of the IRN of both diseases which has not previously been computed. Not only are we able to write down explicit IRN expressions, we are also successful in interpreting these quantities and investigating how variations in key parameter values impact them. Through Figure 3.4, we see that altered infectivity of hosts has a greater impact on the IRNs than the altered infectivity of vectors. In addition, the k_d and k_z variables can be used to determine when the presence of one disease makes it easier or harder for the other to spread (i.e when each pathogen's IRN will

be greater than or less than its BRN). Regardless of the level of ADE, we find that Zika will always spread more easily in dengue endemic regions than it would on its own. However, this is not the case with dengue. For dengue, the effect of ADE has to be high enough (i.e. $k_z > 5.2$) in order for the presence of Zika to facilitate the establishment of dengue. This allows for interesting scenarios where Zika and dengue will have opposite effects on each other. For example, when $k_z > 1$ and $1 < k_d < 5.2$, high dengue propagates the spread of Zika (i.e. $\tilde{R}_z > R_z$), but high Zika prevalence impedes the invasion of dengue (i.e.$\tilde{R}_d < R_d$).

In addition to Figure 3.4, Figures 3.2 and 3.3 provide valuable insight on how the Zika and dengue viruses affect each other on the population level. With or without altered infectivity of humans, the presence of Zika makes it possible for dengue to persist in a population in which it would not be able to persist by itself. However, our results show that ADE (i.e. $k_z > 1$) is essential for Zika to benefit from the presence of dengue. Without ADE, it is possible for Zika's BRN to be greater than 1, but Zika not be able to suscessfully invade a population because of the presence of dengue. Both of these results are due to the baseline ν_d but ν_z values that allow coinfected mosquitoes to be better at transmitting dengue than Zika. Furthermore, as altered host infectivity parameters increase, the region of copersitence of both viruses widens, showing a mutualistic relationship between Zika and dengue due to ADE.

From this research, it is clear that the impact of ADE on the infectivity of hosts plays a crucial role in dengue-Zika dynamics. However, there are no experimental studies that address the epidemiological consequences of ADE, specifically how it affects dengue infectivity of Zika-immune individuals or Zika infectivity of dengue-immune persons. Currently, the studies that address ADE do so on the cellular level, describing its impact on viral titers. We argue that due to the effect of the k_d and k_z parameters on IRN and BRN comparisons and the persistence of Zika and dengue,

there is a need for studies that focus on estimating these values. Using experimentally validated k_d and k_z estimates would allow us to draw more concrete conclusions on the population-wide impact of Zika and dengue, which can potentially inform vaccine development efforts.

In the future, we hope to extend our current dengue-Zika coinfection model to consider vaccinations or include more than one dengue serotype. Explicitly incorporating potential Zika and dengue vaccines will give a clear picture of the possible impact of vaccinations and whether or not the use of one vaccine can indirectly exacerbate the burden of the other pathogen. In addition, since multiple dengue serotypes typically cocirculate within particular regions (and have been shown to exhibit ADE with each other), it would be beneficial to examine how the presence of more than one dengue serotype with Zika affects the long term persistence of the various pathogens.

CHAPTER 4

Invasion Reproductive Numbers for Discrete-Time Models

4.1 Introduction

The basic reproductive number, R_0, is a critical threshold in mathematical epidemiology. This quantity, defined as the "expected number of secondary cases produced, in a completely susceptible population, by a typical infected individual during its entire period of infectiousness" [42, p. 365], is used to determine whether a disease will persist, with $R_0 > 1$ indicating disease persistence. R_0 has been studied in numerous continuous and discrete-time epidemic models (e.g. [7, 72, 73, 74, 75, 76]) and has proved useful for informing disease control strategies. Although the basic reproductive number (BRN) is invaluable, it has its restrictions. One main restriction is that it can only be used to describe disease spread in a naive population.

As many communities around the globe are endemic for at least one pathogen (e.g. Chagas disease in Latin America, malaria in parts of Africa, and dengue in regions of South America), it becomes necessary to study invasion reproductive numbers (IRNs). An IRN describes the number of secondary infections produced by an infected individual in a population where one (or more) other pathogen is endemic [6]. This quantity displays the same threshold behavior as R_0, namely if the IRN of a pathogen is greater than 1, the pathogen can spread in a population endemic with the other disease(s).

IRNs have been utilized frequently in continuous-time models (e.g. [7, 8, 9, 75, 77]); however, they are yet to be explored in discrete-time systems. This may be due to the lack of multiple-pathogen discrete-time models in literature. While

discrete-time competition models have been studied for over forty years and shown to exhibit both competitive exclusion and coexistence under different conditions [78, 79, 80, 81, 82], the only discrete-time multiple-pathogen models, to the best of our knowledge, are discussed in [83] and [84]. In the former article, a discrete-time SIS model of two competing pathogen strains with demography and cross-immunity is analyzed. The basic reproductive number of each strain is calculated and stability analyses are conducted for the disease-free and boundary equilibria. The study also asserts that a coexistence equilibrium exists if and only if the basic reproductive numbers of both strains are identical. Since most parameter values used in this model did not satisfy the coexistence condition, the principle of competitive exclusion is supported. Additionally, through numerical simulations, the author in [83] illustrates how demography can result in complex population dynamics such as period doubling and chaos. It is important to highlight that nowhere in the analysis of [83] is the IRN of the two strains mentioned or alluded to.

In [84], Allen et al. present single-patch and two-patch discrete-time SIS models for n cocirculating pathogens with complete cross-immunity and no demography. Here too, the authors compute the BRNs and address stability of the disease-free and single-strain endemic equilibria. Their analysis reveals that the principle of competitive exclusion holds in a single patch, where the pathogen with the greatest BRN dominates (given that the BRN is greater than 1). However, coexistence of multiple pathogen strains is possible in two patches and is impacted by both dispersal probabilities and BRNs. Although [84] examines disease persistence in a population with multiple pathogen strains, we note that at no point in the study are IRNs mentioned.

The primary purpose of this current work is to extend the derivation of IRNs to discrete-time models, using as illustrative examples a set of two-pathogen SIS models. Unlike [83] and [84], the models that we propose assume that coinfection by both

pathogen strains is possible. Like [84], however, we leave demography implicit (as explained in the next section) because our interest is in developing the concept of IRNs in discrete-time models using the simplest possible multiple-pathogen coinfection scenario. By extending IRNs in this fashion, our research adds to the analytical tools by which discrete-time models can be examined and enriches literature on multiple-pathogen discrete-time systems.

The secondary purpose of this article is to investigate how different assumptions on the ordering of events in discrete-time models impact the BRN and IRN, and ultimately the types of biological conclusions that can be drawn from them. When creating discrete-time models, it is common practice to specify the order of events (e.g. [1, 74, 83, 85, 86, 87]). This is because different orderings can lead to differing conclusions as described in the West Nile virus study of [74] where changing the order of disease-induced mortality, natural mortality, birth, infection, and transfer resulted in distinct forms of the BRN. Although various sequential formulations of our coinfection model can be derived using different ordering of events, we consider only three sequential models where either (a) all infection events occur before recovery, (b) infection and recovery are intertwined, or (c) recovery precedes infection. These three formulations encompass a wide range of infection/recovery patterns that may arise in nature and thus any conclusions obtained from them can be extended to a plethora of other models that follow a similar pattern.

In addition, we consider a formulation of the coinfection model that assumes that events occur simultaneously, as in continuous-time systems. The model of [84] assumes a small enough time step that all event types can occur simultaneously without emptying any of the compartments. Although the structure of the model in [83] is partially ordered, with both infection types occurring simultaneously, a fully simultaneous "ordering" of events, as presented in this work, has not previously been

explored in a discrete-time model using arbitrary time step size. While a specific order of events may be necessary when describing certain biological processes (e.g. animal life cycles), there are instances where events in discrete-time models can occur simultaneously (e.g. when describing disease transmission). In such scenarios, a different formulation of discrete-time models is required, namely the simultaneous formulation that we propose.

The present study extends the single-patch model of [84] in two ways: by formulating it in terms of an arbitrary time step, following notation such as in [74, 79, 88], and by allowing coinfection. The following section develops the different formulations of the two-pathogen discrete-time SIS coinfection model. Next, we derive and compare their respective BRNs and IRNs to develop generalizations about the impact of ordering on these key epidemiological quantities. Finally, the models are applied to a specific example of rhinovirus (RV) and respiratory syncytial virus (RSV) co-circulation to provide insight on the relationship between these two pathogens at the population level.

4.2 Model Formation

The discrete-time models that we will analyze describe the dynamics of two pathogen strains competing for susceptible humans within a population, as shown in Figure 4.1. In the models, humans are compartmentalized into four classes: susceptible (S), infected with pathogen 1 (I_1), infected with pathogen 2 (I_2), and infected with both pathogens (I_{12}). Throughout the following sections, we take the proportion of people infected with pathogen 1 to be $x(t) = \frac{I_1(t)+I_{12}(t)}{N}$, and the proportion of people infected with pathogen 2 to be $y(t) = \frac{I_2(t)+I_{12}(t)}{N}$, where the constant N represents the total human population. The infection and recovery rates of each pathogen are given by $\beta_i, i = 1, 2$ and $\gamma_i, i = 1, 2$ respectively, while the relative

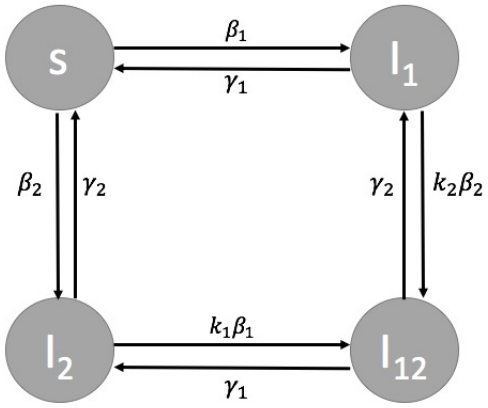

Figure 4.1: **SIS Coinfection Model.**

likelihood of coinfection with pathogen i given infection with the other pathogen is represented by $k_i, i = 1, 2$. We note that ecologically, k_i inversely measures the level of interspecific competition, with high k_i values indicating low interspecific competition. The parameter $b_i = \exp(-\beta_i \Delta t)$ represents the proportion of people who do not get infected with pathogen i by a single infective within a certain time interval and $g_i = \exp(-\gamma_i \Delta t)$, $i = 1, 2$ is the proportion that do not recover from pathogen i in that time interval. In our study, we take the time step, Δt, to be 1. Hence, $b_i = \exp(-\beta_i)$ and $g_i = \exp(-\gamma_i)$. The proportion of people who do not get infected with pathogen i in unit time when x proportion of the population is infectious with pathogen i is therefore represented by b_i^x.

In the subsections below, we develop the simultaneous formulation of the discrete-time SIS coinfection model, referred to as SIM, along with the three sequential formulations which we call SEQ1, SEQ2, and SEQ3.

4.2.1 SIM Model Formation

Unlike traditional formulations of discrete-time models which specify a distinct order of events, if we suppose that the infection and recovery events shown in Figure

4.1 occur simultaneously (i.e. that there is no specific ordering of events), we obtain the following system of difference equations:

$$\begin{aligned}
S(t+1) &= S(t)b_1^{x(t)}b_2^{y(t)} + I_1(t)\frac{\gamma_1}{\gamma_1 + k_2\beta_2 y(t)}(1 - g_1 b_2^{k_2 y(t)}) + I_2(t)\frac{\gamma_2}{\gamma_2 + k_1\beta_1 x(t)}(1 - g_2 b_1^{k_1 x(t)}) \\
I_1(t+1) &= S(t)\frac{\beta_1 x(t)}{\beta_1 x(t) + \beta_2 y(t)}(1 - b_1^{x(t)}b_2^{y(t)}) + I_1(t)g_1 b_2^{k_2 y(t)} + I_{12}(t)\frac{\gamma_2}{\gamma_1 + \gamma_2}(1 - g_1 g_2) \\
I_2(t+1) &= S(t)\frac{\beta_2 y(t)}{\beta_1 x(t) + \beta_2 y(t)}(1 - b_1^{x(t)}b_2^{y(t)}) + I_2(t)g_2 b_1^{k_1 x(t)} + I_{12}(t)\frac{\gamma_1}{\gamma_1 + \gamma_2}(1 - g_1 g_2) \\
I_{12}(t+1) &= I_1(t)\frac{k_2\beta_2 y(t)}{\gamma_1 + k_2\beta_2 y(t)}(1 - g_1 b_2^{k_2 y(t)}) + I_2(t)\frac{k_1\beta_1 x(t)}{\gamma_2 + k_1\beta_1 x(t)}(1 - g_2 b_1^{k_1 x(t)}) + I_{12}(t)g_1 g_2
\end{aligned} \tag{4.1}$$

At time t, a susceptible individual can become infected with either pathogen 1 or pathogen 2. The proportion of people that do not get infected with either pathogen is represented by $b_1^{x(t)}b_2^{y(t)}$. These individuals remain in the susceptible class during the next time step and are joined by people in the I_1 and I_2 classes who recover from infection at time t. The term $1 - g_2 b_1^{k_1 x(t)}$ describes the proportion of people in I_2 who leave due to recovery or coinfection with pathogen 1. Of those that leave the I_2 class, a proportion $\frac{\gamma_2}{\gamma_2 + k_1\beta_1 x(t)}$ become susceptible due to recovery. Likewise, of those that leave the I_1 class at time t, a proportion $\frac{\gamma_1}{\gamma_1 + k_2\beta_2 y(t)}$ recover and become susceptible.

The individuals in I_1 at time $t+1$ consist of those in I_1 who neither recovered from their infection nor were coinfected at the previous time step ($I_1(t)g_1 b_2^{k_2 y(t)}$), a proportion $\frac{\beta_1 x(t)}{\beta_1 x(t) + \beta_2 y(t)}$ of the susceptibles who were infected by pathogen 1, and a proportion $\frac{\gamma_1}{\gamma_1 + \gamma_2}$ of the I_{12} who recovered from infection with pathogen 2. The population in I_2 at each time step is composed in a similar fashion.

Humans in the coinfected class, I_{12}, who remain in that class at time $t+1$ are those who neither recovered from infection with pathogen 1 nor pathogen 2 during the previous time step ($I_{12}(t)g_1 g_2$). Adding to this class is a proportion $\frac{k_1\beta_1 x(t)}{\gamma_2 + k_1\beta_1 x(t)}(1 - g_2 b_1^{k_1 x(t)})$ of individuals from I_2 and a proportion $\frac{k_2\beta_2 y(t)}{\gamma_1 + k_2\beta_2 y(t)}(1 - g_1 b_2^{k_2 y(t)})$

of individuals in I_1 who were coinfected at time t. We note that this model assumes that a susceptible individual cannot be coinfected with both pathogens during one time step.

Intuitively, one expects for model (4.1) to be reduced to a system of two difference equations denoted by $\tilde{S}_2(t+1) = S(t+1) + I_1(t+1)$ and $\tilde{I}_2(t+1) = I_2(t+1) + I_{12}(t+1)$ when $k_2 = 1$, as is the case with an analogous continuous-time coinfection model. This is because $k_2 = 1$ indicates that infection with pathogen 2 is completely independent of infection with pathogen 1. Since those in the S and I_1 classes are infected with and recover from infection with pathogen 2 at the same rate, one expects that these classes can be grouped into a single susceptible class and that the I_2 and I_{12} classes together can constitute a single infectious class. However, due to the structure of model (4.1), such a reduction for $k_2 = 1$ (and similarly for $k_1 = 1$) cannot be achieved.

4.2.2 SEQ1 Model Formation (I_1, I_2, R_1, R_2)

In the first sequential model formulation of the discrete-time SIS model, we assume that infection with pathogen 1 occurs first and is followed by infection with pathogen 2, then recovery from pathogen 1, and finally recovery from pathogen 2. From this ordering of events, we obtain the following system of difference equations for the SEQ1 model (a step-by-step formulation of this system is provided in Appendix B.1):

$$
\begin{aligned}
S(t+1) &= S(t)[b_1^{x(t)}(b_2^{y(t)} + (1-b_2^{y(t)})(1-g_2)) + (1-b_1^{x(t)})(1-g_1)(b_2^{k_2y(t)} + (1-b_2^{k_2y(t)})(1-g_2))] \\
&\quad + I_1(t)(1-g_1)[b_2^{k_2y(t)} + (1-b_2^{k_2y(t)})(1-g_2)] \\
&\quad + I_2(t)(1-g_2)[b_1^{k_1x(t)} + (1-b_1^{k_1x(t)})(1-g_1)] \\
&\quad + I_{12}(t)[(1-g_1)(1-g_2)] \\
I_1(t+1) &= S(t)(1-b_1^{x(t)})g_1[b_2^{k_2y(t)} + (1-b_2^{k_2y(t)})(1-g_2)] \\
&\quad + I_1(t)g_1[b_2^{k_2y(t)} + (1-b_2^{k_2y(t)})(1-g_2)] \\
&\quad + I_2(t)[(1-b_1^{k_1x(t)})g_1(1-g_2)] \\
&\quad + I_{12}[g_1(1-g_2)] \\
I_2(t+1) &= S(t)g_2[b_1^{x(t)}(1-b_2^{y(t)}) + (1-b_1^{x(t)})(1-b_2^{k_2y(t)})(1-g_1)] \\
&\quad + I_1(t)[(1-b_2^{k_2y(t)})(1-g_1)g_2] \\
&\quad + I_2(t)g_2[b_1^{k_1x(t)} + (1-b_1^{k_1x(t)})(1-g_1)] \\
&\quad + I_{12}(t)[(1-g_1)g_2] \\
I_{12}(t+1) &= S(t)[(1-b_1^{x(t)})(1-b_2^{k_2y(t)})g_1g_2] \\
&\quad + I_1(t)[(1-b_2^{k_2y(t)})g_1g_2] \\
&\quad + I_2(t)[(1-b_1^{k_1x(t)})g_1g_2] \\
&\quad + I_{12}(t)[g_1g_2].
\end{aligned}
\tag{4.2}
$$

We note that for the special case $k_2 = 1$, model (4.2) simplifies to

$$
\begin{aligned}
\tilde{S}_2(t+1) &= \tilde{S}_2(t)[b_2^{\frac{\tilde{I}_2(t)}{N}} + (1-b_2^{\frac{\tilde{I}_2(t)}{N}})(1-g_2)] + \tilde{I}_2(t)[1-g_2] \\
\tilde{I}_2(t+1) &= \tilde{S}_2(t)[g_2(1-b_2^{\frac{\tilde{I}_2(t)}{N}})] + \tilde{I}_2(t)g_2
\end{aligned}
\tag{4.3}
$$

where $\tilde{S}_2(t+1)$ and $\tilde{I}_2(t+1)$ are as defined in section 4.2.1. A similar reduction of model (4.2) can be obtained when $k_1 = 1$. For this case, model (4.2) simplifies to

$$\begin{aligned}\tilde{S}_1(t+1) &= \tilde{S}_1(t)[b_1^{\frac{\tilde{I}_1(t)}{N}} + (1 - b_1^{\frac{\tilde{I}_1(t)}{N}})(1-g_1)] + \tilde{I}_1(t)[1-g_1] \\ \tilde{I}_1(t+1) &= \tilde{S}_1(t)[g_1(1 - b_1^{\frac{\tilde{I}_1(t)}{N}})] + \tilde{I}_1(t)g_1\end{aligned} \tag{4.4}$$

where $\tilde{S}_1(t) = S(t) + I_2(t)$ and $\tilde{I}_1(t) = I_1(t) + I_{12}(t)$. Since the total population, N, is constant, systems (4.3) and (4.4) can further be written respectively as

$$\tilde{I}_2(t+1) = (N - \tilde{I}_2(t))[g_2(1 - b_2^{\frac{\tilde{I}_2(t)}{N}})] + \tilde{I}_2(t)g_2 \tag{4.5}$$

$$\tilde{I}_1(t+1) = (N - \tilde{I}_1(t))[g_1(1 - b_1^{\frac{\tilde{I}_1(t)}{N}})] + \tilde{I}_1(t)g_1. \tag{4.6}$$

4.2.3 SEQ2 Model Formation (I_1, R_1, I_2, R_2)

The second sequential formulation of the SIS model assumes the following order of events: infection with pathogen 1, recovery from pathogen 1, infection with pathogen 2, and finally recovery from pathogen 2. From this, we obtain the system of difference equations for the SEQ2 model:

$$\begin{aligned}S(t+1) = {} & S(t)(b_1^{x(t)} + (1 - b_1^{x(t)})(1-g_1))(b_2^{y(t)} + (1 - b_2^{y(t)})(1-g_2)) \\ & + I_1(t)(1-g_1)[b_2^{y(t)} + (1 - b_2^{y(t)})(1-g_2)] \\ & + I_2(t)(1-g_2)[b_1^{k_1 x(t)} + (1 - b_1^{k_1 x(t)})(1-g_1)] \\ & + I_{12}(t)[(1-g_1)(1-g_2)] \\ I_1(t+1) = {} & S(t)(1 - b_1^{x(t)})g_1[b_2^{k_2 y(t)} + (1 - b_2^{k_2 y(t)})(1-g_2)] \\ & + I_1(t)g_1[b_2^{k_2 y(t)} + (1 - b_2^{k_2 y(t)})(1-g_2)] \\ & + I_2(t)[(1 - b_1^{k_1 x(t)})g_1(1-g_2)] \\ & + I_{12}[g_1(1-g_2)]\end{aligned} \tag{4.7}$$

$$
\begin{aligned}
I_2(t+1) = {} & S(t)g_2[b_1^{x(t)}(1-b_2^{y(t)}) + (1-b_1^{x(t)})(1-g_1)(1-b_2^{y(t)})] \\
& + I_1(t)[(1-g_1)(1-b_2^{y(t)})g_2] \\
& + I_2(t)g_2[b_1^{k_1x(t)} + (1-b_1^{k_1x(t)})(1-g_1)] \\
& + I_{12}(t)[(1-g_1)g_2] \\
I_{12}(t+1) = {} & S(t)[(1-b_1^{x(t)})g_1(1-b_2^{k_2y(t)})g_2] \\
& + I_1(t)[g_1(1-b_2^{k_2y(t)})g_2] \\
& + I_2(t)[(1-b_1^{k_1x(t)})g_1g_2] \\
& + I_{12}(t)[g_1g_2].
\end{aligned}
$$

For $k_i = 1, i = 1$ or 2, this model has the same simplifications as SEQ1.

4.2.4 SEQ3 Model Formation (R_1, R_2, I_1, I_2)

In the third sequential model, we assume that recovery from pathogen 1 occurs first and is followed by recovery from pathogen 2, then infection with pathogen 1, and finally infection with pathogen 2. The system of difference equations for SEQ3 is

$$
\begin{aligned}
S(t+1) = {} & S(t)[b_1^{x(t)g_1}b_2^{y(t)g_2}] \\
& + I_1(t)[(1-g_1)b_1^{x(t)g_1}b_2^{y(t)g_2}] \\
& + I_2(t)[(1-g_2)b_1^{x(t)g_1}b_2^{y(t)g_2}] \\
& + I_{12}(t)[(1-g_1)(1-g_2)b_1^{x(t)g_1}b_2^{y(t)g_2}] \\
I_1(t+1) = {} & S(t)[(1-b_1^{x(t)g_1})b_2^{k_2y(t)g_2}] \\
& + I_1(t)b_2^{k_2y(t)g_2}[g_1 + (1-g_1)(1-b_1^{x(t)g_1})] \\
& + I_2(t)[(1-g_2)(1-b_1^{x(t)g_1})b_2^{k_2y(t)g_2}] \\
& + I_{12}(t)(1-g_2)b_2^{k_2y(t)g_2}[g_1 + (1-g_1)(1-b_1^{x(t)g_1})]
\end{aligned}
\tag{4.8}
$$

$$
\begin{aligned}
I_2(t+1) = S(t)[b_1^{x(t)g_1}(1-b_2^{y(t)g_2})] \\
&+ I_1(t)[(1-g_1)b_1^{x(t)g_1}(1-b_2^{y(t)g_2})] \\
&+ I_2(t)[g_2 b_1^{k_1 x(t)g_1} + (1-g_2)b_1^{x(t)g_1}(1-b_2^{y(t)g_2})] \\
&+ I_{12}(t)(1-g_1)[g_2 b_1^{k_1 x(t)g_1} + (1-g_2)b_1^{x(t)g_1}(1-b_2^{y(t)g_2})] \\
I_{12}(t+1) = S(t)[(1-b_1^{x(t)g_1})(1-b_2^{k_2 y(t)g_2})] \\
&+ I_1(t)(1-b_2^{k_2 y(t)g_2})[g_1 + (1-g_1)(1-b_1^{x(t)g_1})] \\
&+ I_2(t)[g_2(1-b_1^{k_1 x(t)g_1}) + (1-g_2)(1-b_1^{x(t)g_1})(1-b_2^{k_2 y(t)g_2})] \\
&+ I_{12}(t)[g_1(g_2 + (1-g_2)(1-b_2^{k_2 y(t)g_2})) \\
&+ (1-g_1)(g_2(1-b_1^{k_1 x(t)g_1}) + (1-g_2)(1-b_1^{x(t)g_1})(1-b_2^{k_2 y(t)g_2})].
\end{aligned}
$$

The SEQ3 model can be simplified for $k_i = 1, i = 1, 2$. However, this simplification is different from that of SEQ1 and SEQ2 due to the fact that recovery from each pathogen occurs before infection in SEQ3, while recovery occurs after infection in SEQ1 and SEQ2. For $k_2 = 1$ and $k_1 = 1$ respectively, the SEQ3 model becomes

$$
\tilde{I}_2(t+1) = (N - \tilde{I}_2(t))[1 - b_2^{\frac{\tilde{I}_2(t)}{N} g_2}] + \tilde{I}_2(t)[g_2 + (1-g_2)(1 - b_2^{\frac{\tilde{I}_2(t)}{N} g_2})] \tag{4.9}
$$

$$
\tilde{I}_1(t+1) = (N - \tilde{I}_1(t))[1 - b_1^{\frac{\tilde{I}_1(t)}{N} g_1}] + \tilde{I}_1(t)[g_1 + (1-g_1)(1 - b_1^{\frac{\tilde{I}_1(t)}{N} g_1})]. \tag{4.10}
$$

4.3 BRNs

The BRN of each model is calculated using the next generation matrix approach outlined in [73]. When modeling scenarios with n pathogens, it is common for the BRN to have the form $R_0 = \max(R_i)$, $i = 1, 2, ..., n$. While R_0 measures the ability of any combination of pathogens to invade the population, R_i measures the

ability of pathogen i to invade when it is the only pathogen present. In the following subsections, we denote the overall BRN of each model by R_{0_k}, $k = s, 1, 2, 3$, where k describes the model at hand (s indicating the simultaneous model and 1, 2, and 3 indicating each of the sequential models). Additionally, we represent each model's pathogen i-only BRN by R_{i_k}.

4.3.1 SIM BRN

Our analysis begins with the calculation of the basic reproductive number of the simultaneous model. Using the next generation matrix approach of [73], we obtain the vector of new infections that survive the time interval

$$F = \begin{pmatrix} S(t)\frac{\beta_1 x(t)}{\beta_1 x(t) + \beta_2 y(t)}(1 - b_1^{x(t)} b_2^{y(t)}) \\ S(t)\frac{\beta_2 y(t)}{\beta_1 x(t) + \beta_2 y(t)}(1 - b_1^{x(t)} b_2^{y(t)}) \\ 0 \end{pmatrix},$$

and the vector of all other transitions

$$T = \begin{pmatrix} I_1(t) g_1 b_2^{k_2 y(t)} + I_{12}(t)\frac{\gamma_2}{\gamma_1 + \gamma_2}(1 - g_1 g_2) \\ I_2(t) g_2 b_1^{k_1 x(t)} + I_{12}(t)\frac{\gamma_1}{\gamma_1 + \gamma_2}(1 - g_1 g_2) \\ I_1(t)\frac{k_2\beta_2 y(t)}{\gamma_1 + k_2\beta_2 y(t)}(1 - g_1 b_2^{k_2 y(t)}) + I_2(t)\frac{k_1\beta_1 x(t)}{\gamma_2 + k_1\beta_1 x(t)}(1 - g_2 b_1^{k_1 x(t)}) + I_{12}(t) g_1 g_2 \end{pmatrix}.$$

Differentiating these with respect to the infected states (I_1, I_2, I_{12}) and evaluating at the unique disease-free equilibrium (N,0,0,0), we have

$$F = \begin{pmatrix} \beta_1 & 0 & \beta_1 \\ 0 & \beta_2 & \beta_2 \\ 0 & 0 & 0 \end{pmatrix} \quad \text{and} \quad T = \begin{pmatrix} g_1 & 0 & \frac{\gamma_2(1 - g_1 g_2)}{\gamma_1 + \gamma_2} \\ 0 & g_2 & \frac{\gamma_1(1 - g_1 g_2)}{\gamma_1 + \gamma_2} \\ 0 & 0 & g_1 g_2 \end{pmatrix}.$$

As described in [73], we require $\rho(T) < 1$. Indeed, $\rho(T) = \max(g_1, g_2) < 1$. We note that the spectral radius of the T matrices used in the SEQ models' BRN calcu-

lations is also $\max(g_1, g_2)$. Thus the requirement $\rho(T) < 1$ holds in the computations of sections 4.3.2- 4.3.4.

The basic reproductive number of the simultaneous model, R_{0_s}, is calculated as $\rho(F(I-T)^{-1}) = \max(\frac{\beta_1}{1-g_1}, \frac{\beta_2}{1-g_2}) = \max(R_{1_s}, R_{2_s})$. In this expression, $\frac{\beta_i}{1-g_i}$ can be interpreted as the product of the number of infections in one time step (β) by the average duration of infection in time steps ($\frac{1}{1-g_i} = \sum_{n=0}^{\infty} g_i^n$).

4.3.2 SEQ1 BRN (I_1, I_2, R_1, R_2)

Using the next generation operator method to calculate the BRN of the SEQ1 model, our F and T matrices are

$$F = \begin{pmatrix} S(t)[(1-b_1^{x(t)})b_2^{k_2 y(t)} g_1 + (1-b_1^{x(t)})(1-b_2^{k_2 y(t)})g_1(1-g_2)] \\ S(t)[b_1^{x(t)}(1-b_2^{y(t)})g_2 + (1-b_1^{x(t)})(1-b_2^{k_2 y(t)})(1-g_1)g_2] \\ S(t)[(1-b_1^{x(t)})(1-b_2^{k_2 y(t)})g_1 g_2] \end{pmatrix}$$

and

$$T = \begin{pmatrix} I_1(t)[b_2^{k_2 y(t)} g_1 + (1-b_2^{k_2 y(t)})g_1(1-g_2)] + I_2(t)[(1-b_1^{k_1 x(t)})g_1(1-g_2)] + I_{12}[g_1(1-g_2)] \\ I_1(t)[(1-b_2^{k_2 y(t)})(1-g_1)g_2] + I_2(t)[b_1^{k_1 x(t)} g_2 + (1-b_1^{k_1 x(t)})(1-g_1)g_2] + I_{12}(t)[(1-g_1)g_2] \\ I_1(t)[(1-b_2^{k_2 y(t)})g_1 g_2] + I_2(t)[(1-b_1^{k_1 x(t)})g_1 g_2] + I_{12}(t)[g_1 g_2] \end{pmatrix}.$$

Differentiating with respect to the infected classes (I_1, I_2, I_{12}) and evaluating at the unique disease-free equilibrium (N,0,0,0), we have

$$F = \begin{pmatrix} \beta_1 g_1 & 0 & \beta_1 g_1 \\ 0 & \beta_2 g_2 & \beta_2 g_2 \\ 0 & 0 & 0 \end{pmatrix} \quad \text{and} \quad T = \begin{pmatrix} g_1 & 0 & g_1(1-g_2) \\ 0 & g_2 & g_2(1-g_1) \\ 0 & 0 & g_1 g_2 \end{pmatrix}.$$

The BRN of the SEQ1 model, R_{0_1}, is calculated as

$$\rho(F(I-T)^{-1}) = \max(\tfrac{\beta_1 g_1}{1-g_1}, \tfrac{\beta_2 g_2}{1-g_2}) = \max(\beta_1 \textstyle\sum_{n=1}^{\infty} g_1^n, \beta_2 \sum_{n=1}^{\infty} g_2^n) = \max(R_{1_1}, R_{2_1}),$$

It is clear that $R_{0_1} < R_{0_s}$. The reason for this is embedded in the order of events in SEQ1. Since recovery follows infection in SEQ1, an infected individual must avoid recovery in order to be counted as infected after each time step. A proportion g_i of infected individuals do not recover, hence the g_i term in $R_{0_1}, i = 1, 2$. This g_i term is not present in R_{0_s} due to the concurrent nature of infection and recovery events in the simultaneous model.

4.3.3 SEQ2 BRN (I_1, R_1, I_2, R_2)

To calculate the BRN of the SEQ2 model, we use the following F and T matrices

$$F = \begin{pmatrix} S(t)[(1-b_1^{x(t)})g_1 b_2^{k_2 y(t)} + (1-b_1^{x(t)})g_1(1-b_2^{k_2 y(t)})(1-g_2)] \\ S(t)[b_1^{x(t)}(1-b_2^{y(t)})g_2 + (1-b_1^{x(t)})(1-g_1)(1-b_2^{y(t)})g_2] \\ S(t)[(1-b_1^{x(t)})g_1(1-b_2^{k_2 y(t)})g_2] \end{pmatrix}$$

and

$$T = \begin{pmatrix} I_1(t)[g_1 b_2^{k_2 y(t)} + g_1(1-b_2^{k_2 y(t)})(1-g_2)] + I_2(t)[(1-b_1^{k_1 x(t)})g_1(1-g_2)] + I_{12}[g_1(1-g_2)] \\ I_1(t)[(1-g_1)(1-b_2^{y(t)})g_2] + I_2(t)[b_1^{k_1 x(t)} g_2 + (1-b_1^{k_1 x(t)})(1-g_1)g_2] + I_{12}(t)[(1-g_1)g_2] \\ I_1(t)[g_1(1-b_2^{k_2 y(t)})g_2] + I_2(t)[(1-b_1^{k_1 x(t)})g_1 g_2] + I_{12}(t)[g_1 g_2] \end{pmatrix}.$$

Differentiating with respect to the infected classes (I_1, I_2, I_{12}) and evaluating at the unique disease-free equilibrium (N,0,0,0), we have

$$F = \begin{pmatrix} \beta_1 g_1 & 0 & \beta_1 g_1 \\ 0 & \beta_2 g_2 & \beta_2 g_2 \\ 0 & 0 & 0 \end{pmatrix} \quad \text{and} \quad T = \begin{pmatrix} g_1 & 0 & g_1(1-g_2) \\ 0 & g_2 & g_2(1-g_1) \\ 0 & 0 & g_1 g_2 \end{pmatrix}.$$

The BRN for the SEQ2 model, R_{0_2}, is calculated as

$$\rho(F(I-T)^{-1}) = \max(\tfrac{\beta_1 g_1}{1-g_1}, \tfrac{\beta_2 g_2}{1-g_2}) = \max(\beta_1 \textstyle\sum_{n=1}^{\infty} g_1^n, \beta_2 \sum_{n=1}^{\infty} g_2^n) = \max(R_{1_2}, R_{2_2}).$$

Here, the R_{0_2} expression matches that of R_{0_1}. This is because just as in SEQ1, recovery from a given pathogen follows infection in the SEQ2 model.

4.3.4 SEQ3 BRN (R_1, R_2, I_1, I_2)

Finally, we compute the BRN for the SEQ3 model. In this case, we use

$$F = \begin{pmatrix} S(t)[(1-b_1^{x(t)g_1})b_2^{k_2 y(t) g_2}] \\ S(t)[b_1^{x(t)g_1}(1-b_2^{y(t)g_2})] \\ S(t)[(1-b_1^{x(t)g_1})(1-b_2^{k_2 y(t) g_2})] \end{pmatrix}$$

and

$$T = \begin{pmatrix} I_1(t)[g_1 b_2^{k_2 y(t) g_2} + (1-g_1)(1-b_1^{x(t)g_1}) b_2^{k_2 y(t) g_2}] + I_2(t)[(1-g_2)(1-b_1^{x(t)g_1}) b_2^{k_2 y(t) g_2}] \\ +I_{12}[g_1(1-g_2) b_2^{k_2 y(t) g_2} + (1-g_1)(1-g_2)(1-b_1^{x(t)g_1}) b_2^{k_2 y(t) g_2}] \\ \\ I_1(t)[(1-g_1) b_1^{x(t)g_1}(1-b_2^{y(t)g_2})] + I_2(t)[g_2 b_1^{k_1 x(t) g_1} + (1-g_2) b_1^{x(t)g_1}(1-b_2^{y(t)g_2})] \\ +I_{12}[(1-g_1) g_2 b_1^{k_1 x(t) g_1} + (1-g_1)(1-g_2) b_1^{x(t)g_1}(1-b_2^{y(t)g_2})] \\ \\ I_1(t)[g_1(1-b_2^{k_2 y(t) g_2}) + (1-g_1)(1-b_1^{x(t)g_1})(1-b_2^{k_2 y(t) g_2})] + I_2(t)[g_2(1-b_1^{k_1 x(t) g_1}) \\ +(1-g_2)(1-b_1^{x(t)g_1})(1-b_2^{k_2 y(t) g_2})] + I_{12}(t)[g_1 g_2 + (1-g_1) g_2(1-b_1^{k_1 x(t) g_1}) \\ +g_1(1-g_2)(1-b_2^{k_2 y(t) g_2}) + (1-g_1)(1-g_2)(1-b_1^{x(t)g_1})(1-b_2^{k_2 y(t) g_2})] \end{pmatrix}.$$

Differentiating with respect to the infected classes (I_1, I_2, I_{12}) and evaluating at the unique disease-free equilibrium (N,0,0,0), we have

$$F = \begin{pmatrix} \beta_1 g_1 & 0 & \beta_1 g_1 \\ 0 & \beta_2 g_2 & \beta_2 g_2 \\ 0 & 0 & 0 \end{pmatrix} \quad \text{and} \quad T = \begin{pmatrix} g_1 & 0 & g_1(1-g_2) \\ 0 & g_2 & g_2(1-g_1) \\ 0 & 0 & g_1 g_2 \end{pmatrix}.$$

The BRN of the SEQ3 model, R_{0_3}, is calculated as

$$\rho(F(I-T)^{-1}) = \max(\tfrac{\beta_1 g_1}{1-g_1}, \tfrac{\beta_2 g_2}{1-g_2}) = \max(\beta_1 \textstyle\sum_{n=1}^{\infty} g_1^n, \beta_2 \sum_{n=1}^{\infty} g_2^n) = \max(R_{1_3}, R_{2_3}).$$

Note that that $R_{0_3} = R_{0_1}$. This occurs because the SEQ1 and SEQ3 models describe the same infection cycle (infection, recovery, infection, recovery, etc.). The only difference between them is the point at which the population is observed within that cycle; in SEQ1 it is observed after recovery and in SEQ3 after infection. As a result, one expects that the BRN of the two models should be identical.

4.4 Endemic Equilibria Stability Analysis

Before computing IRNs, an attempt was made to perform a general stability analysis of the single pathogen endemic equilibria for the SEQ and SIM models. However, due to the complexity of the models, no tangible conclusions were obtained analytically. Thus, we focus our attention on the stability analysis of the endemic equilibria for the SEQ models when either $k_1 = 1$ or $k_2 = 1$, since these models simplify and are mathematically tractable under this assumption.

Recall that for $k_2 = 1$, the SEQ1 & SEQ2 models simplify to (4.5) and for $k_1 = 1$ these models can be rewritten as (4.6). The proof of the stability of the endemic equilibria for both of these special cases can be obtained by studying the stability of the endemic equilibrium for the more general equation

$$\tilde{I}(t+1) \;=\; (N - \tilde{I}(t))[g(1 - b^{\frac{\tilde{I}(t)}{N}})] + \tilde{I}(t)g. \tag{4.11}$$

Notice that this equation is similar to (4.5) and (4.6) but does not include subscripts. Hence, any results obtained using (4.11) can be extended to (4.5) or (4.6) by incorporating the appropriate subscripts.

Theorem 4.4.1. *For* (4.11)*, when* $\frac{\beta g}{1-g} > 1$*, the unique endemic equilibrium (EE) is locally asymptotically stable (LAS).*

Proof. The existence and uniqueness of an EE for system (4.11) can be proved in the same manner as described in Appendix B.2 (with the exception that the term $1 - g_1$ in the function $f(x)$ of Appendix B.2 be replaced with $\frac{1-g}{g}$). Using this proof, we find that the EE for (4.1), which satisfies $y(1 + \frac{1-g}{(1-b^y)g}) = 1$ where $y = \frac{\tilde{I}}{N}$ is the proportion of the population infected with pathogen two, exists and is unique when $\frac{\beta g}{1-g} > 1$. Let $G(\tilde{I}) = (N - \tilde{I})[g(1-b)^{\frac{\tilde{I}}{N}})] + \tilde{I}g$. For the EE to be LAS, we require $\mid G'(\tilde{I}) \mid = gb^y(1 + \beta(1-y)) < 1$.

Since we cannot solve explicitly for y in the EE expression (as $y(1+\frac{1-g}{(1-b^y)g}) = 1$ is transcendental for y), we consider the inverse and view β as a function of y. Given $y(1+\frac{1-g}{(1-b^y)g}) = 1$, we have

$$\begin{aligned}
\tfrac{1-g}{g(1-\exp(-\beta y))} &= \tfrac{1-y}{y} \\
1-\exp(-\beta y) &= \tfrac{y}{1-y}\tfrac{1-g}{g} \\
\exp(-\beta y) &= 1-\tfrac{y}{1-y}\tfrac{1-g}{g} \\
-\beta y &= \ln(1-\tfrac{y}{1-y}\tfrac{1-g}{g}) \\
\beta &= \tfrac{1}{y}\ln(\tfrac{g-gy}{g-y}).
\end{aligned}$$

Notice that in the second line of equalities, $1-\exp(-\beta y) = \frac{y}{1-y}\frac{1-g}{g}$ is less than 1. This forces $\frac{y}{1-y} < \frac{g}{1-g}$ which implies that $y < g$ since the function $\frac{x}{1-x}$ is monotone increasing on (0,1). Substituting β into $\mid G'(\tilde{I}) \mid$ we obtain

$$\mid G'(\tilde{I}) \mid = F(g,y) = \tfrac{g-y}{1-y} + \tfrac{g-y}{y}\ln(\tfrac{g-gy}{g-y}).$$

To prove $F(g,y) < 1$, we wish to show, using techniques from multivariable calculus, that max $F(g,y) < 1$ on $0 < y < g < 1$. Notice that the domain does not include the boundary (i.e. $y = 0$ or $g = 1$). This is because $y = 0$ implies $\frac{\beta g}{1-g} = 1$ (as $\lim_{y\to 0}[y(1+\frac{1-g}{(1-b^y)g})] = \frac{1-g}{\beta g} = 1$ iff $\frac{\beta g}{1-g} = 1$), a contradiction to our assumption that $\frac{\beta g}{1-g} > 1$. In addition, $g = 1$ implies that $y = 1$ (from $y(1+\frac{1-g}{(1-b^y)g}) = 1$), a contradiction to the requirement that $y < g$.

Note that F has no critical points in $0 < y < g < 1$. We will prove this by showing that $F_g > 0$ on its domain (since a critical point in the domain must satisfy $F_g = F_y = 0$). For $0 < y < g < 1$, we require

$$h_1(y) = \frac{y}{1-y} + \ln(1-y) > \frac{y}{g} + \ln(1-\frac{y}{g}) = h_2(y).$$

If we let $h_1(z) = \frac{z}{1-z} + \ln(1-z)$, we obtain $h_1'(z) = \frac{z}{(1-z)^2} > 0$ on $(0,1)$ and $h_1(0) = 0$. Hence, $h_1 > 0$ on $(0,1)$. Likewise, letting $h_2(z) = z + \ln(1-z)$, we notice $h_2'(z) =$

$-\frac{z}{1-z} < 0$ on $(0,1)$ and $h_2(0) = 0$, meaning that $h_2 < 0$ on the domain. This proves that $F_g > 0$. We note that, similarly, $F_y < 0$ on the interior of $0 < y < g < 1$.

Since $\lim_{y\to 0} F_g = \lim_{y\to 0}[\frac{1}{1-y} - \frac{1}{g} + \frac{1}{y}\ln(\frac{g-gy}{g-y})] = 0$ and $\lim_{g\to 1} F_y = \lim_{g\to 1}[\frac{(1-g)(1-2y)}{y(1-y)^2} - \frac{g}{y^2}\ln(\frac{g-gy}{g-y})] = 0$, $(1,0)$ is a critical point of F. Also, $\lim_{g\to 1} F(g,y) = 1$, for $0 < y < 1$, $\lim_{y\to 0} F(g,y) = 1$, for $0 < g < 1$, and $F(g,g) = 0$, for $0 < g < 1$. Thus, $\max F(g,y) = 1$ and is attained on the boundary lines $y = 0$ and $g = 1$. Since the boundary is not included in our domain, we have $\mid G'(\tilde{I}) \mid = F(g,y) < 1$. This proves that the unique EE is LAS. □

A proof analogous to that of Theorem 4.4.1 can be done to show that the unique endemic equilibria of the SEQ3 simplifications (4.9) and (4.10) are LAS when their respective BRNs are greater than one. In this proof, the term $\frac{1-g_1}{1-b_1^x}$ in the function $f(x)$ of Appendix B.2 is replaced with $\frac{(1-g)b^{yg}}{(1-b^{yg})}$ and the y's in the $\mid G'(\tilde{I}) \mid$ and β equations are replaced with yg.

In our exploration of the stability of the single-pathogen endemic equilibria for the general SEQ models, we found that one eigenvalue in each of the Jacobians used to determine the stability of the equilibria has the same form as the $\mid G'(\tilde{I}) \mid$ expression. Thus, our analysis of the special cases for the SEQ models proves that the magnitude of that eigenvalue is less than one. However, because of the complexity of the other eigenvalues, the question of whether their magnitude is less than one (which is required for stability of the single pathogen endemic equilibria) was explored solely numerically.

4.5 IRNs

4.5.1 SIM IRN

To obtain the invasion reproductive number (IRN) when pathogen 1 is endemic (i.e. $R_{1_s} > 1$), we reclassify the infectious classes and use the next generation operator method. The infectious classes are now taken to be I_2 and I_{12}. Letting

$$F = \begin{pmatrix} S(t)\dfrac{\beta_2 y(t)}{\beta_1 x(t) + \beta_2 y(t)}(1 - b_1^{x(t)} b_2^{y(t)}) \\ I_1(t)\dfrac{k_2\beta_2 y(t)}{\gamma_1 + k_2\beta_2 y(t)}(1 - g_1 b_2^{k_2 y(t)}) \end{pmatrix},$$

and

$$T = \begin{pmatrix} \\ I_2(t) g_2 b_1^{k_1 x(t)} + I_{12}(t)\dfrac{\gamma_1}{\gamma_1 + \gamma_2}(1 - g_1 g_2) \\ I_2(t)\dfrac{k_1\beta_1 x(t)}{\gamma_2 + k_1\beta_1 x(t)}(1 - g_2 b_1^{k_1 x(t)}) + I_{12}(t) g_1 g_2 \end{pmatrix},$$

we evaluate the resulting F and T matrices at the unique pathogen 1 endemic equilibrium $(N - I_1^*, I_1^*, 0, 0)$. Proof of the existence of a unique endemic equilibrium for the SIM model can be found in Appendix B.2. At this equilibrium, we have

$$F = \begin{pmatrix} \dfrac{\beta_2(1-x^*)}{\beta_1 x^*}(1 - b_1^{x^*}) & \dfrac{\beta_2(1-x^*)}{\beta_1 x^*}(1 - b_1^{x^*}) \\ \dfrac{\beta_2 k_2 x^*}{\gamma_1}(1 - g_1) & \dfrac{\beta_2 k_2 x^*}{\gamma_1}(1 - g_1) \end{pmatrix}$$

and

$$T = \begin{pmatrix} g_2 b_1^{k_1 x^*} & \dfrac{\gamma_1}{\gamma_1 + \gamma_2}(1 - g_1 g_2) \\ \dfrac{\beta_1 k_1 x^*}{\gamma_2 + \beta_1 k_1 x^*}(1 - g_2 b_1^{k_1 x^*}) & g_1 g_2 \end{pmatrix}$$

with $x^* = \frac{I_1^*}{N}$ being the unique root of $x(1 + \frac{1-g_1}{1-b_1^x}) = 1$. By the Jury criterion [89], $\rho(T) < 1$ if and only if

$$|\ \mathrm{tr}\ T\ | < \det T + 1 < 2.$$

Here, $\det T = g_1 g_2^2 b_1^{k_1 x} - \frac{\gamma_1}{\gamma_1+\gamma_2}(1-g_1 g_2)\frac{\beta_1 k_1 x}{\beta_1 k_1 x+\gamma_2}(1-g_2 b_1^{k_1 x})$ and $|\ \mathrm{tr}\ T\ | = g_2 b_1^{k_1 x} + g_1 g_2$. Since the entries in T are all less than 1 (as is the case with the entries in the T

matrices used in the IRN calculations for the SEQ models), $\det T < 1$, and thus the condition $\det T + 1 < 2$ is satisfied. Also, notice that $|\operatorname{tr} T| = g_2 b_1^{k_1 x} + g_1 g_2 < \det T + 1$. This is obtained from the following inequality,

$$\det T > g_1 g_2^2 b_1^{k_1 x} - (1 - g_1 g_2)(1 - g_{2b_1^{k_1 x}}) = g_2 b_1^{k_1 x} + g_1 g_2 - 1.$$

Using the F and T matrices, we obtain

$$F(I-T)^{-1} = \frac{1}{dc(1-ge)} \begin{pmatrix} h(c+ed) & h(gc+d) \\ j(c+ed) & j(gc+d) \end{pmatrix} = \begin{pmatrix} \frac{h}{d}\frac{1}{1-ge} + \frac{h}{c}\frac{e}{1-ge} & \frac{h}{d}\frac{g}{1-ge} + \frac{h}{c}\frac{1}{1-ge} \\ \frac{j}{d}\frac{1}{1-ge} + \frac{j}{c}\frac{e}{1-ge} & \frac{j}{d}\frac{g}{1-ge} + \frac{j}{c}\frac{1}{1-ge} \end{pmatrix},$$

where $c = 1 - g_1 g_2$, $d = (1 - g_2 b_1^{k_1 x^*})$, $e = \frac{\beta_1 k_1 x^*}{\gamma_2 + \beta_1 k_1 x^*}$, $g = \frac{\gamma_1}{\gamma_1 + \gamma_2}$, $h = \frac{\beta_2 (1 - x^*)}{\beta_1 x^*}(1 - b_1^{x^*})$, and $j = \frac{\beta_2 k_2 x^*}{\gamma_1}(1 - g_1)$.

To find the invasion capability of pathogen 2, we rewrite

$$F(I-T)^{-1} = \begin{pmatrix} \frac{h}{d}\frac{1}{1-ge} + \frac{he}{c}\frac{1}{1-ge} & \frac{h}{c}\frac{1}{1-ge} + \frac{hg}{d}\frac{1}{1-ge} \\ \frac{j}{d}\frac{1}{1-ge} + \frac{je}{c}\frac{1}{1-ge} & \frac{j}{c}\frac{1}{1-ge} + \frac{jg}{d}\frac{1}{1-ge} \end{pmatrix} = \begin{pmatrix} A & B \\ C & D \end{pmatrix}.$$

Biologically, A represents the mean number of I_2's produced by an I_2. The production of new pathogen 2 infections can be made from an I_2 residing in the I_2 class ($\frac{h}{d}$) and from an I_2 that moved to the I_{12} compartment ($\frac{he}{c}$). The second entry, B, in the next generation matrix describes the average number of I_2's created by an I_{12} while in the I_{12} ($\frac{h}{c}$) class and by an I_{12} that transitioned to the I_2 class ($\frac{hg}{d}$). C depicts the mean number of I_{12}'s created by an I_2 while in the I_2 class ($\frac{j}{d}$) plus those that were produced by an I_2 that transitioned to I_{12} ($\frac{je}{c}$) . Lastly, D is the sum of the mean number of I_{12}'s produced by an I_{12} during it's stay in I_{12} ($\frac{j}{c}$) and the mean number of I_{12}'s produced by an I_{12} that moved to the I_2 compartment ($\frac{jg}{d}$) . Depending on which compartment one starts in, the fraction $\frac{1}{1-ge}$ can represent the average number of times that an I_2 visits the I_2 class before recovering or the average

number of times that an I_{12} visits the I_{12} class before recovery. A list of the biological interpretation of the different terms in the $F(I-T)^{-1}$ matrix is in Table 4.1.

Table 4.1: Biological Interpretation of $F(I-T)^{-1}$ Matrix Terms

Term	Biological Interpretation
h/d	Mean number of of I_2's produced by an I_2
h/c	Mean number of I_2's produced by an I_{12}
j/d	Mean number of of I_{12}'s produced by an I_2
j/c	Mean number of I_{12}'s produced by an I_{12}
c	Percentage of people that leave I_{12} class
d	Percentage of people that leave I_2 class
e	Percentage of I_2 that go to I_{12}
g	Percentage of I_{12} that go to I_2

The eigenvalues of $F(I-T)^{-1}$ are roots of the characteristic polynomial $p(z) = z^2 - (A+D)z + q$. Notice that $q = AD - CB = 0$. Thus, the roots of $p(z)$ are 0 and $A+D$. Since $\tilde{R}_{2_s} = \rho(F(I-T)^{-1})$, we have that $\tilde{R}_{2_s} = A+D$, the mean number of I_2's produced by an I_2 plus the mean number of I_{12}'s produced by an I_{12}. Calculation of the IRN for pathogen 1 at the pathogen 2 endemic equilibrium is performed in a similar manner and we obtain $\tilde{R}_{1_s} = A' + D'$. Here, A' and D' are essentially A and D from R_{2_s} with the following modifications: in A', y^* replaces the x^* in A and subscripts are switched from 1 to 2 (i.e γ_1 in A is replaced with γ_2 in A', b_2 in A is replaced with b_1 in A', etc.). In A', y^* is the root of $y(1 + \frac{1-g_2}{1-b_2^y}) = 1$. Notice that unlike the SEQ models below, the SIM model IRNs do not simplify to their corresponding BRNs when $k_i = 1$.

4.5.2 SEQ1 IRN (I_1, I_2, R_1, R_2)

To obtain the IRN of the SEQ1 model when pathogen 1 is endemic (i.e. $R_{1_1} > 1$), we reclassify the infectious classes and use the next generation operator method. The infectious classes are now taken to be I_2 and I_{12}. Letting

$$F = \begin{pmatrix} S(t)[b_1^{x(t)}(1-b_2^{y(t)})g_2 + (1-b_1^x(t))(1-b_2k_2^{y(t)})(1-g_1)g_2] \\ \qquad\qquad + I_1(t)[(1-b_2k_2^{y(t)})(1-g_1)g_2] \\ \\ S(t)[(1-b_1^{x(t)})(1-b_2^{k_2y(t)})g_1g_2] + I_1(t)[(1-b_2^{k_2y(t)})g_1g_2] \end{pmatrix}$$

and

$$T = \begin{pmatrix} I_2(t)[b_1^{k_1x(t)}g_2 + (1-b_1^{k_1x(t)})(1-g_1)g_2] + I_{12}(t)[(1-g_1)g_2] \\ \\ I_2(t)[(1-b_1^{k_1x(t)})g_1g_2] + I_{12}(t)g_1g_2 \end{pmatrix},$$

we evaluate the resulting F and T matrices at the unique pathogen 1 endemic equilibrium $(N-I_1^*, I_1^*, 0, 0)$ (see Appendix B.2 for details regarding single-pathogen endemic equilibria for all models).

$$F = \begin{pmatrix} a & a \\ b & b \end{pmatrix} \quad \text{and} \quad T = \begin{pmatrix} g_2 - g_1g_2(1-b_1^{k_1x^*}) & g_2(1-g_1) \\ g_1g_2(1-b_1^{k_1x^*}) & g_1g_2 \end{pmatrix},$$

where

$$a = \beta_2k_2g_2[(1-x^*)(1-g_1+b_1^{x^*}g_1 - b_1^{x^*} + \frac{b_1^{x^*}}{k_2}) + x^*(1-g_1)],$$

and

$$b = \beta_2k_2g_2[(1-x^*)(g_1 - b_1^{x^*}g_1) + x^*g_1].$$

Here, $\det T = g_1 g_2^2 b_1^{k_1 x}$ and $|\ \mathrm{tr}\ T\ | = g_2 + g_1 g_2 b_1^{k_1 x}$. Since $\det T < 1$, the Jury criterion requirement $\det T + 1 < 2$ is satisfied. Through the set of inequalities

$$\begin{aligned} g_1 g_2 b_1^{k_1 x} &< 1 \\ g_1 g_2 b_1^{k_1 x}(1 - g_2) &< 1 - g_2 \\ g_1 g_2 b_1^{k_1 x} - g_1 g_2^2 b_1^{k_1 x} &< 1 - g_2 \\ g_2 + g_1 g_2 b_1^{k_1 x} &< 1 + g_1 g_2^2 b_1^{k_1 x}, \end{aligned}$$

we see that $\mathrm{tr}\ T < \det T + 1$ and thus $\rho(T) < 1$.

Using the F and T matrices, $\tilde{R}_{2_1} = \rho(F(I - T)^{-1}) = R_{2_1}[(1 - x^*)b_1^{x^*} + k_2(1 - (1 - x^*)b_1^{x^*})]$. In this model, the pathogen 1 prevalence x^* is the unique root of $x(1 + \frac{1-g_1}{(1-b_1^x)g_1}) = 1$. The IRN when pathogen 2 is endemic is computed in a similar manner as $\tilde{R}_{2_1}$ and calculated to be $\tilde{R}_{1_1} = R_{1_1}[(1 - y^*) + k_1 y^*]$. Here, the pathogen 2 prevalence y^* is the unique solution to $y(1 + \frac{1-g_2}{(1-b_2^y)g_2}) = 1$. We note that when $k_2 = 1$, $\tilde{R}_{2_1} = R_{2_1}$ and when $k_1 = 1$, $\tilde{R}_{1_1} = R_{1_1}$.

$\tilde{R}_{2_1}$ is a multiple of R_{2_1} that is the weighted average of 1 and k_2. The value 1 is weighted by the proportion of the population that started out not infected by pathogen 1 and remained uninfected by pathogen 1 during one time step, while k_2 is weighed by the rest of the population. Likewise, $\tilde{R}_{1_1}$ is a multiple of R_{1_1} that consists of a weighted average of 1 and k_1, with 1 weighted by the proportion of the population that is not infected with pathogen 2 and k_1 weighted by the proportion that is infected with pathogen 2.

4.5.3 SEQ2 IRN (I_1, R_1, I_2, R_2)

We obtain the IRN when pathogen 1 is endemic in a similar manner as above. Here, we let

$$F = \begin{pmatrix} S(t)[b_1^{x(t)}(1-b_2^{y(t)})g_2 + (1-b_1^{x(t)})(1-g_1)(1-b_2^{y(t)})g_2] \\ \qquad\qquad + I_1(t)[(1-g_1)(1-b_2^{y(t)})g_2] \\ \\ S(t)[(1-b_1^{x(t)})g_1(1-b_2^{k_2 y(t)})g_2] + I_1(t)[g_1(1-b_2^{k_2 y(t)})g_2] \end{pmatrix}$$

and

$$T = \begin{pmatrix} I_2(t)[b_1^{k_1 x(t)}g_2 + (1-b_1^{k_1 x(t)})(1-g_1)g_2] + I_{12}(t)[(1-g_1)g_2 \\ \\ I_2(t)[(1-b_1^{k_1 x(t)})g_1 g_2] + I_{12}(t)[g_1 g_2] \end{pmatrix}.$$

and evaluating the resulting F and T matrices at the unique pathogen 1 endemic equilibrium $(N - I_1^*, I_1^*, 0, 0)$, we have

$$F = \begin{pmatrix} a_2 & a_2 \\ b_2 & b_2 \end{pmatrix} \quad \text{and} \quad T = \begin{pmatrix} g_2 - g_1 g_2(1-b_1^{k_1 x^*}) & g_2(1-g_1) \\ g_1 g_2(1-b_1^{k_1 x^*}) & g_1 g_2 \end{pmatrix}$$

where

$$a_2 = \beta_2 g_2[(1-x^*)(1-g_1+b_1^{x^*}g_1)+x^*(1-g_1)], \quad \text{and} \quad b_2 = \beta_2 k_2 g_2[(1-x^*)(g_1-b_1^{x^*}g_1)+x^* g_1].$$

Since the T matrix presented here is identical to that of Section 4.5.2, we know that $\rho(T) < 1$.

With these F and T matrices, we obtain

$$\tilde{R}_{2_2} = \rho(F(I-T)^{-1}) = R_{2_2}[1-(1-(1-x^*)b_1^{x^*})g_1 + k_2(1-(1-x^*)b_1^{x^*})g_1],$$

where x^* is the same as that in SEQ1. The factor which R_{2_2} is multiplied by in the expression for $\tilde{R}_{2_2}$ is a simplification of

$$[(x^* + (1-x^*)(1-b_1^{x^*}))(1-g_1) + (1-x^*)b_1^{x^*}] + k_2[(x^* + (1-x^*)(1-b_1^{x^*}))g_1].$$

In this expression, the value 1 is weighted by the sum of the proportion of individuals who were initially infected with pathogen 1 but recovered ($x^*(1-g_1)$), the proportion of people initially uninfected with pathogen 1 who became infected with pathogen 1 and recovered from said infection ($(1-x^*)(1-b_1^{x^*})(1-g_1)$), and the proportion of people initially uninfected by pathogen 1 who remained uninfected during one time step ($(1-x^*)b_1^{x^*}$). Moreover, k_2 is weighted by the sum of the proportion of individuals who were infected with pathogen one at the beginning of the time step and did not recover (x^*g_1), and the proportion of individuals initially uninfected with pathogen1 who became infected and did not recover within the time period ($(1-x^*)(1-b_1^{x^*})g_1$).

The IRN when pathogen 2 is endemic is calculated to be

$$\tilde{R}_{1_2} = R_{1_2}[(1-y^*) + k_1 y^*],$$

where y^* is the same as that in SEQ1. This is identical to $\tilde{R}_{1_1}$ and results from the fact that infection with pathogen 1 occurs first in both SEQ1 and SEQ2. Therefore, the point at which we count the number of secondary pathogen 1 infections is identical for both models and occurs when the population is divided into only two categories: those infected with pathogen 2 and those not infected with pathogen 2. In addition, when $k_2 = 1$, $\tilde{R}_{2_2} = R_{2_2}$ and when $k_1 = 1$, $\tilde{R}_{1_2} = R_{1_2}$.

4.5.4 SEQ3 IRN (R_1, R_2, I_1, I_2)

To calculate the IRN of the SEQ3 model when pathogen 1 is endemic, we use

$$F = \begin{pmatrix} S(t)[b_1^{x(t)g_1}(1-b_2^{y(t)g_2})] + I_1(t)[(1-g_1)b_1^{x(t)g_1}(1-b_2^{y(t)g_2})] \\ \\ S(t)[(1-b_1^{x(t)g_1})(1-b_2^{k_2y(t)g_2})] + I_1(t)(1-b_2^{k_2y(t)g_2})[g_1 + (1-g_1)(1-b_1^{x(t)g_1})] \end{pmatrix}$$

and

$$T = \begin{pmatrix} I_2(t)[g_2 b_1^{k_1 x(t) g_1} + (1-g_2) b_1^{x(t) g_1}(1 - b_2^{y(t) g_2})] \\ +I_{12}[(1-g_1) g_2 b_1^{k_1 x(t) g_1} + (1-g_1)(1-g_2) b_1^{x(t) g_1}(1 - b_2^{y(t) g_2})] \\ \\ I_2(t)[g_2(1 - b_1^{k_1 x(t) g_1}) + (1-g_2)(1 - b_1^{x(t) g_1})(1 - b_2^{k_2 y(t) g_2})] \\ +I_{12}(t)[g_2(g_1 + (1-g_1)(1 - b_1^{k_1 x(t) g_1})) + (1-g_2)(1 - b_2^{k_2 y(t) g_2})(g_1 + (1-g_1)(1 - b_1^{x(t) g_1}))] \end{pmatrix}.$$

Evaluating the resulting F and T matrices at the unique pathogen 1 endemic equilibrium $(N - I_1^*, I_1^*, 0, 0)$ we have

$$F = \begin{pmatrix} a_3 & a_3 \\ b_3 & b_3 \end{pmatrix} \quad \text{and} \quad T = \begin{pmatrix} g_2 b_1^{k_1 x^* g_1} & g_2 b_1^{k_1 x^* g_1}(1-g_1) \\ g_2(1 - b_1^{k_1 x^* g_1}) & g_2(1 - b_1^{k_1 x^* g_1}(1-g_1)) \end{pmatrix}$$

where

$$a_3 = \beta_2 g_2 b_1^{x^* g_1}[(1-x^*) + x^*(1-g_2)] \quad \text{and} \quad b_3 = \beta_2 k_2 g_2[(1-x^*)(1-b_1^{x^* g_1}) - x^* b_1^{x^* g_1}(1-g_1)].$$

Here, $\det T = g_1 g_2^2 b_1^{k_1 x g_1}$ and $|\operatorname{tr} T| = g_2 + g_1 g_2 b_1^{k_1 x g_1}$. To prove that $\rho(T) < 1$, we use the approach described in Section 4.5.2, but replace x (in the determinant and trace expressions of Section 4.5.2) with $x g_1$.

With these F and T matrices,

$$\tilde{R}_{2_3} = \rho(F(I-T)^{-1}) = R_{2_3}[(1 - x^* g_1) b_1^{x^* g_1} + k_2(1 - (1 - x^* g_1) b_1^{x^* g_1})],$$

where x^* is the unique solution to $x(1 + \frac{(1-g_1) b_1^{x g_1}}{1 - b_1^{x g_1}}) = 1$. The factor by which R_{2_3} is multiplied in the expression for $\tilde{R}_{2_3}$ is a simplification of

$$[x^*(1-g_1) + (1-x^*)] b_1^{x^* g_1} + k_2[x^* g_1 + (x^*(1-g_1) + (1-x^*))(1 - b_1^{x^* g_1})].$$

In this expression, 1 is weighted by the sum of the proportion of people originally infected with pathogen 1 who recovered and were not reinfected with the pathogen

and the proportion of people who were originally uninfected with pathogen 1 and remained uninfected during one time step. The parameter k_2 is weighted by the sum of the proportion of people originally infected with pathogen 1 who did not recover, the proportion of people originally infected with pathogen 1 who recovered and were re-infected, and the proportion of people originally uninfected with pathogen 1 but who got infected with the pathogen during one time step. Infections are transmitted by the proportion x^*g_1 of people who do not recover from infection with pathogen 1.

The IRN when pathogen 2 is endemic is $\tilde{R}_{1_3} = R_{1_3}[(1 - y^*g_2) + k_1 y^* g_2]$, where y^* is the unique root of $y(1 + \frac{(1-g_2)b_2^{yg_2}}{1-b_2^{yg_2}}) = 1$. R_{1_3} is multiplied by a weighted average of 1 and k_1, with k_1 weighted by the proportion of people originally infected with pathogen 2 who did not recover in one time step and 1 is weighted by the rest of the population. This $\tilde{R}_{1_3}$ expression is similar to that of $\tilde{R}_{1_2}$ and $\tilde{R}_{1_1}$ except for the fact that y^* is multiplied by g_2 in $\tilde{R}_{1_3}$ (y^*g_2 represents the proportion of people who do not recover from infection with pathogen 2). The inclusion of the g_2 factor is due to recovery occurring first in the SEQ3 model, hence an individual must fail to recover from infection with pathogen 2 in order to be counted in the IRN. Although the IRNs for the SEQ1 and SEQ3 models appear to be different, they are in fact identical as detailed in Appendix B.4. Lastly, notice that when $k_2 = 1$, $\tilde{R}_{2_3} = R_{2_3}$ and when $k_1 = 1$, $\tilde{R}_{1_3} = R_{1_3}$.

4.6 BRN/IRN Threshold Comparisons

Through the above computations, it is evident that there is great variation in the IRN expressions for the SIM, SEQ1, SEQ2, and SEQ3 models. However, what remains unclear is how the different models' IRN thresholds compare (i.e. whether one model's threshold is more or less restrictive than another). To better analyze the IRNs, we create IRN threshold curves for when $\tilde{R}_1$ and $\tilde{R}_2$ for the various models equal 1 and

Model	BRN	$\tilde{R}_1$	$\tilde{R}_2$
SEQ1	$\max(\frac{\beta_1 g_1}{1-g_1}, \frac{\beta_2 g_2}{1-g_2})$	$\tilde{R}_{1_1} = R_{1_1}[(1-y^*) + k_1 y^*]$	$\tilde{R}_{2_1} = R_{2_1}[(1-x^*)b_1^{x^*} + k_2(1-(1-x^*)b_1^{x^*})]$
SEQ2	same as SEQ1	same as SEQ1	$\tilde{R}_{2_2} = \tilde{R}_{2_1} g_1 + R_{2_1}(1-g_1)$
SEQ3	same as SEQ1	same as SEQ1	same as SEQ1
SIM	$\max(\frac{\beta_1}{1-g_1}, \frac{\beta_2}{1-g_2})$	$\tilde{R}_{1_s} = A' + D'$	$\tilde{R}_{2_s} = A + D$

Table 4.2: **Summary of BRNs and IRNs**

Endemic Equilibria	SEQ1, SEQ2	SEQ3	SIM
x^* is unique root of	$x(1+\frac{1-g_1}{(1-b_1^x)g_1}) = 1$	$x(1+\frac{(1-g_1)b_1^{xg_1}}{1-b_1^{xg_1}}) = 1$	$x(1+\frac{1-g_1}{1-b_1^x}) = 1$
y^* is unique root of	$y(1+\frac{1-g_2}{(1-b_2^y)g_2}) = 1$	$y(1+\frac{(1-g_2)b_2^{yg_2}}{1-b_2^{yg_2}}) = 1$	$y(1+\frac{1-g_2}{1-b_2^y}) = 1$

Table 4.3: **Pathogen 1 & 2 Endemic Equilibria.** In this table, x^* is the proportion of people infected with pathogen 1 at the pathogen 1 endemic equilibrium and y^* is the proportion of people infected with pathogen 2 at the pathogen 2 endemic equilibrium.

begin by plotting these curves on the R_1 vs. R_2 axes in Mathematica. The R_1 vs. R_2 plane has been utilized in previous studies on co-circulating pathogens (e.g. [7, 8, 90]) and allows for a primarily epidemiological comparison of our different models. As seen in Figures 4.2 and 4.3, the threshold curves divide the plane into four distinct regions of possible model outcomes (extinction of both pathogens, E_0, persistence of only pathogen 1, E_1, persistence of only pathogen 2, E_2, and co-persistence of both pathogens, E_3).

As an example of how these curves were generated, consider the $\tilde{R}_1 = 1$ curve. We fixed the g_i and k_i parameters while varying β_2. For each value of β_2, we solved for the pathogen 2 endemic equilibrium, and used this equilibrium value to numerically solve for β_1 in the equation $\tilde{R}_1 = 1$. With this pair of β_1 and β_2 values, we calculated R_1 and R_2 for the respective models. Generating the $\tilde{R}_2 = 1$ curves was done in a similar manner while varying β_1 and solving for the pathogen 1 endemic equilibrium. To minimize the effect of parameter values on the threshold graphs, we keep $k_1 = k_2$ and $g_1 = g_2$ in Figures 4.2 and 4.3. We find that while the SEQ2 model predicts a larger region of co-persistence of both pathogens than the other models for $k_i < 1$, it predicts a smaller region of co-persistence for $k_i > 1$.

While the SEQ1 and SEQ3 IRN curves and the SEQ1 and SEQ2 $\tilde{R}_1 = 1$ curves will always overlap due to the models' identical $\tilde{R}_1$ and/or $\tilde{R}_2$ expressions, in general, the ordering of the curves in Figures 4.2 and 4.3 is not always consistent. For example, since $\tilde{R}_{2_2} > \tilde{R}_{2_1}$ if and only if $k_2 < 1$ (meaning that it is easier for strain two to survive in SEQ2 than SEQ1 for $k_2 < 1$), and vice versa for $k_2 > 1$, we find that the SEQ1 $\tilde{R}_2$ threshold curve will be above that of SEQ2 for $k_2 < 1$, with the ordering switched for $k_2 > 1$ (Appendix B.3). In addition, the position of the SIM model curves relative to other curves varies with parameter values. For example, if

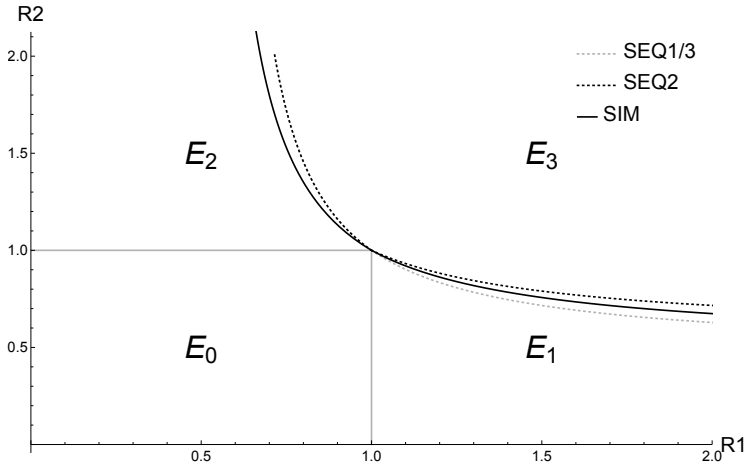

Figure 4.2: **BRN/IRN Threshold Curves** $k_i > 1$**.** In this graph, $g_1 = g_2 = 0.4$ and $k_1 = k_2 = 2$. In region E_0, we see extinction of both pathogens, in E_1, the persistence of only pathogen 1, in E_2, the persistence of only pathogen 2, and in E_3, co-persistence of both pathogens.

$g_1 = g_2 = 0.05, \beta_1 = 0.1, k_1 = k_2 = 1.01$, we have $\tilde{R}_{2_3} < \tilde{R}_{2_s}$, but for a different set of g_i values, namely, $g_1 = g_2 = 0.4$, we have $\tilde{R}_{2_3} > \tilde{R}_{2_s}$.

In addition to focusing on the epidemiological variation between the models in the R_1 vs. R_2 plane, we can observe how the behavior of each model changes with respect to raw parameter values such as β_1 and β_2. Since the various models have different BRN's, viewing the IRN threshold curves on a β_1 vs. β_2 axis allows for the visualization of an additional region where certain models predict disease extinction while others do not. This is the case depicted in Figure 4.4. The region between the gray and black boxes illustrates β_1 and β_2 values for which the sequential models predict disease extinction but the SIM model does not. In fact, parts of that space represent the E_1, E_2, and E_3 regions predicted by the SIM models. In addition, the L shaped region created by the two sets of $\tilde{R}_1 = 1$ and $\tilde{R}_2 = 1$ curves illustrates a space where the SIM model predicts co-persistence of both pathogens but the sequential models do not. The region of co-persistence predicted by the SIM model in this

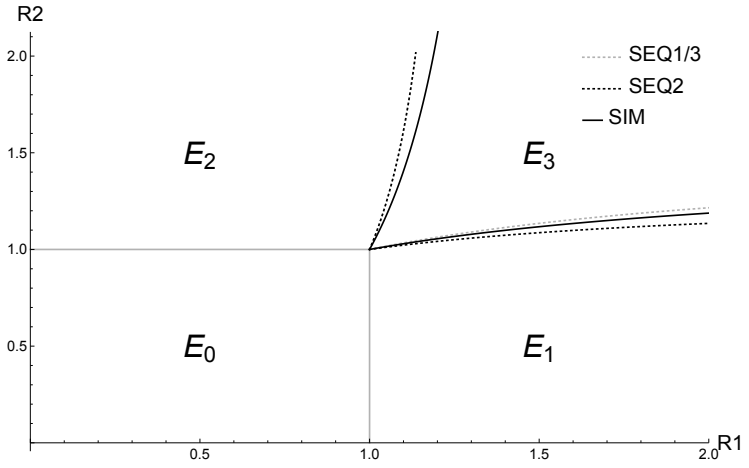

Figure 4.3: **BRN/IRN Threshold Curves for $k_i < 1$.** In this graph, $g_1 = g_2 = 0.4$ and $k_1 = k_2 = 0.7$. In region E_0, we see extinction of both pathogens, in E_1, the persistence of only pathogen 1, in E_2, the persistence of only pathogen 2, and in E_3, co-persistence of both pathogens.

case is larger than that of the sequential models. This results from the fact that recovery occurs after infection in the sequential models. Infected individuals must escape recovery in order to be counted in the BRNs of these models, which reduces the BRNs and thus makes it less likely to predict persistence of the pathogens.

Through numerical simulations, we are able to investigate how the different model BRN/IRN threshold curves behave as the likelihood of coinfection approaches zero or infinity. For all of the discrete-time models, we find that the region of co-persistence of the two pathogens widens as $k_i, i = 1, 2$ increases, but becomes smaller as k_i decreases (as illustrated in Figures 4.2 and 4.3). As the likelihood of coinfection increases, the interspecific competition between the two pathogens decreases. This causes the relationship between the pathogens to become more and more mutualistic, resulting in both strains aiding each other to become established within the community. Surprisingly, when $k_1 = k_2 = 0$ (i.e. when the two strains exhibit cross-immunity and interspecific competition is at its maximum), we see that for a wide range of parameter values (one of which is shown in Figures 4.5 and 4.6), all

of the sequential models predict a region of co-persistence of both pathogens, while the simultaneous model predicts competitive exclusion. In fact, for the SIM model, coexistence is only possible when the BRNs of both pathogens are equal. The proof of this is essentially the same as that of Lemma 3.3 in [83] (except for the fact that the SIM model has a constant total population, N, instead of an asymptotically constant population T_∞ and does not consider deaths). Since it is highly unlikely that two pathogens in nature will have identical BRNs, the simultaneous model supports the notion that only one pathogen can successfully invade the population.

To further explore the contradiction in competition dynamics between the SEQ and SIM models under cross-immunity, we observe what happens in the limit as $\Delta t = T$ approaches zero (recall that in formulating the discrete-time models, we assume $\Delta t = 1$). In this scenario, we find that all of the models have the same BRN and IRNs. The BRN in this case is $\max(R_1, R_2)$ =max $(\frac{\beta_1}{\gamma_1}, \frac{\beta_2}{\gamma_2})$, the pathogen 1 IRN ($\tilde{R}_1$) is $\frac{\beta_1}{\gamma_1}(1 - y^*)$, and pathogen 2 IRN ($\tilde{R}_2$) is $\frac{\beta_2}{\gamma_2}(1 - x^*)$, where $y^* = 1 - \frac{1}{R_2}$ and $x^* = 1 - \frac{1}{R_1}$. Notice that the BRN and IRN expressions are similar to what one expects to find in a continuous-time formulation of the coinfection models. Co-persistence of the two pathogen strains is possible if R_1, R_2, $\tilde{R}_1$, and $\tilde{R}_2$ are greater than 1. As shown in Theorem 4.6.1, it is impossible for both IRNs to be greater than 1. This means that in the limit as T approaches 0, competitive exclusion occurs if R_1 and R_2 are greater than 1.

Theorem 4.6.1. *$\tilde{R}_1$ and $\tilde{R}_2$ cannot both be greater than 1 in the limit as T approaches 0.*

Proof. Notice that $\lim_{T\to 0} \tilde{R}_1 = \lim_{T\to 0} \frac{R_1}{R_2}$, and $\lim_{T\to 0} \tilde{R}_2 = \lim_{T\to 0} \frac{R_2}{R_1}$. Consequently $\lim_{T\to 0} \tilde{R}_1 \cdot \lim_{T\to 0} \tilde{R}_2 = 1$. Since they are reciprocals of each other, they cannot both exceed 1. □

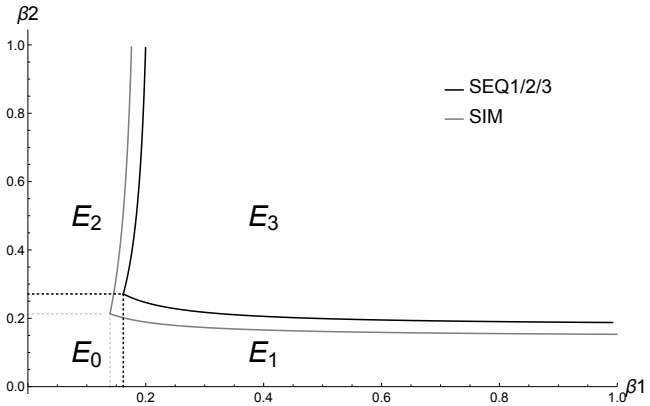

Figure 4.4: **BRN/IRN Threshold Curves β_1 vs. β_2.** In this graph, $g_1 = 0.15$, $g_2 = 0.24$, $k_1 = 0.7$ and $k_2 = 1.5$. In region E_0, we see extinction of both pathogens, in E_1, the persistence of only pathogen 1, in E_2, the persistence of only pathogen 2, and in E_3, co-persistence of both pathogens. The dotted gray box delineates the E_0 region for the SIM model while the dotted black box delineates the E_0 region for the SEQ1, SEQ2, and SEQ3 models.

4.7 RV and RSV Coinfection

We now apply the above models to describe RV and RSV circulation within a human population. RV and RSV are two of the main causes of common respiratory tract infections such as pneumonia, bronchiolitis, and the common cold. Since there are currently no vaccines for these viruses, reinfection by either pathogen, and even co-infection by both pathogens have been reported [91, 92, 93]. During co-infections, it is believed that RSV and RV behave in an antagonistic manner. This is supported by numerous studies which show that infection by one virus is associated with a reduced likelihood of infection by the other virus [92, 94, 95].

Most previous RV/RSV mathematical models have examined these viruses individually (e.g.[91, 96, 97]). The only model to consider RV and RSV coinfection [96] focuses on the within-host competition dynamics of the two viruses. There is currently no model that considers RV and RSV co-circulation at the population level. In addition, although RV and RSV hospital case reports are given in daily, weekly,

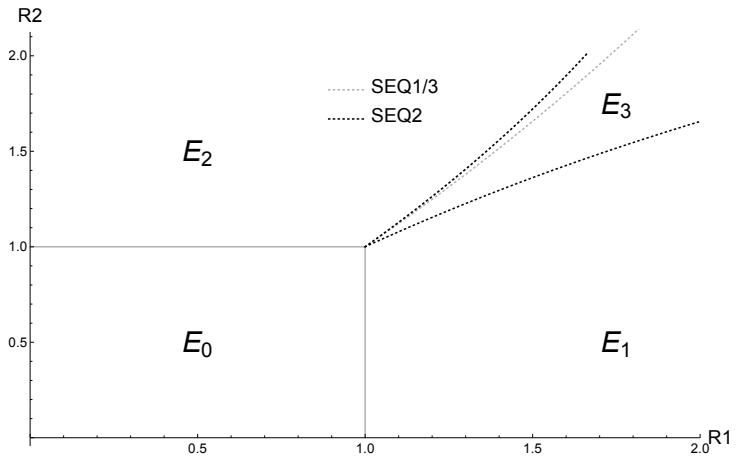

Figure 4.5: **Coexistence in SEQ Models.** The parameter values used to generate this figure are $g_1 = 0.15, g_2 = 0.24, k_1 = k_2 = 0$. With these parameter values, we witness the possibility of coexistence of the two pathogen strains in the SEQ models.

or monthly intervals as mentioned in [98, 99, 100], none of the existing models are situated in discrete time. Given the available viral infection data sets, it is natural (and one may even argue more appropriate) to consider a discrete-time model of RV and RSV as we do here.

In all of our models, pathogen 1 is taken to be RSV and pathogen 2 is RV. Most of the parameter values used in the models were obtained from previously published studies and are shown in Table 4.4. The transmission rate for RV is the average of the estimated child to child, adult to child, and adult to adult transmission rates found in [100]. Due to the inhibitory relationship between the two viruses, we take $k_i < 1, i = 1, 2$.

To illustrate the kind of variation in results that may occur when using the discrete-time models to describe RV and RSV spread, we take $k_1 = k_2 = 0.05$. The BRNs and IRNs obtained for this particular choice of k_i are in Table 4.5. These values place us within the E1 region of SEQ1 and SEQ3 and the E3 region of the SEQ2 and SIM models. While all of the models predict that RV can spread in a

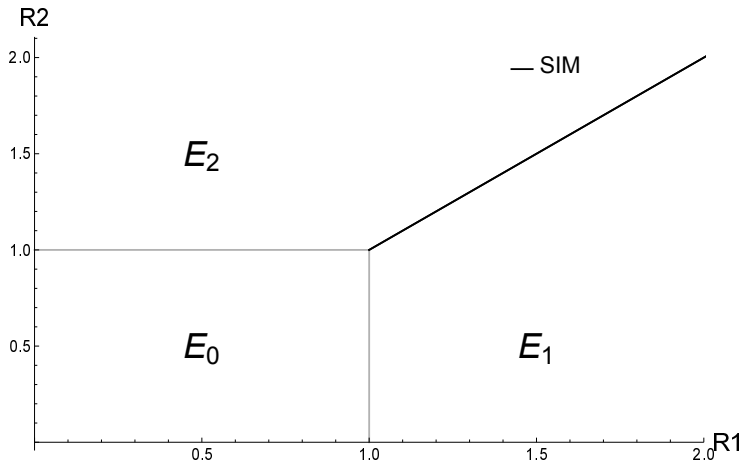

Figure 4.6: **Competitive Exclusion in SIM Model** The parameter values used to generate this figure are $g_1 = 0.15, g_2 = 0.24, k_1 = k_2 = 0$. With these parameter values, we witness competitive exclusion in the SIM model.

Symbol	Value/Range	Source
β_1	0.28 days^{-1}	[101]
β_2	0.36 days^{-1}	[100]
γ_1	0.1 days^{-1}	[99]
γ_2	0.14 days^{-1}	[102]
k_1,k_2	$(0, 1)$	Assumed

Table 4.4: **RV & RSV Parameter Values.** RSV is taken to be pathogen 1 in the discrete-time models and RV is pathogen 2.

Model	R_1	R_2	$\tilde{R}_1$	$\tilde{R}_2$
SEQ1	2.66	2.40	1.29	0.91
SEQ2	2.66	2.40	1.29	1.05
SEQ3	2.66	2.40	1.29	0.91
SIM	2.94	2.76	1.16	1.03

Table 4.5: **BRNs and IRNs for RV (pathogen 1) and RSV (pathogen 2).** Calculations use values from Table 4.4 and $k_1 = k_2 = 0.05$.

completely susceptible population, only the SEQ2 and SIM models predict that the virus will spread in a population endemic with RSV. On the other hand, the SEQ1 and SEQ3 models illustrate the unusual phenomenon that the presence of one virus (RSV) actually protects against invasion by another (RV), a phenomenon also depicted in [7] for two co-circulating HPV strains. Switching the order of RSV and RV, namely letting RSV be pathogen 2 and RV be pathogen 1 while keeping $k_1 = k_2 = 0.05$, shows that our discrete-time systems are sensitive to the order of each pathogen. In this scenario (not depicted here), the IRN for both pathogens is greater than 1 in all

of the models. Conflicting results such as these show how model assumptions about the order of disease infection and recovery events impact epidemiological conclusions.

4.8 Discussion and Concluding Remarks

Discrete-time systems are sensitive to ordering and are more prone to chaotic and other complex behavior than continuous-time models, but may nevertheless be more appropriate to describe scenarios where the biology of a system demands discrete representation. However, it is important to note that the conclusions obtained from these models depend on underlying assumptions about the sequencing of events. In this paper, we develop multiple formulations of a novel two-pathogen discrete-time coinfection model and provide a detailed analysis of how differences in the ordering of infection and recovery events impact two critical quantities, the BRN and IRN, for each pathogen. Our work is the first to extend the derivation of IRNs to discrete-time systems and to introduce a discrete-time model that assumes simultaneous occurrence of disease events.

Our results show that whether events in a discrete-time model are sequenced or not impacts the BRN and simplification of the model. Due to the order of events in the sequential models, a g_i term appears in their BRNs. This occurs because an individual must fail to recover during a time step in order to be counted in the BRN. Since events occur simultaneously in the SIM model, an infected individual does not need to evade recovery in order to be counted in the BRN, hence the lack of a g_i term in the SIM model's BRN expression. This difference in BRNs makes it possible to find parameter values such that the sequential models predict disease extinction ($R_0 < 1$) while the SIM model predicts disease invasion ($R_0 > 1$), a contradiction that can be especially alarming from a public health standpoint. In addition, the natural simplifications observed with the SEQ models and their IRNs for $k_i = 1, i = 1, 2$ are

not observed with the SIM model. Although interesting, we note that this may affect how biologically reasonable the results of the SIM model may be.

One peculiar finding of this research is the potential for the SEQ and SIM models to predict drastically different coexistence results. While all of the sequential models indicate that a region of coexistence for the two pathogen strains will always exist, the SIM model indicates that competitive exclusion occurs when the pathogens exhibit cross-immunity. The result of the SIM model under the assumption of cross-immunity is typical of autonomous continuous-time models (e.g. [103]) and resembles that of the partially ordered model in [83], where only infection events occur simultaneously. The fact that competitive exclusion is seen in both the Perez-Velazquez model and our SIM model indicates that simultaneity of infection alone is sufficient for competitive exclusion to occur. Thus, even the slightest inclusion of simultaneously occurring events is key in formulations of discrete-time models and should be explored in greater detail. Although the SIM model does not naturally simplify under certain special cases (i.e. $k_i = 1, i = 1, 2$), and analysis of the model is more complex than that of the sequential models (as seen in the IRN calculations), this formulation is important in that it preserves the competitive exclusion principle and has important consequences for disease prevention and control strategies. For example, assuming cross-immunity, the SIM model suggests that control strategies should target the pathogen that is more likely to spread, while the sequential models suggest that control aimed at both pathogens may be needed.

A possible explanation for the difference observed between the SIM and SEQ models under the assumption of complete cross-immunity can be found in the ecological framework of character displacement. This framework describes the divergence of similar species in regions where they co-exist. In order for similar species to co-exist, the theory of character displacement states that there must be some degree of

variation between them (e.g. in resource use or reproduction) [104]. This variation lessens the competition between the species and makes coexistence possible [105]. In our particular case, we believe that the ordering of events in the SEQ models results in enough variation between the two pathogens for there to be coexistence. However, due to the the simultaneous infection and recovery events in the SIM model, there is no clear distinguishing factor between the pathogens, and as a result competitive exclusion occurs.

As shown in Theorem 4.6.1, the apparent contradiction in competition dynamics between the various models is resolved in the limit as $\Delta t = T$ approaches 0. Under this scenario, all of the discrete-time models predict competitive exclusion and have BRN and IRN expressions similar to those of a continuous-time formulation of the coinfection model. This result shows that it becomes more difficult for both IRNs to exceed 1 for small time steps, and that the region of co-persistence in the R_1 vs. R_2 graphs constricts for small T. Furthermore, the result illustrates that time steps are crucial in the study of discrete-time systems since different time steps can produce fundamentally different model conclusions. In addition, the fact that all of the models behave in a similar manner in the limit as Δt approaches 0 supports the argument of character displacement as a justification for the variation observed when $\Delta t = 1$. As the time step becomes small, it is harder to separate infection and recovery events, and in turn to differentiate between the two pathogens. Therefore, the principle of competitive exclusion prevails.

Given that events in the coinfection model are ordered, our work illustrates that ordering affects the IRN but not the BRN of the two pathogens. As seen in Table 4.2, the IRN (especially the pathogen 2 IRN) is more sensitive to assumptions on the sequence of events than the BRN. This is because many factors are involved in calculating the IRN that are not needed for the BRN, factors such as whether

an individual was infected with the endemic strain at the beginning of a time step, whether he or she recovered from the endemic strain, became infected with the invading strain, etc. It is common knowledge in discrete-time mathematical modeling that ordering of events can affect important epidemiological quantities such as the BRN [74]. However, since IRNs have not been studied in discrete time until now, this research shows that ordering has implications that mathematical biologists working with discrete-time models may not previously have been aware of.

Results obtained from our various model formulations are analogous to the findings of [85] and [1] which are situated in the context of population ecology. In [85], Hilker and Liz investigate whether hydra effect, the unusual increase in a species' population size in response to an increase in its mortality rate, is impacted by the timing of harvesting and reproduction in discrete-time models of standard harvesting strategies. Through rigorous mathematical proofs, they find no qualitative distinctions between two models that differ in the ordering of harvesting and reproduction because the models essentially describe the same process (harvesting, reproduction, harvesting, reproduction, etc.). This result is further echoed in the predator-prey models of [1], where switching the order of density-dependent prey regulation and predation results in identical qualitative conclusions. In our study, we also find that when the general order of events is preserved between models, as seen in SEQ1 and SEQ3, which simply take census at different points in the process, there is no difference in the BRN or IRN of the models. However, differences become apparent when we consider the SEQ2 model which describes a completely different order than SEQ1 and SEQ3. This illustrates that the order of events in discrete-time models matters when more than two interacting events are involved, as altering the order of a subset of events can result in distinct disease cycles.

Our application of the different formulations of the discrete-time coinfection model to RSV and RV co-circulation provides a concrete illustration of the wide array of results that can be obtained from these models. Under certain assumptions, only the SEQ1 and SEQ3 models show the potential for the presence of RSV to protect a population from invasion of RV. This conclusion, however, changes with the order of each pathogen, indicating that the protective ability of RSV is only observed when it is given the advantage of infecting the population first since infection with pathogen 2 is then applied to a less receptive population. This conclusion stresses the importance of the biological assumptions embedded in mathematical models.

While this current work provides valuable insight into the dynamics of various formulations of discrete-time coinfection models, we acknowledge that the model that we propose is simplistic in nature. In reality, the dynamics of co-circulating pathogen strains can lead to complex mathematical systems, some examples of which are described in [7, 75, 106]. In our future work, we will extend this discrete-time coinfection model to incorporate various transmission routes, such as vector-borne transmission, so that it can be applicable to a wider range of diseases. We hope that this initial exploration of IRNs in discrete-time systems, and the simultaneous formulation of such systems, will serve as a catalyst for other researchers to contribute to the study of multiple-pathogen discrete-time models, paying careful attention to how model assumptions on the order of events (or the lack thereof) affect key epidemiological conclusions.

CHAPTER 5

Conclusion

In this dissertation, we analyze ZIKV transmission and multiple pathogen interactions from a mathematical modeling perspective. Our work is the first to incorporate several secondary transmission pathways of Zika, examine the dengue-Zika interplay, and extend IRNs to discrete-time models. We illustrate how some of the complexities of Zika (particularly secondary transmission pathways and cocirculation with dengue) impact the spread and control of the disease. In addition, through the coinfection models of Chapters 3 and 4, we highlight the importance of IRNs in the study of multiple interacting pathogens and their sensitivity to model assumptions (assumptions such as ADE and altered vector infectivity in Chapter 3 and ordering of discrete-time models in Chapter 4).

Although transmission via mosquito bites is known to drive Zika outbreaks, we argue that the effects of Zika's additional transmission pathways, as discussed in Chapter 2, should not be overlooked. When compared to the vector-only model, these additional pathways increase Zika's BRN by 5%, cause an outbreak to occur two weeks sooner, and result in up to 2.5 times more ZIKV infections at the peak of an outbreak. Fitting the vector-only model to initial disease incidence data, reveals that the qualitative changes on the course of an outbreak caused by secondary transmission pathways can result in an overestimation of Zika's BRN. Furthermore, neglecting these transmission mechanisms when determining the timing of control strategies may cause public health officials to delay the enactment of controls and ultimately risk increasing ZIKV infections by approximately 30%.

In Chapter 3, ADE is identified as a critical component of the dengue-Zika interplay. When comparing IRN threshold curves for these diseases, we find that ADE has a greater impact on the persistence of each disease than altered vector infectivity. Furthermore, as the effect of ADE on human infectivity increases, the region of copersistence of dengue and Zika widens dramatically. Our research also shows that ADE can be used to determine threshold conditions for when the endemic presence of one disease promotes the spread of the other. While ADE will always facilitate invasion of Zika in a dengue endemic population, its effect must be high enough (i.e. $k_d > 5.2$) for strong Zika presence to facilitate dengue spread. These results support the need for experimental studies that focus on the true impact of ADE on human dengue and Zika infectivity.

The discrete-time coinfection models in Chapter 4 show that the IRN, BRN, and competition dynamics of two cocirculating pathogens are sensitive to the order of events. It is a well-known fact that different sequences of events in discrete-time models can result in different conclusions. However, our work is the first to address the effect of sequencing on IRNs. Given that infection and recovery events are ordered, we discover that these variations do not change the BRN but do alter the IRN. Furthermore, the lack of sequencing in the SIM model results in a lower BRN than the SEQ models. This allows for the possibility of the SIM model to predict disease invasion while the SEQ models predict disease extinction. In addition, while the SEQ models predict copersistence under the assumption of complete cross-immunity, the SIM model preserves the principle of competitive exclusion. As the time step approaches zero however, we show that the SEQ models predict competitive exclusion (under cross immunity), a phenomenon that can be explained through the ecological framework of character displacement.

Combining the various chapters of this dissertation leads to two resounding conclusions on the study of Zika and use of IRNs to examine multiple pathogen interactions. From Chapters 2 and 3, it is clear that to have a better understanding of the spread of Zika, one must study the pathogen from multiple angles. Individually, these various angles reveal important aspects of the disease. For example, we find that secondary transmission pathways can be used to inform Zika control and that ADE is critical in determining how Zika fares in the presence of dengue (and vice versa). Chapters 3 and 4 illustrate the usefulness of IRNs in identifying key factors that foster invasion of a disease into areas endemic with another disease(s) and reveal the variation of IRNs with model assumptions. In Chapter 3, the IRN played a significant role in determining the impact of ADE and altered vector infectivity on dengue and Zika interactions. In addition to this, the discrete-time models in Chapter 4 show that IRNs can vary drastically with ordering assumptions.

Future extensions of this work include validating the Zika models of Chapters 2 and 3 using epidemiological data. Validation of these models will strengthen their conclusions and potentially allow them to be used to inform disease prevention and control in various countries. In addition, we hope to incorporate multiple dengue strains in studying the dengue-Zika interplay. Since there are five dengue serotypes, many of which cocirculate within the same regions, this will enable us to investigate how competition dynamics between Zika and dengue are altered by the presence of multiple dengue strains. Similar to [84], we hope to extend the discrete-time coinfection model of Chapter 4 to incorporate n pathogens ($n > 2$) so that the model can be used to describe disease transmission in regions with more than two cocirculating pathogens.

REFERENCES

[1] V. Weide, M. C. Varriale, and F. M. Hilker, "Hydra effect and paradox of enrichment in discrete-time predator-prey models," *Mathematical Biosciences*, vol. 310, pp. 120–127, 2019.

[2] World Health Organization, "A global brief on vector-borne diseases." `https://apps.who.int/iris/bitstream/handle/10665/111008/WHO_DCO_WHD_2014.1_eng.pdf?sequence=1`, 2014.

[3] D. L. Smith, K. E. Battle, S. I. Hay, C. M. Barker, T. W. Scott, and F. E. McKenzie, "Ross, Macdonald, and a theory for the dynamics and control of mosquito-transmitted pathogens," *PLOS Pathogens*, vol. 8, no. 4, p. e1002588, 2012.

[4] T. C. Pierson and M. S. Diamond, "The emergence of Zika virus and its new clinical syndromes," *Nature*, vol. 560, no. 7720, p. 573, 2018.

[5] S. Thangamani, J. Huang, C. E. Hart, H. Guzman, and R. B. Tesh, "Vertical transmission of Zika virus in *Aedes aegypti* mosquitoes," *The American Journal of Tropical Medicine and Hygiene*, vol. 95, no. 5, pp. 1169–1173, 2016.

[6] T. C. Porco and S. M. Blower, "Designing HIV vaccination policies: subtypes and cross-immunity," *Interfaces*, vol. 28, no. 3, pp. 167–190, 1998.

[7] B. Crawford and C. M. Kribs, "The impact of vaccination and coinfection on HPV and cervical cancer," *Discrete and Continuous Dynamical Systems Series B*, vol. 12, no. 2, pp. 279–304, 2009.

[8] M. Martcheva and S. S. Pilyugin, "The role of coinfection in multidisease dynamics," *SIAM Journal on Applied Mathematics*, vol. 66, no. 3, pp. 843–872, 2006.

[9] M. Nuno, G. Chowell, X. Wang, and C. Castillo-Chavez, "On the role of cross-immunity and vaccines on the survival of less fit flu-strains," *Theoretical Population Biology*, vol. 71, no. 1, pp. 20–29, 2007.

[10] D. Gao, Y. Lou, D. He, T. C. Porco, Y. Kuang, G. Chowell, and S. Ruan, "Prevention and control of Zika as a mosquito-borne and sexually transmitted disease: a mathematical modeling analysis," *Scientific Reports*, vol. 6, p. 28070, 2016.

[11] Pan American Health Organization and World Health Organization, "Zika suspected and confirmed cases reported by countries and territories in the Americas cumulative cases, 2015-2017." `https://www.paho.org/hq/dmdocuments/2017/2017-jan-27-phe-ZIKV-cases.pdf`, 2017.

[12] R. Hamel, F. Liégeois, S. Wichit, J. Pompon, F. Diop, L. Talignani, F. Thomas, P. Desprès, H. Yssel, and D. Missé, "Zika virus: epidemiology, clinical features and host-virus interactions," *Microbes and Infection*, vol. 18, no. 7-8, pp. 441–449, 2016.

[13] R. Leon, "Sexual transmission of dengue viruses by *Aedes albopictus*," *The American Journal of Tropical Medicine and Hygiene*, vol. 37, no. 2, pp. 398–402, 1987.

[14] C. Manore and M. Hyman, "Mathematical models for fighting Zika virus," *Siam News, Philadelphia*, 2016.

[15] A. J. Kucharski, S. Funk, R. M. Eggo, H.-P. Mallet, W. J. Edmunds, and E. J. Nilles, "Transmission dynamics of Zika virus in island populations: a

modelling analysis of the 2013–14 French Polynesia outbreak," *PLoS Negl Trop Dis*, vol. 10, no. 5, p. e0004726, 2016.

[16] S. Towers, F. Brauer, C. Castillo-Chavez, A. K. Falconar, A. Mubayi, and C. M. Romero-Vivas, "Estimate of the reproduction number of the 2015 Zika virus outbreak in Barranquilla, Colombia, and estimation of the relative role of sexual transmission," *Epidemics*, vol. 17, pp. 50–55, 2016.

[17] O. Maxian, A. Neufeld, E. J. Talis, L. M. Childs, and J. C. Blackwood, "Zika virus dynamics: When does sexual transmission matter?," *Epidemics*, vol. 21, pp. 48–55, 2017.

[18] D. Baca-Carrasco and J. X. Velasco-Hernández, "Sex, mosquitoes and epidemics: an evaluation of zika disease dynamics," *Bulletin of Mathematical Biology*, vol. 78, no. 11, pp. 2228–2242, 2016.

[19] S. Bewick, W. F. Fagan, J. M. Calabrese, and F. Agusto, "Zika virus: endemic versus epidemic dynamics and implications for disease spread in the Americas," *bioRxiv*, p. 041897, 2016.

[20] A. Lloyd, "Sensitivity of model-based epidemiological parameter estimation to model assumptions," in *Mathematical and Statistical Estimation Approaches in Epidemiology*, pp. 123–141, Springer, 2009.

[21] M. A. Nowak, A. L. Lloyd, G. M. Vasquez, T. A. Wiltrout, L. M. Wahl, N. Bischofberger, J. Williams, A. Kinter, A. S. Fauci, V. M. Hirsch, *et al.*, "Viral dynamics of primary viremia and antiretroviral therapy in simian immunodeficiency virus infection.," *Journal of Virology*, vol. 71, no. 10, pp. 7518–7525, 1997.

[22] A. L. Lloyd, "The dependence of viral parameter estimates on the assumed viral life cycle: limitations of studies of viral load data," *Proceedings of the Royal Society of London B: Biological Sciences*, vol. 268, no. 1469, pp. 847–854, 2001.

[23] H. J. Wearing, P. Rohani, and M. J. Keeling, "Appropriate models for the management of infectious diseases," *PLoS Medicine*, vol. 2, no. 7, p. e174, 2005.

[24] D. P. Shutt, C. A. Manore, S. Pankavich, A. T. Porter, and S. Y. Del Valle, "Estimating the reproductive number, total outbreak size, and reporting rates for Zika epidemics in South and Central America," *Epidemics*, vol. 21, pp. 63–79, 2017.

[25] T. Fréour, S. Mirallié, B. Hubert, C. Splingart, P. Barrière, M. Maquart, and I. Leparc-Goffart, "Sexual transmission of Zika virus in an entirely asymptomatic couple returning from a Zika epidemic area, France, April 2016," *Eurosurveillance*, vol. 21, no. 23, 2016.

[26] B. E. Dawes, C. A. Smalley, B. L. Tiner, D. W. Beasley, G. N. Milligan, L. M. Reece, J. Hombach, and A. D. Barrett, "Research and development of Zika virus vaccines," *npj Vaccines*, vol. 1, p. 16007, 2016.

[27] A. Fagbami, "Zika virus infections in Nigeria: virological and seroepidemiological investigations in Oyo State," *Journal of Hygiene*, vol. 83, no. 02, pp. 213–219, 1979.

[28] D. M. Dudley, M. T. Aliota, E. L. Mohr, A. M. Weiler, G. Lehrer-Brey, K. L. Weisgrau, M. S. Mohns, M. E. Breitbach, M. N. Rasheed, C. M. Newman, *et al.*, "A rhesus macaque model of asian-lineage Zika virus infection," *Nature Communications*, vol. 7, 2016.

[29] E. S. Paixão, F. Barreto, M. da Glória Teixeira, M. da Conceição N. Costa, and L. C. Rodrigues, "History, epidemiology, and clinical manifestations of Zika: a systematic review," *American Journal of Public Health*, vol. 106, no. 4, pp. 606–612, 2016.

[30] V. Duong, L. Lambrechts, R. E. Paul, S. Ly, R. S. Lay, K. C. Long, R. Huy, A. Tarantola, T. W. Scott, A. Sakuntabhai, *et al.*, "Asymptomatic humans

transmit dengue virus to mosquitoes," *Proceedings of the National Academy of Sciences*, vol. 112, no. 47, pp. 14688–14693, 2015.

[31] W. H. Thompson and B. J. Beaty, "Venereal transmission of La Crosse virus from male to female *Aedes triseriatus.*," *The American Journal of Tropical Medicine and Hygiene*, vol. 27, no. 1 Pt 1, pp. 187–196, 1978.

[32] D. Musso and D. J. Gubler, "Zika virus," *Clinical Microbiology Reviews*, vol. 29, no. 3, pp. 487–524, 2016.

[33] M. Aubry, V. Richard, J. Green, J. Broult, and D. Musso, "Inactivation of Zika virus in plasma with amotosalen and ultraviolet a illumination," *Transfusion*, vol. 56, no. 1, pp. 33–40, 2016.

[34] D. Focks, S. Sackett, D. L. Bailey, and D. Dame, "Observations on container-breeding mosquitoes in New Orleans, Louisiana, with an estimate of the population density of *Aedes aegypti*(l.)," *The American Journal of Tropical Medicine and Hygiene*, vol. 30, no. 6, pp. 1329–1335, 1981.

[35] C. R. Williams, P. Johnson, T. Ball, and S. Ritchie, "Productivity and population density estimates of the dengue vector mosquito *Aedes aegypti* (*Stegomyia aegypti*) in Australia," *Medical and Veterinary Entomology*, vol. 27, no. 3, pp. 313–322, 2013.

[36] S. A. Ritchie, B. L. Montgomery, and A. A. Hoffmann, "Novel estimates of *Aedes aegypti* (Diptera: Culicidae) population size and adult survival based on Wolbachia releases," *Journal of Medical Entomology*, vol. 50, no. 3, pp. 624–631, 2013.

[37] C. A. Manore, K. S. Hickmann, S. Xu, H. J. Wearing, and J. M. Hyman, "Comparing dengue and chikungunya emergence and endemic transmission in *Aedes aegypti* and *Aedes albopictus*," *Journal of Theoretical Biology*, vol. 356, pp. 174–191, 2014.

[38] A. T. Ciota, S. M. Bialosuknia, D. J. Ehrbar, and L. D. Kramer, "Vertical transmission of Zika virus by *Aedes aegypti* and *Aedes albopictus* mosquitoes," *Emerging Infectious Diseases*, vol. 23, no. 5, p. 880, 2017.

[39] H. Yang, M. d. L. d. G. Macoris, K. Galvani, M. Andrighetti, and D. Wanderley, "Assessing the effects of temperature on the population of *Aedes aegypti*, the vector of dengue," *Epidemiology & Infection*, vol. 137, no. 8, pp. 1188–1202, 2009.

[40] L. Esteva and H. M. Yang, "Mathematical model to assess the control of *Aedes aegypti* mosquitoes by the sterile insect technique," *Mathematical Biosciences*, vol. 198, no. 2, pp. 132–147, 2005.

[41] B. Byttebier, M. S. De Majo, and S. Fischer, "Hatching response of *Aedes aegypti* (Diptera: Culicidae) eggs at low temperatures: Effects of hatching media and storage conditions," *Journal of Medical Entomology*, vol. 51, no. 1, pp. 97–103, 2014.

[42] O. Diekmann, J. A. P. Heesterbeek, and J. A. Metz, "On the definition and the computation of the basic reproduction ratio R0 in models for infectious diseases in heterogeneous populations," *Journal of Mathematical Biology*, vol. 28, no. 4, pp. 365–382, 1990.

[43] L. Arriola and J. M. Hyman, "Sensitivity analysis for uncertainty quantification in mathematical models," in *Mathematical and Statistical Estimation Approaches in Epidemiology*, pp. 195–247, Springer, 2009.

[44] World Health Organization and Special Programme for Research and Training in Tropical Diseases, *Dengue: guidelines for diagnosis, treatment, prevention and control*. World Health Organization, 2009.

[45] World Health Organization, "Global strategy for dengue prevention and control 2012–2020," *WHO Library Cataloguing-in-Publication Data, Switzerland*, 2012.

[46] K. Kumar, P. K. Singh, J. Tomar, and S. Baijal, "Dengue: epidemiology, prevention and pressing need for vaccine development," *Asian Pacific Journal of Tropical Medicine*, vol. 3, no. 12, pp. 997–1000, 2010.

[47] M. Mustafa, V. Rasotgi, S. Jain, and V. Gupta, "Discovery of fifth serotype of dengue virus (denv-5): A new public health dilemma in dengue control," *Medical Journal Armed Forces India*, vol. 71, no. 1, pp. 67–70, 2015.

[48] M. Dupont-Rouzeyrol, O. O'Connor, E. Calvez, M. Daures, M. John, J.-P. Grangeon, and A.-C. Gourinat, "Co-infection with Zika and dengue viruses in 2 patients, New Caledonia, 2014," *Emerging Infectious Diseases*, vol. 21, no. 2, p. 381, 2015.

[49] M. Y. Carrillo-Hernández, J. Ruiz-Saenz, L. J. Villamizar, S. Y. Gómez-Rangel, and M. Martínez-Gutierrez, "Co-circulation and simultaneous co-infection of dengue, chikungunya, and Zika viruses in patients with febrile syndrome at the Colombian-Venezuelan border," *BMC Infectious Diseases*, vol. 18, no. 1, p. 61, 2018.

[50] J. J. Waggoner, L. Gresh, M. J. Vargas, G. Ballesteros, Y. Tellez, K. J. Soda, M. K. Sahoo, A. Nuñez, A. Balmaseda, E. Harris, *et al.*, "Viremia and clinical presentation in Nicaraguan patients infected with Zika virus, chikungunya virus, and dengue virus," *Clinical Infectious Diseases*, p. ciw589, 2016.

[51] N. M. Iovine, J. Lednicky, K. Cherabuddi, H. Crooke, S. K. White, J. C. Loeb, E. Cella, M. Ciccozzi, M. Salemi, and J. G. Morris Jr, "Coinfection with Zika and dengue-2 viruses in a traveler returning from Haiti, 2016: clinical presentation and genetic analysis," *Clinical Infectious Diseases*, p. ciw667, 2016.

[52] C. Rückert, J. Weger-Lucarelli, S. M. Garcia-Luna, M. C. Young, A. D. Byas, R. A. Murrieta, J. R. Fauver, and G. D. Ebel, "Impact of simultaneous exposure

to arboviruses on infection and transmission by *Aedes aegypti* mosquitoes," *Nature Communications*, vol. 8, p. 15412, 2017.

[53] E. P. Abrao and B. A. L. da Fonseca, "Infection of mosquito cells (c6/36) by dengue-2 virus interferes with subsequent infection by yellow fever virus," *Vector-Borne and Zoonotic Diseases*, vol. 16, no. 2, pp. 124–130, 2016.

[54] T. Magalhaes, A. Robison, M. Young, W. Black, B. Foy, G. Ebel, and C. Rückert, "Sequential infection of *Aedes aegypti* mosquitoes with chikungunya virus and Zika virus enhances early Zika virus transmission," *Insects*, vol. 9, no. 4, p. 177, 2018.

[55] B. A. Chaves, A. S. Orfano, P. M. Nogueira, N. B. Rodrigues, T. B. Campolina, R. Nacif-Pimenta, A. C. A. M. Pires, A. B. V. Júnior, A. Paz, E. Vaz, *et al.*, "Coinfection with Zika virus (ZIKV) and dengue virus results in preferential ZIKV transmission by vector bite to vertebrate host," *The Journal of Infectious Diseases*, 2018.

[56] S. S. Whitehead, J. E. Blaney, A. P. Durbin, and B. R. Murphy, "Prospects for a dengue virus vaccine," *Nature Reviews Microbiology*, vol. 5, no. 7, p. 518, 2007.

[57] L. M. Paul, E. R. Carlin, M. M. Jenkins, A. L. Tan, C. M. Barcellona, C. O. Nicholson, S. F. Michael, and S. Isern, "Dengue virus antibodies enhance Zika virus infection," *Clinical & Translational Immunology*, vol. 5, no. 12, p. e117, 2016.

[58] A. S. Charles and R. C. Christofferson, "Utility of a dengue-derived monoclonal antibody to enhance Zika infection in vitro," *PLoS Currents*, vol. 8, 2016.

[59] W. Dejnirattisai, P. Supasa, W. Wongwiwat, A. Rouvinski, G. Barba-Spaeth, T. Duangchinda, A. Sakuntabhai, V.-M. Cao-Lormeau, P. Malasit, F. A. Rey, *et al.*, "Dengue virus sero-cross-reactivity drives antibody-dependent enhance-

ment of infection with Zika virus," *Nature Immunology*, vol. 17, no. 9, p. 1102, 2016.

[60] A. P. Durbin, "Dengue antibody and Zika: Friend or foe?," *Trends in Immunology*, vol. 37, no. 10, pp. 635–636, 2016.

[61] A. B. Kawiecki and R. C. Christofferson, "Zika virus–induced antibody response enhances dengue virus serotype 2 replication in vitro," *The Journal of Infectious Diseases*, vol. 214, no. 9, pp. 1357–1360, 2016.

[62] K. Stettler, M. Beltramello, D. A. Espinosa, V. Graham, A. Cassotta, S. Bianchi, F. Vanzetta, A. Minola, S. Jaconi, F. Mele, *et al.*, "Specificity, cross-reactivity and function of antibodies elicited by Zika virus infection," *Science*, p. aaf8505, 2016.

[63] M. Andraud, N. Hens, C. Marais, and P. Beutels, "Dynamic epidemiological models for dengue transmission: a systematic review of structural approaches," *PloS ONE*, vol. 7, no. 11, p. e49085, 2012.

[64] J. P. Braselton and I. Bakach, "A survey of mathematical models of dengue fever," *Journal of Computer Science Systems Biology*, vol. 8, no. 5, p. 255, 2015.

[65] A. Wiratsudakul, P. Suparit, and C. Modchang, "Dynamics of Zika virus outbreaks: an overview of mathematical modeling approaches," *PeerJ*, vol. 6, p. e4526, 2018.

[66] R. Isea and K. E. Lonngren, "A preliminary mathematical model for the dynamic transmission of dengue, chikungunya and Zika," *American Journal of Modern Physics and Application*, vol. 3, pp. 11–15, 2016.

[67] K. O. Okuneye, J. X. Velasco-Hernandez, and A. B. Gumel, "The "unhol" chikungunya–dengue–Zika trinity: A theoretical analysis," *Journal of Biological Systems*, vol. 25, no. 04, pp. 545–585, 2017.

[68] G. H. Moraes, E. de Fátima Duarte, and E. C. Duarte, "Determinants of mortality from severe dengue in Brazil: a population-based case-control study," *The American Journal of Tropical Medicine and Hygiene*, vol. 88, no. 4, pp. 670–676, 2013.

[69] Pan American Health Organization, "Provisional remarks on Zika virus infection in pregnant women: document for health care professionals." `http://iris.paho.org/xmlui/handle/123456789/18600`, 2016.

[70] O. Olawoyin and C. Kribs, "Effects of multiple transmission pathways on Zika dynamics," *Infectious Disease Modelling*, vol. 3, pp. 331–344, 2018.

[71] P. van den Driessche and J. Watmough, "Reproduction numbers and subthreshold endemic equilibria for compartmental models of disease transmission," *Mathematical Biosciences*, vol. 180, no. 1-2, pp. 29–48, 2002.

[72] L. J. Allen, "Some discrete-time SI, SIR, and SIS epidemic models," *Mathematical Biosciences*, vol. 124, no. 1, pp. 83–105, 1994.

[73] L. J. Allen and P. van den Driessche, "The basic reproduction number in some discrete-time epidemic models," *Journal of Difference Equations and Applications*, vol. 14, no. 10-11, pp. 1127–1147, 2008.

[74] M. A. Lewis, J. Rencławowicz, P. van den Driessche, and M. Wonham, "A comparison of continuous and discrete-time west nile virus models," *Bulletin of Mathematical Biology*, vol. 68, no. 3, pp. 491–509, 2006.

[75] Z. Qiu, Q. Kong, X. Li, and M. Martcheva, "The vector–host epidemic model with multiple strains in a patchy environment," *Journal of Mathematical Analysis and Applications*, vol. 405, no. 1, pp. 12–36, 2013.

[76] N. Hernandez-Ceron, Z. Feng, and P. van den Driessche, "Reproduction numbers for discrete-time epidemic models with arbitrary stage distributions," *Jour-*

nal of Difference Equations and Applications, vol. 19, no. 10, pp. 1671–1693, 2013.

[77] P. Zhang, G. J. Sandland, Z. Feng, D. Xu, and D. J. Minchella, "Evolutionary implications for interactions between multiple strains of host and parasite," *Journal of Theoretical Biology*, vol. 248, no. 2, pp. 225–240, 2007.

[78] M. P. Hassell and H. N. Comins, "Discrete time models for two-species competition," *Theoretical Population Biology*, vol. 9, no. 2, pp. 202–221, 1976.

[79] H. L. Smith and X.-Q. Zhao, "Competitive exclusion in a discrete-time, size-structured chemostat model," *Discrete and Continuous Dynamical Systems, Series B*, vol. 1, no. 2, pp. 183–191, 2001.

[80] J. E. Franke and A.-A. Yakubu, "Mutual exclusion versus coexistence for discrete competitive systems," *Journal of Mathematical Biology*, vol. 30, no. 2, pp. 161–168, 1991.

[81] J. M. Cushing, S. Levarge, N. Chitnis, and S. M. Henson, "Some discrete competition models and the competitive exclusion principle," *Journal of difference Equations and Applications*, vol. 10, no. 13-15, pp. 1139–1151, 2004.

[82] J. Edmunds, J. M. Cushing, R. F. Costantino, S. M. Henson, B. Dennis, and R. A. Desharnais, "Park's Tribolium competition experiments: a non-equilibrium species coexistence hypothesis," *Journal of Animal Ecology*, vol. 72, no. 5, pp. 703–712, 2003.

[83] J. Perez-Velazquez, "Competitive exclusion in a discrete-time epidemic model with two competing strains," Tech. Rep. BU-1514-M, Biometric Department, MTBI Cornell University, 01 1999.

[84] L. J. Allen, N. Kirupaharan, and S. M. Wilson, "SIS epidemic models with multiple pathogen strains," *Journal of Difference Equations and Applications*, vol. 10, no. 1, pp. 53–75, 2004.

[85] F. M. Hilker and E. Liz, "Harvesting, census timing and "hidden" hydra effects," *Ecological Complexity*, vol. 14, pp. 95–107, 2013.

[86] P. Klepac and H. Caswell, "The stage-structured epidemic: linking disease and demography with a multi-state matrix approach model," *Theoretical Ecology*, vol. 4, no. 3, pp. 301–319, 2011.

[87] R. Bravo de la Parra, M. Marvá, E. Sánchez, and L. Sanz, "Discrete models of disease and competition," *Discrete Dynamics in Nature and Society*, vol. 2017, 2017.

[88] C. Castillo-Chavez and A.-A. Yakubu, "Dispersal, disease and life-history evolution," *Mathematical Biosciences*, vol. 173, no. 1, pp. 35–53, 2001.

[89] F. Brauer and C. Kribs, *Dynamical systems for biological modeling: An introduction*. CRC Press, 2015.

[90] C. M. Kribs and C. Mitchell, "Host switching vs. host sharing in overlapping sylvatic *Trypanosoma cruzi* transmission cycles," *Journal of Biological Dynamics*, vol. 9, no. 1, pp. 247–277, 2015.

[91] A. B. Hogan, K. Glass, H. C. Moore, and R. S. Anderssen, "Exploring the dynamics of respiratory syncytial virus (RSV) transmission in children," *Theoretical Population Biology*, vol. 110, pp. 78–85, 2016.

[92] R. M. Greer, P. McErlean, K. E. Arden, C. E. Faux, A. Nitsche, S. B. Lambert, M. D. Nissen, T. P. Sloots, and I. M. Mackay, "Do rhinoviruses reduce the probability of viral co-detection during acute respiratory tract infections?," *Journal of Clinical Virology*, vol. 45, no. 1, pp. 10–15, 2009.

[93] K. T. Zlateva, J. J. de Vries, F. E. Coenjaerts, A. M. van Loon, T. Verheij, P. Little, C. C. Butler, H. Goossens, M. Ieven, and E. C. Claas, "Prolonged shedding of rhinovirus and re-infection in adults with respiratory tract illness," *European Respiratory Journal*, pp. erj01721–2013, 2014.

[94] S. Karppinen, L. Toivonen, L. Schuez-Havupalo, M. Waris, and V. Peltola, "Interference between respiratory syncytial virus and rhinovirus in respiratory tract infections in children," *Clinical Microbiology and Infection*, vol. 22, no. 2, pp. 208–e1, 2016.

[95] E. T. Martin, M. P. Fairchok, Z. J. Stednick, J. Kuypers, and J. A. Englund, "Epidemiology of multiple respiratory viruses in childcare attendees," *The Journal of Infectious Diseases*, vol. 207, no. 6, pp. 982–989, 2013.

[96] L. Pinky and H. M. Dobrovolny, "Coinfections of the respiratory tract: viral competition for resources," *PLOS ONE*, vol. 11, no. 5, p. e0155589, 2016.

[97] F. R. Adler and P. S. Kim, "Models of contrasting strategies of rhinovirus immune manipulation," *Journal of Theoretical Biology*, vol. 327, pp. 1–10, 2013.

[98] M. Leecaster, P. Gesteland, T. Greene, N. Walton, A. Gundlapalli, R. Rolfs, C. Byington, and M. Samore, "Modeling the variations in pediatric respiratory syncytial virus seasonal epidemics," *BMC Infectious Diseases*, vol. 11, no. 1, p. 105, 2011.

[99] A. Weber, M. Weber, and P. Milligan, "Modeling epidemics caused by respiratory syncytial virus (RSV)," *Mathematical Biosciences*, vol. 172, no. 2, pp. 95–113, 2001.

[100] R. M. Eggo, J. G. Scott, A. P. Galvani, and L. A. Meyers, "Respiratory virus transmission dynamics determine timing of asthma exacerbation peaks: evidence from a population-level model," *Proceedings of the National Academy of Sciences*, p. 201518677, 2016.

[101] H. C. Moore, P. Jacoby, A. B. Hogan, C. C. Blyth, and G. N. Mercer, "Modelling the seasonal epidemics of respiratory syncytial virus in young children," *PLOS ONE*, vol. 9, no. 6, p. e100422, 2014.

[102] J. M. Gwaltney, J. O. Hendley, G. Simon, and W. S. Jordan, "Rhinovirus infections in an industrial population: Ii. characteristics of illness and antibody response," *JAMA*, vol. 202, no. 6, pp. 494–500, 1967.

[103] P. Pelosse and C. M. Kribs, "The role of the ratio of vector and host densities in the evolution of transmission modes in vector-borne diseases. the example of sylvatic *Trypanosoma cruzi*," *Journal of Theoretical Biology*, vol. 312, pp. 133–142, 2012.

[104] W. L. Brown and E. O. Wilson, "Character displacement," *Systematic Zoology*, vol. 5, no. 2, pp. 49–64, 1956.

[105] K. S. Pfennig and D. W. Pfennig, "Character displacement: ecological and reproductive responses to a common evolutionary problem," *The Quarterly Review of Biology*, vol. 84, no. 3, pp. 253–276, 2009.

[106] C. M. Kribs and A. Mubayi, "The role of adaptations in two-strain competition for sylvatic *Trypanosoma cruzi* transmission," *Journal of Biological Dynamics*, vol. 6, no. 2, pp. 813–835, 2012.

APPENDIX A

A.1 Proof of Lemma 3.3.1

Proof. A brief inspection of the dengue-only equilibrium reveals that this equilibrium point exists (i.e. consists of nonnegative terms) iff $I_d^* > 0$. Notice that

$$\begin{aligned}
I_d^* &> 0 \iff \\
\tfrac{\mu N_h(\beta_{hd}\beta_{vd}N_v - \mu_v N_h(\gamma_d+\mu))}{\beta_{vd}(\gamma_d+\mu)(\mu N_h+\beta_{hd}N_v)} &> 0 \iff \\
\mu N_h(\beta_{hd}\beta_{vd}N_v - \mu_v N_h(\gamma_d+\mu)) &> 0 \iff \\
\mu N_h\beta_{hd}\beta_{vd}N_v &> \mu\mu_v N_h^2(\gamma_d+\mu) \iff \\
\tfrac{\mu N_h\beta_{hd}\beta_{vd}N_v}{\mu\mu_v N_h^2(\gamma_d+\mu)} &> 1 \iff \\
\tfrac{N_v}{N_h}\tfrac{\beta_{vd}}{\mu_v}\tfrac{\beta_{hd}}{\mu+\gamma_d} &> 1 \iff \\
\sqrt{\tfrac{N_v}{N_h}\tfrac{\beta_{vd}}{\mu_v}\tfrac{\beta_{hd}}{\mu+\gamma_d}} &> 1.
\end{aligned}$$

Thus, a unique dengue-only equilibrium exists iff $R_d > 1$. □

APPENDIX B

B.1 Formulation of SEQ1 Model

For the SEQ1 model, let t_1, t_2, t_3, and $t_4 = t + 1$ represent the time when infection with pathogen 1, infection with pathogen 2, recovery from pathogen 1, and recovery from pathogen 2 occur respectively, with $t < t_1 < t_2 < t_3 < t_4$. In addition, let $y(t_i) = \frac{I_2(t_i)+I_{12}(t_i)}{N}$. The system of difference equations obtained after infection with pathogen 1 is

$$\begin{aligned} S(t_1) &= S(t)b_1^{x(t)} \\ I_1(t_1) &= S(t)(1 - b_1^{x(t)}) + I_1(t) \\ I_2(t_1) &= I_2(t)b_1^{k_1 x(t)} \\ I_{12}(t_1) &= I_2(t)(1 - b_1^{k_1 x(t)}) + I_{12}(t). \end{aligned}$$

After infection with pathogen 2 we have,

$$\begin{aligned} S(t_2) &= S(t_1)b_2^{y(t_1)} \\ I_1(t_2) &= I_1(t_1)b_2^{k_2 y(t_1)} \\ I_2(t_2) &= I_2(t_1) + S(t_1)(1 - b_2^{y(t_1)}) \\ I_{12}(t_2) &= I_{12}(t_1) + I_1(t_1)(1 - b_2^{k_2 y(t_1)}). \end{aligned}$$

After recovery from pathogen 1, we obtain

$$\begin{aligned} S(t_3) &= S(t_2) + I_1(t_2)(1 - g_1) \\ I_1(t_3) &= I_1(t_2)g_1 \\ I_2(t_3) &= I_2(t_2) + I_{12}(t_2)(1 - g_1) \\ I_{12}(t_3) &= I_{12}(t_2)g_1. \end{aligned}$$

After recovery from pathogen 2, we have

$$S(t_4) = S(t_3) + I_2(t_3)(1 - g_2)$$

$$I_1(t_4) = I_1(t_3) + I_{12}(t_3)(1 - g_2)$$

$$I_2(t_4) = I_2(t_3)g_2$$

$$I_{12}(t_4) = I_{12}(t_3)g_2.$$

Since $y(t_1) = y(t)$, the system of equations for the SEQ1 model can be written as

$$\begin{aligned}
S(t+1) &= S(t_3)b_1^{x(t)}b_2^{y(t)} + (I_1(t) + S(t)(1 - b_1^{x(t)}))b_2^{k_2 y(t)}(1 - g_1) \\
&\quad + [I_2(t)b_1^{k_1 x(t)} + S(t)b_1^{x(t)}(1 - b_2^{y(t)}) + (I_{12}(t) + I_2(t)(1 - b_1^{k_1 x(t)}) \\
&\quad + (I_1(t) + S(t)(1 - b_1^{x(t)}))(1 - b_2^{k_2 y(t)}))(1 - g_1)](1 - g_2) \\
I_1(t+1) &= (I_1(t) + S(t)(1 - b_1^{x(t)}))b_2^{k_2 y(t)} g_1 \\
&\quad + [(I_{12}(t) + I_2(t)(1 - b_1^{k_1 x(t)}) + (I_1(t) + S(t)(1 - b_1^{x(t)}))(1 - b_2^{k_2 y(t)}))g_1](1 - g_2) \\
I_2(t+1) &= [I_2(t)b_1^{k_1 x(t)} + S(t)b_1^{x(t)}(1 - b_2^{y(t)}) + (I_{12}(t) + I_2(t)(1 - b_1^{k_1 x(t)}) \\
&\quad + (I_1(t) + S(t)(1 - b_1^{x(t)}))(1 - b_2^{k_2 y(t)}))(1 - g_1)]g_2 \\
I_{12}(t+1) &= [(I_{12}(t) + I_2(t)(1 - b_1^{k_1 x(t)}) + (I_1(t) + S(t)(1 - b_1^{x(t)}))(1 - b_2^{k_2 y(t)}))]g_1 g_2.
\end{aligned} \tag{B.1}$$

The system of difference equations for the SEQ2 and SEQ3 models can be obtained step-by-step in a similar fashion.

B.2 Endemic Equilibrium

To find the pathogen 1 endemic equilibrium for the SIM model, we set $I_1 = I_{12} = 0$. With this, the system of equations for the SIM model becomes

$$I_1(t+1) = (N - I_1(t))(1 - b_1^{\frac{I_1(t)}{N}}) + I_1(t)g_1.$$

The fixed point condition

$$I_1^* = (N - I_1^*)(1 - b_1^{\frac{I_1^*}{N}}) + I_1^* g_1$$

can be rewritten as

$$(N - I_1^*) = I_1^* \frac{1 - g_1}{(1 - b_1^{\frac{I_1^*}{N}})}$$

(or else $I_1^* = 0$). Adding I_1^* to both sides and dividing by N yields

$$f(x) = x \left(1 + \frac{1 - g_1}{(1 - b_1^x)}\right) = 1,$$

where $x = \frac{I_1^*}{N}$.

Differentiating with respect to x, we have

$$f'(x) = 1 + \frac{(1 - g_1)}{(1 - b_1^x)^2}[1 - b_1^x + b_1^x \log b_1^x].$$

The last term, $h(b_1^x)$ where $h(y) = 1 - y + y \log y$, is positive since $h'(y) = \log y < 0$ on (0,1) and $h(1) = 0$ (note $0 < b_1^x < 1$)). Thus, $f'(x) > 0$ on $(0, 1)$, meaning that f is monotone increasing within that interval.

Since f is positive and increasing on (0,1) and $f(1) > 1$, $f(x) = 1$ has a unique solution in (0,1) if and only if $\lim_{x \to 0^+} f(x) = \frac{1-g_1}{-\log b_1} < 1$. Thus, a unique pathogen 1 endemic equilibrium (and hence a unique root of f) exists if and only if $1 - g_1 < -\log b_1 = \beta_1$, which is equivalent to $R_{1_s} = \frac{\beta_1}{1-g_1} > 1$.

Proof of a unique pathogen 2 endemic equilibrium for the SIM model as well as of a unique pathogen 1 and pathogen 2 endemic equilibria for the SEQ1, 2, and 3 models (and their simplified versions (4.5), (4.6), (4.9), and (4.10)) can be obtained using a similar approach.

B.3 SEQ1 & SEQ2 $\tilde{R}_2$ Threshold Curve

To prove that $\tilde{R}_{2_2} > \tilde{R}_{2_1}$ iff (if and only if) $k_2 < 1$, notice the following sequence of inequalities which follow iff the previous inequality is satisfied:

$$\begin{aligned}
\tilde{R}_{2_2} &> \tilde{R}_{2_1} \\
R_{2_1} &> \tilde{R}_{2_1} \\
R_{2_1} - \tilde{R}_{2_1} &> 0 \\
R_{2_1} - R_{2_1}[(1-x^*)b_1x^*(1-k_2)+k_2] &> 0 \\
R_{2_1}[(1-k_2) - (1-x^*)b_1x^*(1-k_2)] &> 0 \\
R_{2_1}[(1-k_2)(1-(1-x^*)b_1x^*] &> 0 \\
1-k_2 &> 0 \\
k_2 &< 1.
\end{aligned}$$

A similar proof can be given to show $\tilde{R}_{2_2} < \tilde{R}_{2_1}$ iff$k_2 > 1$

B.4 SEQ1 & SEQ3 IRN Expressions

Since $R_{1_1} = R_{1_3}$, we will prove that the SEQ1 and SEQ3 $\tilde{R}_1$ equations are identical by showing that $y_1^* = y_3^* g_2$, where $y_1^* \in (0,1)$ is the unique root of $y\left(1 + \frac{(1-g_2)}{(1-b_2^y)g_2}\right) = 1$ and $y_3^* \in (0,1)$ is the unique root of $y\left(1 + \frac{(1-g_2)b_2^{yg_2}}{(1-b_2^{yg_2})}\right) = 1$ (uniqueness of these roots is discussed in Appendix B.2).

To see this, note that

$$\begin{aligned}
1 &= y_3^* \left(1 + \frac{(1-g_2) b_2^{y_3^* g_2}}{(1-b_2^{y_3^* g_2})} \right) \\
&= y_3^* \left(\frac{(1-b_2^{y_3^* g_2} g_2)}{(1-b_2^{y_3^* g_2})} \right) \\
&= y_3^* \left(\frac{(g_2 - b_2^{y_3^* g_2} g_2 + 1 - g_2)}{(1-b_2^{y_3^* g_2})} \right) \\
&= y_3^* \left(g_2 + \frac{(1-g_2)}{(1-b_2^{y_3^* g_2})} \right) \\
&= y_3^* g_2 \left(1 + \frac{1-g_2}{(1-b_2^{y_3^* g_2}) g_2} \right).
\end{aligned}$$

This shows that $y_3^* g_2$ is a root of $f(y) = y \left(1 + \frac{1-g_2}{(1-b_{2_1}^{y}) g_2} \right) = 1$. Since y_1^* is the unique root of $f(y)$, we have $y_1^* = y_3^* g_2$.

An analogous proof showing that $x_1^* = x_3^* g_1$, where $x_1^* \in (0,1)$ is the unique root of $x \left(1 + \frac{(1-g_1)}{(1-b_1^x) g_1} \right) = 1$ and $x_3^* \in (0,1)$ is the unique root of $x \left(1 + \frac{(1-g_1) b_1^{x g_1}}{(1-b_1^{x g_1})} \right) = 1$, can be used to show that the two models' $\tilde{R}_2$ equations are identical.

BIOGRAPHICAL STATEMENT

Omomayowa Olawoyin was born in Lagos, Nigeria and moved to America at a young age. She earned an Honors Bachelor of Arts in Mathematics at the University of Texas at Arlington (UTA) in May 2015. As an undergraduate student, she participated in research projects through the National Science Foundation sponsored Undergraduate Training in Theoretical and Ecological Research Program and McNair Scholars Summer Research Institute. After receiving her Bachelors degree, Omomayowa entered the mathematics doctoral program at UTA, where she worked under the supervision of Christopher Kribs on projects related to the mathematical modeling of infectious diseases and elementary mathematics education. Omomayowa was awarded the National Science Foundation Graduate Research Fellowship and Ford Foundation Predoctoral Fellowship, of which she accepted the former. During her graduate studies, she became a member of Pi Mu Epsilon and served as secretary for the Society of Industrial and Applied Mathematics, vice president for the UTA chapter American Mathematical Society, and secretary for UTA's College of Science Black Graduate Student Association.